UNIVERSITÀ DEGLI STUDI DI PADOVA

DIPARTIMENTO DI INGEGNERIA INDUSTRIALE

CORSO DI LAUREA MAGISTRALE IN INGEGNERIA CHIMICA E DEI PROCESSI INDUSTRIALI

**Tesi di Laurea Magistrale in
Ingegneria Chimica e dei Processi Industriali**

DYES PHOTODEGRADATION PROMOTED BY GREEN CATALYSTS

Relatore: Prof. Roberta Bertani

Laureando: Pierre Bottarel

ANNO ACCADEMICO 2019-2020

Abstract

In the circular economy context, the aim of the thesis is to evaluate the possible valorisation of waste materials, such as spent coffee grounds and domestic wooden ash, for the preparation of catalyst supports.

The thesis work can be divided into two section. Firstly, the waste materials were treated to prepare catalysts using different metal systems and two preparation techniques: wet impregnation and ball milling. Referring to the impregnation technique, a pre-treatment has been applied with sodium bicarbonate and acetic acid to develop the matrix porosity. Metal systems are copper, manganese and iron salts and titanium dioxide. Catalysts physical and chemical characterization was carried out thoroughly.

Then, some selected catalysts were tested to degrade organic dyes. The dyes considered in the study were rhodamine, erythrosine B and carminic acid.

Experimental investigations were carried out in three sets of reaction.

Firstly, the photodegradation promoted by TiO_2 and TiO_2-supported catalysts was tested, in presence of UV light, allowing to evaluate how the presence of the spent coffee grounds support influenced the reaction, involving on one side a certain adsorption due to the support and partially inhibiting on the other side the catalytic activity of the TiO_2.

 The oxidative degradation promoted by copper-based catalysts was studied using different amounts of catalyst and H_2O_2.

The oxidative degradation promoted by Fe-supported catalysts obtained by ball milling was finally considered.

Riassunto

Nel contest dell'economia circolare, lo tesi si propone di valutare la possibile valorizzazione di materiali di scarto, come i fondi di caffè e le ceneri da combustione domestica di legna, per la preparazione di supporti per catalizzatori.

Il lavoro può essere suddiviso in due aree di studio. In primo luogo, i materiali di scarto sono stati trattati utilizzando diversi sistemi metallici e due tecniche di preparazione: l'impregnazione e la macinazione con un mulino a biglie. Per la preparazione di catalizzatori per impregnazione, è stato applicato un pretrattamento con bicarbonato di sodio e acido acetico per sviluppare la porosità della matrice. I sistemi metallici impiegati sono sali di rame, di manganese e di ferro, nonché diossido di titanio. I catalizzatori sono stati quindi approfonditamente caratterizzati dal punto di vista fisico e chimico. Quindi, alcuni catalizzatori scelti sono stati testate nella degradazione di coloranti organici. I coloranti presi in considerazione sono rodamina, eritrosina B e acido carminico.

L'investigazione sperimentale è stata svolta focalizzando l'attenzione su tre tipologie di reazione.

Per prima è stata testata la fotodegradazione catalitica, promossa rispettivamente da TiO_2 e da catalizzatori supportanti TiO_2 in presenza di luce UV, che ha permesso di valutare come la presenza del supporto a base di fondi di caffè abbia influenzato la reazione, comportando da una parte una componente di assorbimento del colorante nella matrice carboniosa e inibendo dall'altra l'attività catalitica del diossido di titanio.

La degradazione ossidativa della rodamina con catalizzatori a base di rame è stata studiata utilizzando diverse quantità di catalizzatore e di H_2O_2.

Infine, è stata considerata la degradazione ossidativa con catalizzatori a base di ferro ottenuti per macinazione con un mulino a biglie.

Index

Introduction

The thesis is the result of the experimental work carried out from March to October 2020. The initial project was to perform the laboratory experiences in Lisbon, at the Instituto Superior Tecnico, under the supervision of Prof. Armando Pombeiro and Dr. Ana da costa Ribeiro within the Erasmus project. Unfortunately, due to the pandemic situation, it has been preferred to complete the activity in the laboratories of the University of Padua even if the collaboration with the colleagues in Lisbon was preserved and allowed a continuous comparison during the thesis activities.

The objective of the thesis was to develop sustainable heterogeneous catalysts using waste as raw materials for the support preparation. Catalysts have been tested in the oxidative degradation of organic dyes, even if the initial project concerned the oxidation of cyclohexane.

Firstly, some studies present in literature were screened to understand which are the main advantages and the major issues related to the use of spent coffee grounds, which are attracting a great scientific attention due to the composition and the large amount of them, continuously available.

As a novel waste to apply in this field, wooden ash was studied, but, due to the heterogeneity of the morphology and composition it was, for the moment, abandoned.

Then a series of catalysts (containing TiO_2, copper and manganese) has been prepared in the laboratory and physically and chemically characterized, even if some relevant determination were not, up to now, completed, using the instrumentation available in the Department of Industrial Engineering and at the CEASC laboratories.

Finally, an experimental setting was designed to test the degradation reactions with and without the supply of UV light.

Particular attention was dedicated to the carminic acid dye, whose behaviour, being quite complex, has been investigated and its degradation was successfully carried out.

Chapter 1

Waste as raw material for the environmental pollution reduction

The aim of the thesis is the design of sustainable catalysts. The reason of the usage of the term sustainable is due to the dispersing matrix material choice. In fact, the raw material that have been chosen for the application are waste material such as spent coffee grounds and wooden ash. For this reason, it can be said that this study is a concrete chemical engineering application of the circular economy principles. Moreover, this way of proceeding takes into account the green chemistry principles, that underline the importance of the waste prevention and of the catalyst employment.

In this first chapter, the circular economy fundamental aspects and major objectives together with the green chemistry guidelines are briefly summarized, in order to give a contextualization of the experimental investigation direction.

Then the characterization of the raw materials considered for the dispersion matrices creation have been reported. In order to make comparisons with commercially available materials, the same precursors used for the green matrices were employed for the realization of similar catalysts.

The second part of the work focused on the degradation and photodegradation of dyes promoted by the use of catalysts dispersed on green materials. The environmental problem connected with the presence of dyes in wastewater will be considered, underlying the principal techniques applied for their removal.

1.1 Circular economy

One of the major challenges of the XXI century is the shift from a linear economy to a circular economy. The model that characterized most of the companies in the last 150 years is known as linear economic model and is based in the concept of "take, make, waste". The basic assumption of this model is that energy and material resources are unlimited. As this hypothesis appears more and more unrealistic, because of its unsustainability from an environmental and an ethical point of view, in the last two decades a new economic model, known as circular economy, has gained importance. It is

based on the ability of self-regenerating, by mean of the reuse of materials in more production cycles and in the minimization of waste generation.

1.1.1 Moving from a linear economy to a circular economy

Porter said that "Pollution is a form of economic waste that involves the unnecessary, inefficient or uncomplete use of resources. Often emissions are a signal of inefficiency and impose to a company to do an activity that does not generate value, such as the management, the stockage and the disposal of the generated wastes. At the base of the efforts for the waste reduction and for the maximization of the profit there are some common principles such as the efficient use of inputs, the substitution of materials and the minimization of unnecessary activities" [1]. This affirmation well defines and underline the major limits of the concept of linear economy, where companies extract inputs, considered available in unlimited quantities, they transform them, using energy, in outputs, that are distributed to the consumers. The consumers use products and through them away, generating wastes to be disposed.

As underlined by the Onu Resource Panel [2], the growth of global material use has accelerated over the past four decades, while economic growth and population growth have been slowing. This is symptomatic of an economic system that has begun to show important signs of abating. Considering the availability of raw materials, the Ellen Mac Arthur Foundation [3] underlined how in 2010, 65 billion of tons of raw materials have been introduced in the economic system and it is expected that this trend will be enhanced in the next years. In the long term, it is clear that this way of managing raw materials will lead to difficulties on founding resources, less abundant and more expensive. Furthermore, it has been valued that only the 40% of the 65 billion of tons of raw materials will be recovered at the end of their life cycle.

This way of proceeding has a strong impact in the environment, damaging ecosystems all around the word. A parameter that has been estimated by the Global Footprint Network no profit association [4] is the Earth Overshoot Day. The parameter indicates the day of the year when the global population has consumed all the natural resources available for the year. While in the 70's the Earth Overshoot Day was in November, in 2019 it has been the 29th of July, determining the worst result.

These data show the strong limitation of the linear economic system and evidence the need of a shift to a new way of thinking the economy.

The new economic model to which the greatest world powers are turning their attention in the last decades is known as the circular economy. Circular economy is an expression that broadly describes a system where the economic growth is not dependent from the resource consumption. The circular

economy model can self-regenerate, reusing materials in more cycles and minimizing the waste productions. The first industrial applications have taken place in the last 70's.

The Ellen McArthur Foundation, that is one of the most important guideline definers for the circular economy, has individuated three principles that represent the foundations of the new system.

1. Design out waste and pollution. By the fact that waste and pollution are not accidents, decisions must be taken in order to view waste as a design flaw and harnessing new materials and technologies, in order to ensure that waste and pollution are not created in the first place.

2. Keep products and materials in use. Some products and components must be designed so they can be reused, repaired and remanufactured. It is also important to be able to get materials back at the end of their use, so they do not end up in the landfill. This way of considering waste has led to the "design to disassembling" modality of engineering a product, considering during its conception how it will be possible to recover the materials employed.

3. Regenerate natural systems. It is possible to enhance natural resources by returning valuable nutrients to the soil and other ecosystems.

The EU parliament payed a lot of attention to the circular economy, that was inserted in the wider context of the Green New Deal. From the EU parliament reports it is possible to observe the structure of the circular economy system, shown in Fig. 1.1 [5]. Every step that forms the cycle must be think from a circular economy perspective. In this plan, when a product reaches the end of its life, its components are kept within the economy wherever possible; attention is payed also to tackle the planned obsolescence, for which products have limited lifespans to encourage consumers to buy again.

Figure 1.1 Circular Economy scheme

With this in mind, materials that are used can be of two types. The first ones are biological materials, that go back in the biosphere at the end of their cycle of life. They are characterized by being renewable. The second ones are technique materials, that are not renewable, and are designed to go from the production to the consumption without big losses. While in a linear economy companies try to make money by producing new products, in a circular economy wealth is produced by well managing resources. The ultimate goal of the circular economy is the cancellation of waste generation.

1.2 Green chemistry

Beyond the concept of circular economy, that is transforming the entire global economic system year after year, another idea that is influencing more specifically the industrial engineering is the one of Green chemistry. Green chemistry is an expression that was coined by Anastas of the U.S. Environmental Protection Agency (EPA) in 1993 [6], in accord to the growing need of more sustainable process in the industry and particularly in the chemical industry. EPA started in this year the "US Green Chemistry Program", that jointed together different activities, such as the Presidential Green Chemistry Challenge Awards. Industrial engineering has turned its attention to green chemistry projects also before the 1993: particularly, in Italy and Great Britain some project started in the early 1990s.

Sheldon, Arends and Hanefeld [7] provide a working definition of what green chemistry is, saying that "Green chemistry efficiently utilizes (preferably renewable) raw materials, eliminates waste and avoids the use of toxic and/or hazardous reagents and solvents in the manufacture and application of chemical products". This definition is then completed by 12 principles that individuate the green chemistry guidelines.

1. Waste prevention instead of remediation
2. Atomic efficiency
3. Less hazardous/toxic chemicals
4. Safer product by design
5. Innocuous solvents and auxiliaries
6. Energy efficient by design
7. Preferably renewable raw materials
8. Shorter synthesis (avoid derivatizations)
9. Catalytic rather than stoichiometric reagents
10. Design products for degradation

11. Analytical methodologies for pollution prevention

12. Inherently safer processes.

It is evident that many of these points aim this work. In particular the use of coffee and ash as raw material is in agreement with the seventh point, that underline the importance of renewable raw material employment. In this case materials are not only renewable, but also, they are waste. Their treatment would be quite easy because they are not toxic and they do not contain environmental pollutants, but it would take time and resources, for example for their transport, to manage materials without any value. By reusing them it is possible to justify any effort in their treatment with the generation of new valuable products.

The waste used in the study derived from vegetable sources and for this reason they are renewable raw materials.

Secondly the objective of the work is to create dispersing matrix for the catalysis and to test them. Catalysis is a core aspect of the green chemistry, as underlined by the ninth principle. Stoichiometric reagents are still used in many applications, especially in the pharmaceutical and fine chemical industries. Green chemistry's principles want to shift from this way of proceeding to the adoption of catalysis wherever it is possible, in order to minimize the production of wastes during the production process and improve yield, reducing time and energy consumption.

The Green chemistry principles are also the basis of the Green Engineering principles [8].

1. Designers need to strive to ensure that all material and energy inputs and outputs are as inherently nonhazardous as possible.

2. It is better to prevent waste than to treat or clean up waste after it is formed.

3. Separation and purification operations should be designed to minimize energy consumption and materials use.

4. Products, processes, and systems should be designed to maximize mass, energy, space, and time efficiency.

5. Products, processes, and systems should be "output pulled" rather than "input pushed" using energy and materials.

6. Embedded entropy and complexity must be viewed as an investment when making design choices on recycle, reuse, or beneficial disposition.

7. Targeted durability, not immortality, should be a design goal.

8. Design for unnecessary capacity or capability (e.g., "one size fits all") solutions should be considered a design flaw.

9. Material diversity in multicomponent products should be minimized to promote disassembly and value retention.

10. Design of products, processes, and systems must include integration and interconnectivity with available energy and materials flows.

11. Products, processes, and systems should be designed for performance in a commercial "afterlife".

12. Material and energy inputs should be renewable rather than depleting.

1.3 Coffee[9]

The coffee that has been employed in the study is a 100% Arabica blend, but in nature many varieties of coffee exist. Among the more than 70 existent species, only three of them are cultivated.

Coffea arabica L. and *Coffea canephora* Pierre represent the majority of the world production, while *Coffea liberica* is produced in smaller amounts.

C. arabica, also known as Arabica represents the 65-70% of the global production. Its origin remount from Ethiopia and its cultivation is carried out in tropical or subtropical regions, characterized by moderate temperatures. Scientific and economical investments have been done in order to make plants more productive, resistant and ecologically well adapted, by means of hybridization and crossing with non-cultivated species. This blend is characterized by a higher cup quality, more appreciated organoleptic characteristics, lower total soluble solid content respect to the *C. canephora*.

C. canephora, commercially known as Robusta, worldwide production corresponds to the 10-25 % of the total. This species comes from the forest of the Equatorial Africa, but nowadays the production is extended to Asia and South America. Even if it is considered a smaller quality product respect to the Arabica, it has approximately the double caffeine content, it is more resistant to pests and diseases and it has a higher yield of extractable solids.

C. Liberica has a lower economic importance so 98% of the commercial coffee are Arabica or Robusta.
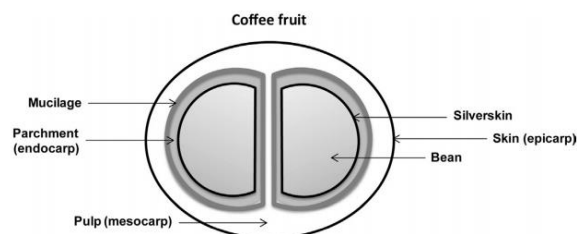

Figure 1.2Structure of a coffee berry

Fig. 1.2 represents the coffee fruit structure. Externally a protective skin envelops the fruit, becoming red from green when the fruit is ripe. Inside there are the mesocarp or pulp and the core, divided in two elliptical hemispheres with flat adjacent parts. The silverskin protects the beans.

According to the International Coffee Organization, during the crop year 2018-2019, the total production of coffee was about 170937 thousands of 60 kg bags. Brazil is the major producer, with almost 63 thousands of 60 kg bags, followed by Vietnam and Colombia.
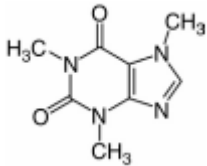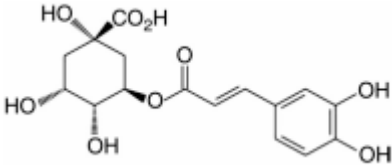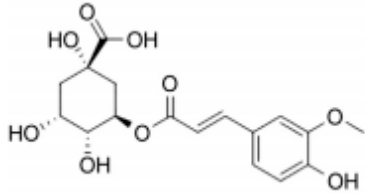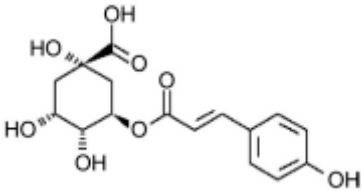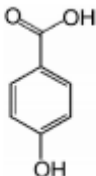
Among the coffee production problems, one of the most important is the waste generation. For example, in Brazil the production of coffee from 2008 to 2013 averaged 2.9 million tons, being generated about 1.4 million tons of wastes each year. Considering all the producing countries, waste generation becomes a serious environmental problem. The valorization of wastes by the companies is crucial from a sustainability perspective but also to generate other incomes. Along the production and consumption chain of the coffee lot of wastes are produces. Among them immature and defective coffee beans have to be considered. They account for the 15-20% of the production and the cause of the most important defects are black, sour, or brown, immature, bored or insect-damaged, and broken beans. One other cause of waste generation is the drying process, where coffee husk is removed. On a dry-weight basis, husk represent around the 12% of the cherry weight, thus for 1 tons of harvested fruit, 0.18 tons of husk waste are generated. Silverskin is very adherent to the beans and it is removed only during roasting. For this reason, it is the main by-product for the coffee-roasting companies, and its collection is mandatory. The final usage of the silverskin is as fuel, for composting and soil fertilization. Finally, there are the spent coffee grounds, that are produced at the end of the chain.

1.3.1 Spent coffee grounds

Spent coffee grounds are the main by-product of the coffee brewing process. They are obtained both domestically, such as at home, at restaurant or at coffee shop, and industrially during the preparation of instantaneous coffee. Comparing the domestic and the industrial ones, it is possible to find much more chemical compounds in the first ones, where the extraction is not optimized. In both cases it is a dark brown solid with a high moisture content. Considering that 11g of fresh coffee grounds are averagely needed for a cup of coffee, six million tons of spent coffee grounds are worldwide wasted every year, estimating that 1 ton of green coffee generates 650kg of spent coffee grounds and, to get 1 ton of soluble coffee, 2 tons of spent coffee grounds are generated, as affirmed by Mussato et al. [10] and Girotto et al. [11]. Accordingly to Ballesteros et al. [12], the nutritional composition of spent coffee grounds derived from mixtures of Arabica and Robusta is rich in polysaccharides, lignin and protein. The ash content is very small, representing the 1.3% of the weight and it is composed by a large variety of elements, such as potassium, that is the predominant, calcium, magnesium, sulphur, phosphorus, iron, manganese, boron and copper.

The bioactive components that are mostly present in spent coffee grounds are reported in Tab. 1.1.

Table 1.1 Principal bioactive components in spent coffee grounds

Caffeine

Caffeoylquinic acids

Feruloylquinic acids

p-Coumaroylquinic acids

4-Hydroxybenzoic acids

These components are not completely extracted during the preparation of the beverage and they are still present in the spent coffee grounds.

Different studies reported in literature have been developed to valorise the spent coffee grounds in a circular economy perspective. Five topics can summarize the major application considered in the studies.

1. It is possible to recover value added chemicals by extraction or enzymatic processes [13][14]. The main products obtained are polysaccharides, that constitute about the 45% on weight and

mainly consists of mannan, galactomannan, arabinogalactana and cellulose [15]. Caffeine is present in a percentual of 18% on weight typically, then other brown-coloured components, such as melanoidins are present. Lipids constitute the 10-20% w/w and are mainly diterpene alcohol esters about 12%, sterols and triaciglycosterols (in particular linoleic, palmitic, stearic, oleic and linolenic acids) as affirmed by Ramon-Goncalves et al. [16], Karmee et al. [17] and Tongumpou et al. [18].

2. Biopolymers and biocomposites achievement can be realized recovering the high content of hemicellulose, cellulose and lignin. As proposed by Moustafa et al. [19], thanks to their composition, spent coffee grounds employment has been evaluated for the reinforcement of polymers.

3. Energy recovery can be achieved using spent coffee grounds [20][21]. The generation of energy sources from spent coffee grounds is a way of proceeding considered by Silva et al. [22], who tried to obtain fuel for industrial boilers and by Machado et al. [23] and Rocha et al. [24] who used them as raw material to get fuel ethanol.

4. Spent coffee grounds have a positive effect as soil amendment, modifying physical and nutritional features, as underlined by Cruz et al. [25], and improving microbial activity and reducing leaching of mineral nitrogen from the arable soil, as affirmed by Elbl et al. [26].

5. Activated carbon can be obtained from spent coffee grounds. Its properties have been studied considering different applications such as the water purification [27][28][29][30][31][32][33]. In particular among the different features, it has been studied the heavy metal removal from waters[34][35][36] , or the diminution of the environmental pollution, proposed by Ching et al.[37], Kim et al.[38], Kim et al.[39] and Rovani et al.[40]. Another application of the activated carbon from spent coffee grounds is the carbon dioxide capture, described by Querejeta et al. [41] and Travis et al. [42], as medium for the hydrogen sulphite separation from air at ambient conditions, studied by Nowicki et al. [43] and Kante et al. [44]. Activated carbon employment has been evaluated also for the storage of small molecules such as methane, hydrogen and lithium, considered in the studies of Kemp et al. [45], Akasaka et al. [46] and Um et al. [47] respectively. The spent coffee grounds derived activated carbon has been studied also as catalyst or support for metal catalysts as proposed by Oh et al. [48] and Goncalves et al. [49]. Finally, recent applications consider the use of activated carbon as cathodic or anodic material in sodium ion and Li-Se batteries, respectively in the work of Lee et al. [50] and Zhao et al. [51]

Other studies are dealing with the usage of spent coffee grounds as animal feed, as proposed by Givens and Barber [52] or for the realization of distilled beverages with coffee aroma, as affirmed by Sampaio et al. [53].

1.4 Wooden ash

Wooden ash and paper mill sludge represent the main waste of the wooden industry in terms of quantity and environmental accumulation. Different sources [54] suggest that considering primary and

secondary wood industry and paper and pulp industry, about 3-5 million Mg of wooden ash are annually produced in the USA.

In the past the majority of the wooden ash waste was disposed in the landfills, but their management is becoming more and more complex due to the more stringent environmental regulations and the minor availability of the landfills, as suggested by Etiegni et al. [55]. In fact, wooden ash is mainly composed by fine particulate matter, which is easily airborne by winds, becoming a source of pollution and a risk to nearby residents [56]. The increase of the complexity in the management of this kind of waste involves an increase in the cost of this type of operation.

In the last decades the discussion about ash was mainly focused on the coal ashes, but in the recent years the attention is more and more focused on the biomass ashes. The reason of this shift is that more and more power plants are built for the generation of energy from renewable sources and among them biomasses are used. Their application as fuel for power generation can be associated or independent from the combustion of coal.

The main risk associated to the wooden ash management is the environmental pollution, that can be generated due to the chemical composition and properties. In fact there is the very strange presumptions that biomass combustion systems are non-polluting or that biomass ash does not contain toxic metals like in the case of coal ash, while it was demonstrated that the concentrations of Ag, As, Ba, Cd, Cl, Cr, Cu, Hg, Mn, Mo, Ni, Pb, S, Sb, Se, Sn, Th, Tl, U, V and Zn in biomass ashes are very disturbing in some studies, as underlined by Vassilev [57]. These elements are in a more mobile and hazardous form rather than in coal ashes. This problem can be managed with a systematic control of the ashes but unfortunately studies concerning the concentration, modes of occurrence, behavior and fate of hazardous phases and trace elements in biomass fuels and their BAs are only at an initial stage of investigation, as affirmed by Vassilev V. [58].

The composition of biomass ashes and in particular of wooden ashes is very different from the one of coal ashes, as studied by Kalembkiewicz et al. [59]. Biomass ashes are rich in plant nutrients, such as calcium, potassium and other microelements. The richness in nutrient component makes the wooden ashes particularly suitable for the use in fertilization.

Another important property of wooden ashes is the high neutralizing potential, that allows their use in reclamation works as substitute of lime.

It is very complex to study the wooden ashes because of the fact that their composition and their properties changes significantly depending on the initial raw material that is combusted and on the combustion condition. As example, Fig. 1.3 represent a ternary diagram where different types of biomass are reported.
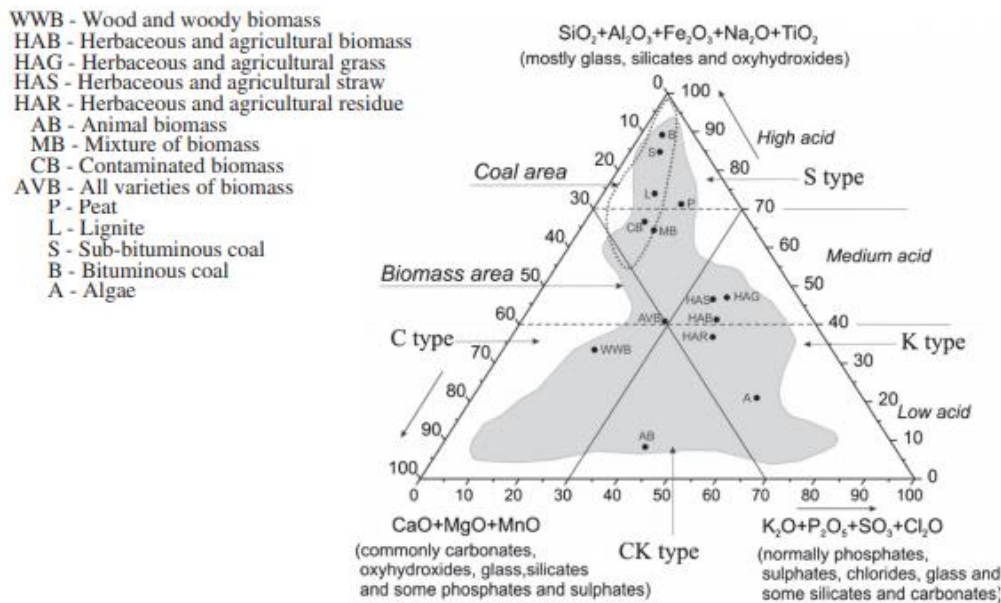
Figure 1.3 Ternary diagram representing the biomass composition

One other feature that strongly influences the final composition and properties of the wooden ash is the process conditions at which it is obtained. Changing the combustion temperature, the yield and the final composition of the wooden ash can change significantly.

1.5   Water pollution

Water quantity and water quality issues are considered as the most critical worldwide ecological problem. Climate change will aggravate these problems even more in the next years, enhancing the melting of the glaciers, accelerating the water cycle, causing potential more floods and droughts and increasing the water temperatures. Focusing on the human health, consequences will involve the lack of improved sanitation, and the related lack of safe drinking water [60]. It is estimated that today about one 25% of the global population suffers from a lack of safe drinking water [61].

More than one third of the accessible renewable freshwater is consumptively used for agriculture, industrial and domestic applications. Most of the applications lead to water contamination, with the dispersion of pollutants such as synthetic and geogenic natural compounds. Being this problem very generalized, water pollution is becoming a concern in almost all parts of the world.

Industrial and agriculture wastewater pollutants can be grouped in three main categories:

1. Bacteria, virus, protozoa and all agents which cause health diseases.
2. Inorganic compounds which are water soluble, such as acids, salts and toxic metals, such as cadmium. Radioactive waste also belongs to this category, since they are unstable compounds decaying with the emission of ionizing radiations.

3. Organic compounds, such as saturated, unsaturated and aromatic hydrocarbons. They are mainly derived by oils, detergents and emulsifiers, plastics and pesticides.

Water organic and inorganic contaminants are mostly as a result of improper treatment of industrial waste, as for example an impropriate sewage planning and management or acid rains from nitrogen oxides due to exhaustion from the combustion process of fossil fuels. Common organic pollutants introduced in waters by chemical and pharmaceutical industries are phenols, bisphenols A, dyes, pharmaceuticals, parabens, endocrine disrupting compounds, phthalates and benzoic acids, as suggested by Al-Hamdi et al. [62]. The problem of the presence of emerging micropollutants and pharmaceuticals is frequently observed in surface water, effluents and drinking water.

Organic water pollutants are very difficult to degrade in water and dyes pollutants discharged in industrial wastewater often receive much more attention due to their coloration and health consequences. In fact, most of the dyes present in waters are undesirable because they are toxic, mutagenic and carcinogenic. Very small quantities of dyes in water can be identified by human eyes, so for some dyes amounts smaller than 1 ppm are considered as an important class of contaminants in wastewater. Dyes coloration is a big issue because it also prevents light penetration and thereby reduces the photosynthetic activities of water streams and disturbs the aquatic equilibrium.

Dyes are used as colouring agents in a variety of industries such as textiles, paper, food, rubber, plastic, cosmetics and leather.

1.5.1 Organic removal from wastewaters

For the removal of organic pollutants and specifically of dyes from wastewater different techniques have been applied. Methods for the pollution removal can be split in conventional and unconventional ones. Among the conventional methods, biological method, chemical precipitation and membrane filtration are the most common ones.

Biological methods are cost effective and environmentally friendly. They also allow a good odour and colour reduction and a high throughput is possible. However, when microalgae are used, the effluent usually needs to be diluted many times because they are not capable to remove high pollutants concentration levels. Moreover, biological processes are difficult to control, needing to handle fluctuation in effluent composition and quantity because of variable wastewater composition and volume. Biological treatments can be applied only to some specific organic pollutant species. For example, food dyes are usually not biodegradable, so the technique is not suitable for them.

Another possibility is to opt for a chemical precipitation treatment, that has the advantage of being simple and having a low energy demand. The technique consists on the flocculation and sedimentation of the organic pollutants. Flocculation consists in the cohesion of particles to form flocks that are sedimented in the further steps. The chemical precipitation shows some disadvantage such as the high non-reusable chemical consumption, considering coagulants, flocculants and aid chemicals, the need of monitoring the pH and the generation of a big quantity of sludge.

An alternative solution for the organic removal from wastewater is the membrane filtration. It is a physical technique that consists on using a porous membrane to trap the pollutants, enabling to obtain purified water. Parameters affecting the performances are the particle size, the solubility, the diffusivity and the charge. The membrane filtration technique is very useful thanks to its simplicity and effectivity. With this method it is possible to rapidly remove also high concentration of pollutants such as solids, microorganism and inorganic matter as exemplified by Strong and Burgess [63] in the wine-related and distillery wastewater treatment. This solution is eco-friendly and does not present problems related to toxicity, corrosivity and plant and animal safety.

Considering the lab-scale, membrane filtration can appear very advantageous from an economical perspective but considering factors such as the maintenance and the operation costs, the convenience disappears for medium and small industries. Moreover, it is quite complicated to find commercial membranes capable of restricting solutes, especially talking about low molecular weight non-charged organics [64]. A major issue of the membrane filtration is fouling, that can determine a loss in performances, causing a los in permeate flux and productivity.
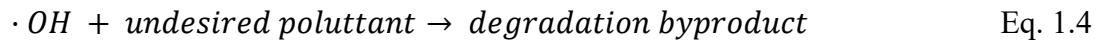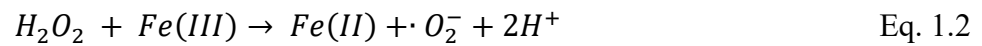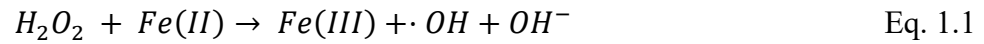
In last decades, advanced oxidation processes, AOPs, have become a promising strategy for the wastewater treatment. They rely on in-situ production of powerful oxidizing radicals, for the effective degradation of the organic pollutants to CO_2 and H_2O, that does not involve environmental of health risks. The AOPs have the great advantage of being able of working at ambient temperature and pressure. AOPs include photocatalysis processes based on near-UV or solar visible irradiation [65], Fenton-based processes, ozonation, electrochemical oxidation and a variety of emerging processes such as the pulsed plasma [66].

Among the AOPs, a technique that shows great potential in organic pollutants degradation is photocatalysis [67]. Heterogeneous photocatalytic oxidation was claimed in 1967 [68], and uses rutile titanium oxide TiO_2 to cause oxidation, considering adequately positive its band gap. The interest of employing this technique is also due to the fact that the activation energy needed to run the reaction can be provided by the solar light. Energy saving and low processes costs are in fact among the main advantages of the photodegradation technique. The photocatalysis, that uses the TiO_2 catalyst is environmentally friendly, since there is not the need of adding any chemicals or to use high consuming energy plants. The simplicity of the technique is ensured by the fact that the catalyst loading is easy to adjust.

The main difficulties on managing the TiO_2-promoted photocatalysis consist on the difficulty of recovering and regeneration of the catalyst and the photocatalyst losses under long term operations.

Other catalytic and photocatalytic organic compound degradation techniques have been proposed in the last years. Among them the Fenton system are decidedly important.

In fact, among the AOPs, the Fenton-based system are the most widely used thanks to the hydrogen peroxide H_2O_2 ability of generating hydroxyl radicals ($\cdot OH$), that are very powerful oxidizing agents. The decomposition of the H_2O_2 is promoted by a catalyst. The most widely used Fenton-based technology is the one that uses iron-based catalysts.

The main reaction involved in the Fenton process are reported in Eq. 1.1 to Eq. 1.4

$$H_2O_2 \ + \ Fe(II) \rightarrow \ Fe(III) + \cdot OH + OH^- \qquad \text{Eq. 1.1}$$
$$H_2O_2 \ + \ Fe(III) \rightarrow \ Fe(II) + \cdot O_2^- + 2H^+ \qquad \text{Eq. 1.2}$$
$$\cdot O_2^- + Fe(III) \rightarrow \ Fe(II) + O_2 + 2H^+ \qquad \text{Eq. 1.3}$$
$$\cdot OH \ + \ undesired \ poluttant \rightarrow \ degradation \ byproduct \qquad \text{Eq. 1.4}$$

However, its application to the organic compound degradation is extremely limited because of the narrow pH window in which it can be applied. In fact, to prevent the Fe (III) precipitation tendency, that is pronounced in the circumneutral pH range, it is necessary to work at pH between 2 and 4. A solution to overcome the problem related to the Fe solubility is to substitute the iron with copper. Using Cu as Fenton catalyst is advantageous because Cu (II) is decidedly more soluble in the pH range of interest, that goes from 3 to 7 [69].

An extensively used technique for the removal of organic compounds from the wastewater is represented by the adsorption. Its strengths are the cost, the ease of operation, the flexibility and simplicity of design and the insensitivity to toxic pollutants. Thanks to their excellent adsorption ability, activated carbon can be considered as a logical choice for the removal of dyes. The main disadvantage of activated carbons regards their cost, so waste-derived material including agriculture wastes, industrial waste, fly ash and clay material such as bentonite are employed for the preparation [70].

Chapter 2

Material and Methods

2.1 General features

Tab. 2.1 summarizes the experiments carried out in the work to create catalysts from wastes as raw materials.

Table 2.1 Recapitulative table of the realized catalysts

Raw Material	Pretreatment	Metal system
Wet Impregnation Technique/Metal systems		
Spent coffee grounds	$NaHCO_3/CH_3COOH$ 1:1, 1:2, 1:5	$Cu(NO_3)_2 \cdot 3H_2O$
		$CuSO_4 \cdot 5H_2O$
		$Mn(NO_3)_2 \cdot 4H_2O$
		TiO_2
Wooden ash	$NaHCO_3/CH_3COOH$ 1:1, 1:2, 1:5	$Cu(NO_3)_2 \cdot 3H_2O$
Spent coffee grounds activated carbon	As it is	$Cu(NO_3)_2 \cdot 3H_2O$
		$Mn(NO_3)_2 \cdot 4H_2O$
		TiO_2
Commercial activated carbon	As it is	$Cu(NO_3)_2 \cdot 3H_2O$
		$Mn(NO_3)_2 \cdot 4H_2O$
		TiO_2
Ball Milling Technique and heating		
Spent coffee grounds		
Commercial activated carbon		

The catalyst preparation was carried out into two steps: the support preparation and the metal system deposition. The support preparation involved different raw materials and the metal impregnation has been achieved with two techniques: the wet impregnation and the ball milling.

The raw materials, the supports and the catalysts have been characterized through the following techniques.

1. Environmental Scanning Electron Microscope ESEM, to get information about the morphology and the atomic abundance of the surface of the material.
2. Porosimetry to evaluate the surface area and pores volume by means of the di Brunauer-Emmett-Teller equation (BET).
3. X-ray scattering techniques XRD, to individuate the amorphous or crystalline structure.

4. Fourier Transformed Infrared Spectroscopy FT-IR, to estimate the presence of functional groups on the surface of the samples.

In Tab. 2.2 the parameters investigated, and the related technique and measurement instrument are summarized.

Table 2.2 Instrumentation utilized for the raw material, support and catalyst characterization

Parameter	Technique	Instrument
Morphology and Atomic abundance	ESEM	FEI-QUANTA200
Porosity	BET	Quantachrome Autosorb iQ
Structure	XRD	X Pert Powder
Functional groups	FT-IR	Spectrum100

In the final part of the chapter the experimental settings for the adsorption and degradation tests with dye solutions are described. The techniques used for the study of the absorption and degradation experiments are the following:

1. UV-visible spectroscopy to understand how the dye concentration varies in time during the process.
2. Electrospray ionization to study the composition of the final solutions.

In Tab. 2.3 the experimental investigated parameters and the corresponding technique applied are reported.

Table 2.3 Instrumentation utilized for the dye's absorption and degradation experiments

Parameter	Technique	Instrument
Dye concentration	UV-Vis	Lamda 25 Perkin Elmer
Final composition	ESI	Finnigan LCQDUO

2.2   Support preparation

2.2.1 Preparation of spent coffee grounds-based supports

The spent coffee grounds are a 100% arabica blend of the Illy's brand, procured in an Italian local cafeteria after espresso coffee brewing. Before the employment of the coffee, some preliminary treatments are carried out. The spent coffee grounds are sieved to remove impurities, stirred to obtain a homogeneous sample and oven-dried at 105°C for 24 hours. To prevent the humidification of the material, it is conserved in a desiccator, as illustrated in Fig. 2.1.

Figure 2.1 Desiccator containing the spent coffee grounds

Once the spent coffee grounds are purified and dried, they can be treated to develop their porosity. The treatment consists in the addition of sodium bicarbonate ($NaHCO_3$) and acetic acid (CH_3COOH) to the spent coffee grounds. Sodium bicarbonate and acetic acid react and release carbon dioxide (CO_2), that hits the raw material matrix, changing its morphology. It has been decided to work with a ratio between sodium bicarbonate and spent coffee grounds of 1:1, 1:2 and 1:5.

Practically, 10g of spent coffee grounds have been weighted. Then sodium bicarbonate has been added in the defined ratio to the spent coffee grounds and the powder has been uniformized by mean of a pestle and a mortar. Then the powder has been put in a flask and the flask has been disposed on a magnetic stirrer. For the 1:1 and 1:2 ratio a straight bar has been employed to provide agitation, while for the 1:5 ratio a cross bar has been used. Initially a defined quantity of acetic acid has been added, depending of the ratio between sodium bicarbonate and spent coffee grounds. By adding the acetic acid, the reaction starts to take place, carbon dioxide was released in small bubbles and the mixture tended to form a cake. Before it assumed a solid consistence, it was important to add other acetic acid, to help the reaction to continue. The complete consumption of the sodium bicarbonate was necessary, without forming solid conglomerates. It was possible to understand that the reaction was still running as long as small bubbles continued to appear on the surface.

The powder mixing procedure is shown for the C1:5 sample as an example in Fig.2.2 and Fig.2.3. The homogenization is quite precise even if small sodium carbonate granules are still present. It is very important that these grains are small otherwise if the mixing is insufficient, they can grow generating rocks of sodium bicarbonate that does not react with acetic acid. That implies on one side that the increasing in porosity will not be achieved and on the other side the fact that on the final support there will be traces of sodium carbonate.

Figure 2.2 Coffee and NaHCO₃ before mixing

Figure 2.3 Coffee and NaHCO3 after mixing

Fig. 2.4 and Fig. 2.5 show the C1:1 and C1:5 support after few seconds of mixing on the magnetic stirrer. The C1:2 case is very similar to the C1:1. In the figure in the left the bubbling phenomenon is less evident than in the right figure. In the right figure the quantity of sodium bicarbonate and acid involved were greater than in the left one, so the reaction had more evident effects.
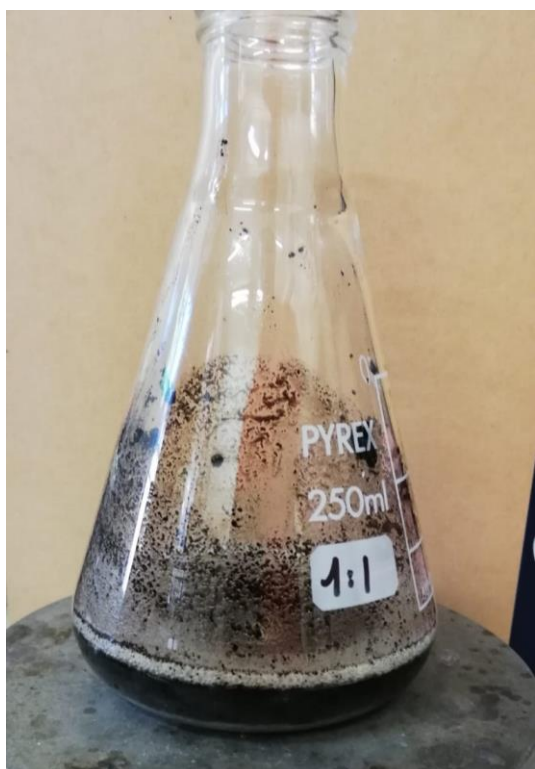

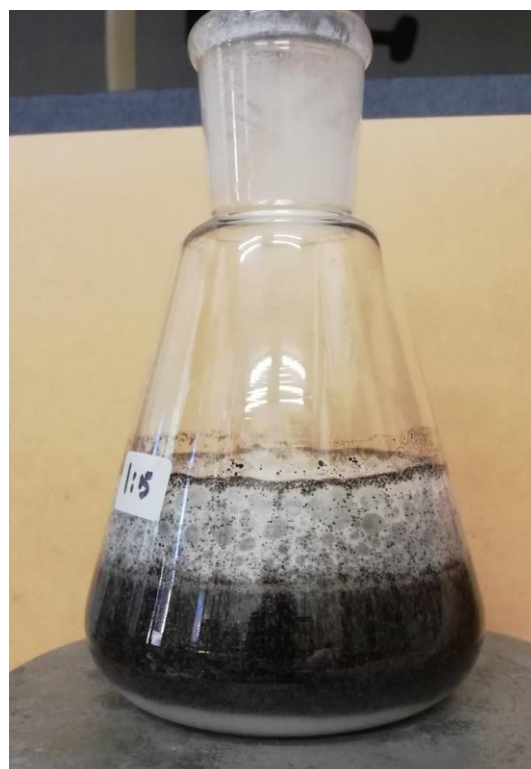*Figure 2.4 C1:1 flask after few seconds of mixing*

Figure 2.5 C1:5 flask after few second of mixing

In the figure related to the C1:5, a certain quantity of sodium carbonate tends to deposit on the back of the flask. It is very important to prevent its deposition and to promote the reaction, improving mixing with a bigger bar, changing the rotation frequency or manually by agitating with a glass rod. In the table below, all the quantities of reactants are summarized for the three ratios are summarized.

Table 2.4 Quantities involved in the coffee-based support realization

	1:1 RATIO	1:2 RATIO	1:5 RATIO
Coffee [g]	10	10	10
Sodium Bicarbonate [g]	10	20	50
Initial Acetic Acid [mL]	20	40	100
Additional Acetic Acid [mL]	30	60	100

After 12 hours the bubbling effect stopped in all cases. At this point the supports were filtrated by means of vacuum filtration and washed with deionized water to remove unreacted acid from the sample. The washing also removed some organic molecules present in the coffee matrix, as shown by the brown colour of the washing water (Fig. 2.6).

Figure 2.6 Acid and water used for the support creation and washing

Then, the filtered powder was put in the oven at 120°C for 12 hours. Finally, the support was recovered and conserved in a plastic box. The loss in weight was around the 20% in the different samples.

2.2.2 Preparation of wooden ash-based supports

The wooden ash employed for the experiments was a grey powder obtained by the combustion of beech tree wood in a domestic fireplace. The initial raw material was very heterogeneous, so it had been sieved to remove partially non-combusted wood and other impurities. With this treatment it has been possible to obtain a more uniform matrix, even if complete homogeneity could not be reached. The ash has been conserved in a glass jar.

As previously reported for spent coffee grounds-based supports, wooden ash was treated to increase its porosity with sodium bicarbonate and acetic acid. Three defined ratios between sodium bicarbonate and ash were fixed and depending of the ratio a certain quantity of acetic acid was added.

The acetic acid was partially added at the beginning to start the reaction and partially during the reaction to prevent the cake formation. Quantities involved in the realization of the ash-based supports are reported in Tab. 2.5.

Table 2.5 Quantities involved in the ash-based support realization

	1:1 RATIO	1:2 RATIO	1:5 RATIO
Ash [g]	10	10	10
Sodium Bicarbonate [g]	10	20	50
Initial Acetic Acid [mL]	20	40	100
Additional Acetic Acid [mL]	40	50	110

In this case the filtration of the support for the acetic acid removal gave a greater material loss. At the end the loss in weight varied a lot among the different samples, but it was always greater than the 50%. The residual acid solution filtered, in this case had a grey coloration, that was caused by the presence of some finer ash particles that were able to migrate through the filter.

2.2.3 Preparation of activated carbon supports

The activated carbon has been obtained by pyrolysis of the spent coffee grounds. After the treatment of removal of impurities, stirring and drying, 60g of powder were mixed with potassium hydroxide (KOH) in a ratio 1:1 by mass, under N_2 atmosphere. Usually, potassium hydroxide was employed as activating agent in order to develop porosity during thermal treatments. The mixture was then pyrolyzed for 4 hours at 800°C in a tubular alumina reactor, under N_2 atmosphere (150cc/min). Operating conditions have been chosen accordingly to Wang et al. [71].

For comparison, a commercial activated carbon has been employed, without making any treatment on it before the metal deposition. The commercial activated carbon was purchased from Ceca Italiana s.r.l. In Tab. 2.6 are collected all the supports that have been created, classified considering the initial raw material used and the amount of sodium bicarbonate employed for the treatment.

Table 2.6 List of prepared supports

	Raw Material	Amount of Raw Material [g]	Amount of NaHCO$_3$ [g]
C1:1	Spent Coffee Grounds	10	10
C1:2	Spent Coffee Grounds	10	20
C1:5	Spent Coffee Grounds	10	50
A1:1	Wooden Ash	10	10
A1:2	Wooden Ash	10	20
A1:5	Wooden Ash	10	50
B	Activated Carbon from spent coffee grounds pyrolysis	No treatment is needed	

CAC	Commercial Activated carbon	No treatment is needed

2.3 Catalyst preparation

2.3.1 Wet impregnation technique

The wet impregnation technique has been employed to disperse the metal, that constitutes the active sites of the catalyst, on the support. Water-soluble salts have been employed as precursors. All the employed supports are characterized by a layer of chemisorbed oxygen that ensures readily wettability by aqueous solutions [72]. By this way water wets the porous surface and metal ions dissolved in it can be dispersed in the matrix. The coordination with complex organic molecules of the matrix lead to the exchange of H^+ attached to the support with positive cations such as Cu^{2+} and Mn^{2+}. The final washing of the catalyst removes traces of the excess of the metal precursor.

In Tab. 2.7 the catalysts prepared with the wet impregnation technique and the experimental details are summarized.

Table 2.7 List of the catalysts obtained by wet impregnation

	Support	Metal Species	Amount of Support [g]	Amount of Metal Species [g]
C1:1Cu	C1:1	$Cu(NO_3)_2·3H_2O$	1	0.02
C1:2Cu	C1:2	$Cu(NO_3)_2·3H_2O$	1	0.02
C1:5Cu	C1:5	$Cu(NO_3)_2·3H_2O$	1	0.02
C1:5Cu1:10	C1:5	$Cu(NO_3)_2·3H_2O$	1	0.10
C1:1Mn	C1:1	$Mn(NO_3)_2·4H_2O$	1	0.02
C1:2Mn	C1:2	$Mn(NO_3)_2·4H_2O$	1	0.02
C1:5Mn	C1:5	$Mn(NO_3)_2·4H_2O$	1	0.02
C1:5Mn1:10	C1:5	$Mn(NO_3)_2·4H_2O$	1	0.10
C1:5Ti	C1:5	TiO_2	1	0.10
C1:1solfCu	C1:1	$CuSO_4·5H_2O$	1	0.02
C1:2solfCu	C1:2	$CuSO_4·5H_2O$	1	0.02
C1:5solfCu	C1:5	$CuSO_4·5H_2O$	1	0.02
A1:1Cu	A1:1	$Cu(NO_3)_2·3H_2O$	1	0.02
A1:2Cu	A1:2	$Cu(NO_3)_2·3H_2O$	1	0.02
A1:5Cu	A1:5	$Cu(NO_3)_2·3H_2O$	1	0.02
B-Cu	B	$Cu(NO_3)_2·3H_2O$	1	0.02
B-Mn	B	$Mn(NO_3)_2·4H_2O$	1	0.02
B-Ti	B	TiO_2	1	0.02
CAC-Cu	CAC	$Cu(NO_3)_2·3H_2O$	1	0.10

CAC-Mn	CAC	Mn(NO₃)₂·4H₂O	1	0.10
CAC-Ti	CAC	TiO₂	1	0.10

Different metal systems have been deposited on the supports surface. Considering firstly the spent coffee grounds-based supports, copper, manganese and titanium dioxide have been dispersed. On the wooden ash-based support only copper has been deposited and on the activated carbon, both on that obtained from spent coffee grounds pyrolysis and the commercial one, copper, manganese and titanium dioxide have been dispersed.

The dispersion of copper on the spent coffee grounds-based supports surface has been carried out by means of two different precursors, copper nitrate trihydrate ($Cu(NO_3)_2 \cdot 3H_2O$, MM 241.60 g/mol; atomic Cu = 26.30 %) and copper sulphate pentahydrate ($CuSO_4 \cdot 5H_2O$, MM 249.69 g/mol, atomic Cu = 25.55 %). Copper nitrate is more soluble than copper sulphate in water.

The deposition has been carried out with the three spent coffee grounds-based supports, mixing support and metal system in a fixed mass ratio of 100:2.

To prepare the catalyst, 1g of support has been weighted and 0.02g of copper-based precursor have been put in a flask with 100mL of water. The flask was left on a magnetic stirrer for 20 hours. Then the solution has been filtered with a Büchner funnel, washed with deionized water to remove the excess of metal, and filtered. Finally, the powder has been dried in an oven at 120°C for 10 hours. The final catalyst has been conserved in a plastic box. The procedure has been repeated in the case of the manganese nitrate tetrahydrate metal system ($Mn(NO_3)_2 \cdot 4H_2O$, MM 251.01 g/mol; atomic Mn = 21.89 %).

Considering the C1:5 support, it has been chosen to disperse copper nitrate and manganese nitrate not only with the usual ratio of 100:2 w/w between support and metal system, but also with a ratio of 100:10 w/w.

Catalysts prepared using the commercial activated carbon as support have been realized with a ratio between support and metal system of 100:10 w/w. To prepare the catalyst 0.1g of titanium dioxide have been added to 1g of C1:5 support and put in a flask. 100mL of water have been added and the flask was put on a magnetic stirrer. After 20 hours, the solution has been filtered and the catalyst was left to dry in the oven at 120°C for 10 hours. The catalyst has finally been conserved in a plastic box. In the case of the titanium dioxide, the procedure was radically different. Titanium dioxide is insoluble in water. The titanium dioxide used for the deposition is a commercial Degussa Titanium dioxide nanopower, whose purity was of the 99.9%. It is composed by an 86% of anatase and a 14% of rutile, as shown by its XRD spectrum, reported in Fig. 2.7.
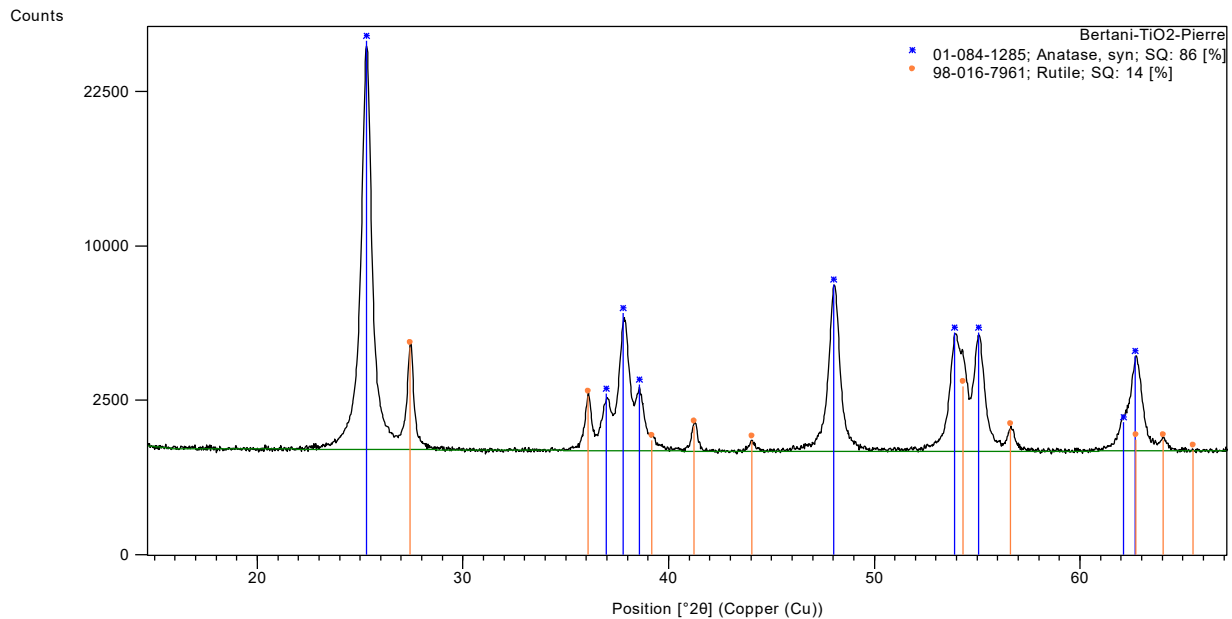
Figure 2.7 XRD Spectrum of TiO₂ used in the thesis

2.4   Physical and chemical characterization techniques

 Characterization has been achieved using different techniques and results of the various samples have been compared.

2.4.1 ESEM

The environmental scanning electron microscope is a microscopic technique that uses a ray of electrons incident on the sample. Electrons, being characterized by a radiation with a wavelength dependent on their kinetic energy, are used to obtain higher resolution power than the optical microscope. The electron beam comes from a tungsten filament, which acts as the cathode. A voltage is applied to the loop, causing it to heat up. The anode, which is positive with respect to the filament, forms powerful attractive forces for electrons. This causes electrons to accelerate toward the anode. The SEM produces various types of signals: secondary electrons, characteristic x-rays, back scattered electrons (BSE), transmitted electrons and sample current. All these require specialized detectors for their detection that are not usually present on a single machine. Secondary electron imaging is the most commonly used detection mode. The SEM can produce very high-resolution images of a sample surface, revealing details about 1 to 5 nm in size in this mode. This is done by collecting low-energy secondary electrons that are ejected from the sample atoms by scattering interactions with beam electrons. Beam electrons that are reflected from the sample are referred to as back-scattered electrons (BSE): the intensity of the BSE signal is strongly related to the atomic number of the sample, thus

images produced by these BSE can provide information about the distribution of different elements in the sample. Through the EDS x-ray detector, it is possible to measure the relative abundance of emitted x-rays versus their energy. To determine the elemental composition of the sampled volume, the spectrum of x-ray energy versus counts is evaluated. The enlargements applied were 100x, 700x and 1500x for all the samples and 20x for some ones where a panning shot on the entire sample was needed. The microanalysis, by EDX embedded, to evaluate the composition on the surface of the sample has been done with the 700x enlargement. This choice is due to the fact that a large region must be considered in order to prevent some inaccuracy due to local irregularity of the sample.

The powder to be analysed is disposed on a metallic small cylinder that is used as support. To guarantee adherence of the sample on the support, double-sided tape is used. The different cylinders are fixed on a metallic disk with other double-sided tape. Finally, the disk is inserted in the microscope to carry out the analysis.

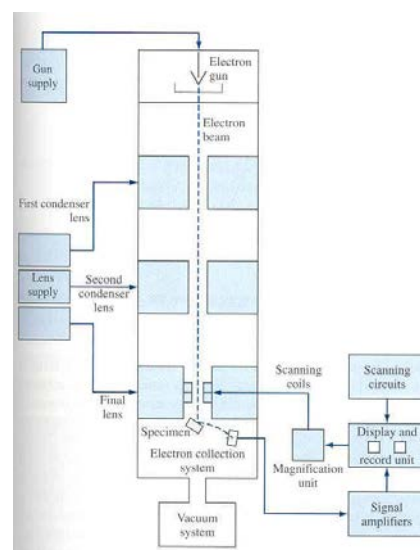*Figure 2.8 Equipment for the ESEM analysis*

Figure 2.9 Basic construction of a SEM

In Fig. 2.8 and in Fig. 2.9, the equipment for the ESEM analysis and the scheme of a SEM are reported. At the right of the desk there is the microscope. In particular, the front view allows to see the door used to introduce the disk supporting the samples. The small knobs help to regulate the position of the disk once the door is closed. On the desk there are the two computer terminals, one used for the morphological analysis and the other for the elementary estimation.

The Environmental Scanning Electron Microscope (ESEM) is a modified version of SEM which can image samples in either the wet state or contained in low vacuum or in a gas with adequate resolution and quality. The greatest use of ESEM is in imaging uncoated, non-metallic or biological specimens. Argon or other gases (H_2O) are typically present around the specimen so that a pressure higher than 500 Pa can be achieved, whereas a vacuum of approximately 10^{-3} Pa to 10^{-4} Pa is required for SEM imaging. At such a vacuum, non-conductive samples do not need to be prepared in advance and it can be observed as it is.

2.4.2 Surface area measurements with the BET determination

The Brunauer Emmet Teller (BET) is an analytical technique that allows to determine the sample specific area and porosity. It is based on the physical adsorption of nitrogen, that happens at 77K. The quantity of gas adsorbed on the solid surface at different pressures after the degassing is evaluated. By this way it is possible to determine an adsorption isotherm, from which the S_{BET} and V_m parameter of the BET equation are obtained. The instrument used to carry out the analysis is the Quantachrome Autosorb iQ.

The equipment is composed by an analyser, a control module and an interface for the data elaboration. Between the pre-sampling line and the analysis there is a vacuum flask with automatic lift to introduce the nitrogen in the system. Controls and indicators are managed with a software that allows the activation of the vacuum system, the degassing valves and the heating coat. Along the sampling line, helium is initially fluxed, in order to measure the dead volume, that corresponds to the place occupied by the sample on the burette. The nitrogen is fluxed and depending on the adsorbed quantity on the sample it is possible to get the surface area.

Figure 2.10 Instrumentation for the BET Analysis

In Fig. 2.10 the instrumentation for the BET analysis is represented. The number 1 indicates the vacuum flask, that is positioned on the lift, indicated with number 2, during the analysis. Number 3 indicates the bags used for the degassing process.

BET measurements have been carried out for SCG derived carbon and for commercial activated carbon, obtaining 1200 m^2/g and 932 m^2/g, respectively.

2.4.3 X-Ray Diffraction

The X-ray diffraction (XRD) is a flexible and non-destructive analytical technique employed to get information about the crystalline structure of powder. In the study the X-ray diffraction has been used to study the wooden ash, the spent coffee grounds-based, the ash-based supports and the C1:5Ti catalyst. The instrument used to carry out the analysis is a powder diffractometer X Pert Powder. The basic idea of the analysis is that an X-ray photon interacts with the sample. During the measurement, a monochromatic ray produced by a copper surface is incident on the sample. The radiations diffracted by the sample are collected by a detector that converts them into electrical impulses. The electrical impulses are then amplified and sent to a computer for the elaboration. To carry out the analysis it is important to very finely grind the sample powder that as to be decidedly homogeneous before putting it on a steel disk for the analysis.

Figure 2.11 XRD analysis instrumentation

Fig. 2.11 shows the instrumentation needed to carry out the XRD analysis. On the right the computer used to compare peaks with information collected in database, in order to identify the crystalline structures.

For some samples, the XRD analysis has been applied not only in a qualitative way, but also in a semiquantitative one. In fact, it is possible to individuate the relative amount between two mineral phases by comparing the high of the principal peaks. This type of evaluation can give quite reliable information only if the two peaks have similar amplitude. The reason of this limitation is that the having larger or tighter peaks influences the quantity of the phase present, so the real quantitative information can be achieved only by considering all the peaks areas. Having peaks with a similar width, it is possible to make acceptable the semiquantitative evaluation.

2.4.4 Fourier Transformed Infrared Spectroscopy

The infrared spectroscopy (IR) is an analytical technique that allows to identify the functional groups present in a molecule. The radiation emitted by the incident radiation, can be absorbed by the bonds in the molecule with the stretching or the bending vibration modes, going from their fundamental state to an excited one. By the fact that each functional group vibrates at specific wavelengths it is possible to know which bonds are present in the sample looking at the effect of sending radiations with different wavelengths.

As a result of the analysis, a plot is obtained where in the abscissa axe the wavelength is plotted, while in the ordinate axe the transmittance is reported. The plot is so characterized by the presence of peaks at defined wavelengths. The base rule is reported in Eq. 2.1.

$$v = \frac{1}{2\pi c}\left(\frac{k}{\mu}\right)^{\frac{1}{2}}$$
Eq.2.1

where k is the elastic constant of the bond and μ is the reduced mass of the two atoms bonded.

The wavelength is defined as wavelength per unit distance and it is expressed in cm^{-1}, while the transmittance can be defined as in Eq. 2.2.

$$T = \frac{I_I}{I_0}$$
Eq.2.2

The transmittance, by definition, is a number between 0 and 1, but in the plots, it is reported as a percentage, so it can vary in the range between 0 and 100.

Among the various quantitative and qualitative applications of the FT-IR, the major one is the identification of the organic compounds present in a sample. In fact, organic compounds give complex spectra in the area of the mid-infrared. Even if the division among far, mid and near infrared is not strict, because it does not depend on chemical or electromagnetic properties, frequency chosen to conduce the experiment usually are between 4000 cm^{-1} and 250 cm^{-1}.

To analyze a solid powder in a FT-IR instrumentation, many ways of proceeding are possible: we used the preparation of pellets. To do that 10 mg of sample powder have been weighted and then they have been grinded with 200 mg of potassium bromide KBr, which is transparent in the IR region. It is very important that the result is extremely uniform. By the fact that the KBr is very hygroscopic, it is important to work very quickly to prevent the adsorption of water of the sample, that can affect the final spectrum. The grinded mixture is collected in a small plastic jar, paying attention to isolate with parafilm. Then, a mechanic press is used to create the pellet. Powder must be uniformly distributed on the support in order to obtain a uniform pellet. The resulting pellet is very thin and fragile, so it must be treated with lot of care. The procedure is repeated for all the samples, paying attention on the cleaning of each instrument, to prevent the sample contamination and particularly the contamination of the pure KBr.

The disks are inserted on the sample holder which will be positioned in the instrument in a fixed position to allow the beam to pass through the sample.

The instrument employed to carry out the analysis is FT-IR PerkinElmer Spectrum 100 with an OMNIC software for the data elaboration.

Figure 2.12 Instrumentation for the FT-IR Analysis

In Fig.2.12 the experimental instrumentation is shown. In the left there is the analyzer, in particular with the number 1 it is indicated the area from where the infrared radiations arrive to the sample and with the number 2 it is indicated the position of the support where the sample disk is put. Finally, number 3 indicates the interface used to elaborate the spectra.

2.5 Adsorption and degradation of dyes

To test the activity of the catalyst, experiments of adsorption and degradation of dyes have been carried out. The dyes whose degradation has been studied were carminic acid, rhodamine and erythrosine B. The concentration of the dye in the time in the solution has been measured by means of a UV-visible spectroscopy while the final composition has been studied by means of an electrospray ionization analysis.

2.5.1 Dyes aqueous solutions

The dyes that have been considered in the study are carminic acid, rhodamine and erythrosine B. Their structure is reported in Tab. 2.8.

Dyes have been employed in aqueous solution in fixed concentration. To do that, once having cleaned the instrumentation with water before and acetone after, the desired quantity of the considered dye, is weighted and put on a glass jar. The dyes considered in the study have a dusty solid form. At this point the dye are solubilized in deionized water and the liquid solution is collected in a glass flask. To get the desired solution concentration, attention is payed to solubilize all the dye, that tends to be quite encrusting, especially in the case of the rhodamine. Usually flasks of 500 mL are prepared each time. Once terminated the process, the flask is closed with a cap and insulated with parafilm. The properties of the aqueous solution of the three dyes are reported in the Tab. 2.10. The pictures used
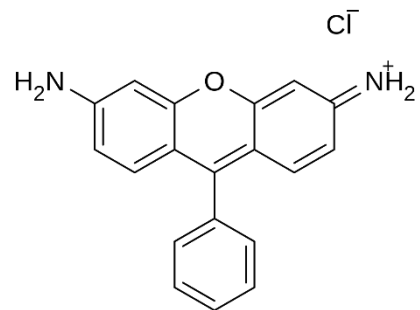
to individuate the initial absorption have been taken using PMMA cuvettes with a white background, in order to do have no differences due to the thickness of the sample or the background colour.

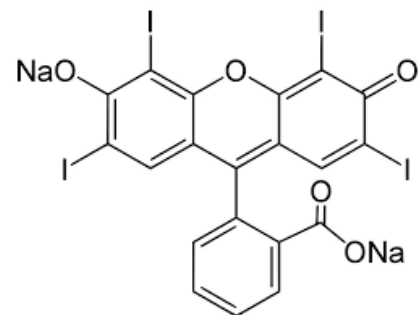*Table 2.8 Dyes tested in the adsorption and degradation processes*

Carminic Acid
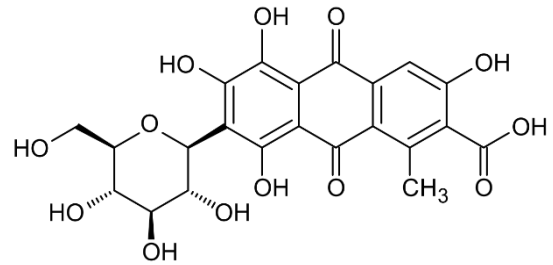
Rhodamine

Erythrosine B

For the different dyes, different concentrations have been used, due to their different molar attenuation coefficients, reported in Table 2.9, in order to have an absorption lower than the maximum value which could be observed in the spectrometer in the visible region.

In Table 2.9 the pH values of the starting solutions of the dyes are reported, too, together with the coloration.

Table 2.9 Dye employed for the experiments

Dye	MW [g/mol]	Massive conc. in water [mg/L]	Molar conc. in water [M]	Molar Attenuation coefficient [M⁻¹cm⁻¹]	λ_{max} [nm]	Coloration	pH
Carminic Acid	492.38	80	$1.625 \cdot 10^{-4}$	7878	495		4.01
Rhodamine	479.02	80	$1.670 \cdot 10^{-4}$	12142	553		5.03
Erythrosine B	879.86	20	$2.273 \cdot 10^{-5}$	81915	526		6.15

2.6   Ultraviolet-visible spectroscopy

To quantify the decreasing of the concentration of dye in the aqueous solution, a UV-visible spectrometer was employed.
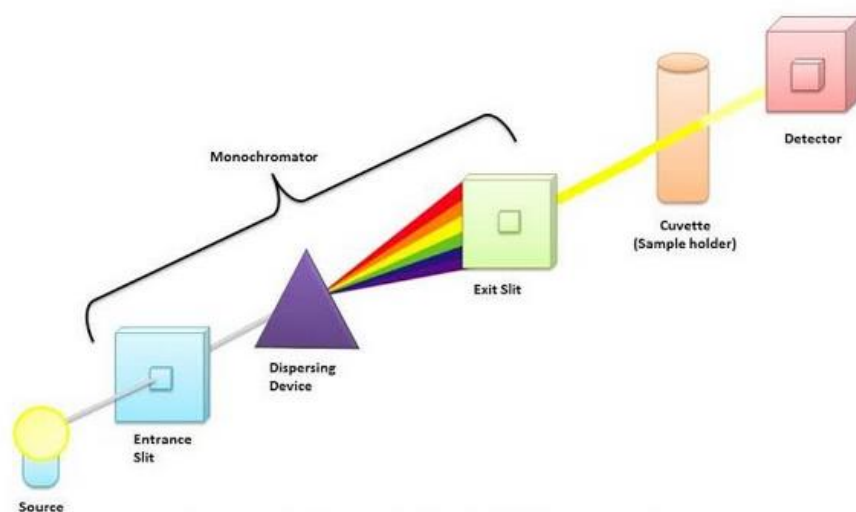
Figure 2.13 UV-Vis instrumentation principle

The instrumentation used is the LAMBDA-25 (Perkin Elmer). This instrumentation is composed by a source, a monochromator, a sustain for the collocation of the cuvettes and a detector. A schematic representation of the functioning of the instrumentation is reported in Fig. 2.13.

The instrumentation works in a double ray modality. For this reason, firstly a blank sample is analyzed, constituted by two cuvettes containing deionized water, then one cuvette is substituted by the sample to be analyzed. By this way it is possible to obtain a relative measurement respect to the initial blank, and by this way prevent to consider the absorption of the water.

As shown in Fig. 2.13 there is a source, that in the case of the employed instrumentation is constituted by two lamps. The first lamp works in the UV range, between 190 nm and 350 nm, while the second lamp works in the visible range, between 350 nm and 800 nm. Making an analysis the instrumentation can switch from a lamp to the other increasing the wavelength. All spectra have been collected with a scanning velocity of 480 nm/s and a band width of 1 nm. The monochromator is used to select precisely a unique wavelength by dispersing the ray and selecting one wavelength with an exit slit. The ray, characterized by a monochromatic light, whose photons have an energy of hv, hits the sample. The sample molecules are able to absorb some radiation thanks to some groups, called chromophore groups. Depending on the types of chromophore groups in the molecules, the absorption of the photons will happen at different wavelengths. Finally, the photodiodes detector measures how many photons hit itself. Looking for a certain wavelength how many photons hits the final detector, it is possible to know how many others have been adsorbed.

Molecules containing bonding and non-bonding electrons (n-electrons) can absorb energy in the form of ultraviolet or visible light to excite these electrons to higher anti-bonding molecular orbitals. The more easily excited the electrons, the longer the wavelength of light it can absorb. There are four possible types of transitions (π–π*, n–π*, σ–σ*, and n–σ*), and they can be ordered as follows: σ–σ* > n–σ* > π–π* > n–π*.

It is possible to correlate the value of absorbance measured to the concentration of dye in the sample referring to the Lambert-Beer Law, whose equation is reported in Eq. 2.3.

$$A = \varepsilon_\lambda l C$$ Eq.2.3

where A represents the value of absorbance, that is non dimensional. ε_λ is the molar attenuation coefficient of the attenuating specie, expressed in $[M^{-1} cm^{-1}]$, l is the optical path length in $[cm]$, usually 1 cm, and finally C is the molar concentration of the attenuating specie, written in $[M]$.

The Lambert-Beer Law can be applied to solution concentrated up to 10^{-2} M. Considering the initial concentration of the three dye always smaller than 10^{-3} M and stated that, being a degradation process, the concentration of the dye can only decrease, the Lambert-Beer Law can be used to obtain the concentration of the dye in the experiments.

The resulting spectrum, for each sample, shows the absorbance as a function of the wavelength. By applying the Lambert-Beer Law at a certain characteristic wavelength it is possible to obtain which is the concentration of the dye in the solution.

For the rhodamine and for the erythrosine B a calibration curve equation is still available and allowed to correlate a certain value of absorbance to a corresponding dye concentration in the solution. The calibration curve plot is reported in Fig. 2.14 for the erythrosine B.
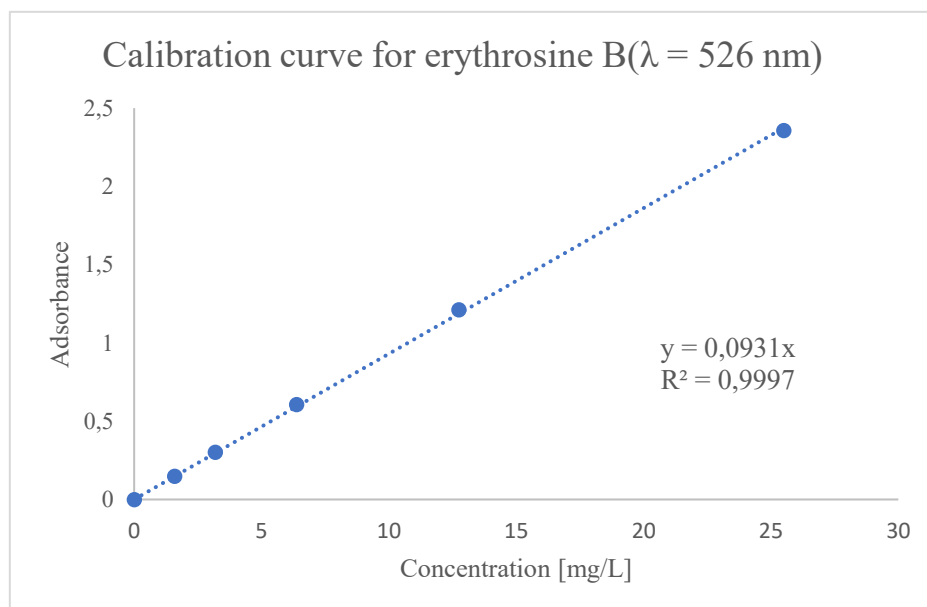

Figure 2.14 Erythrosine B calibration curve

The calibration curve available for erythrosine B correlates a certain value of absorbance with a corresponding molar concentration. The curve has been obtained using a wavelength of 526 nm. The equation of the calibration curve is obtained using six experimental points and has a R^2 very close to one: $y = 0.00931x$

For the rhodamine the calibration curve equation available is reported in Eq. 2.4. for a wavelength of 553 nm.

$$y = 0.025347x \hspace{4cm} \text{Eq. 2.4}$$

Finally, for the calibration curve of the carminic acid, no information was available, thus a calibration curve has been created. A solution of 200 mg/L of carminic acid in water has been prepared and diluted in order to obtain solution with a concentration of 50 mg/L, 25 mg/L, 12.5 mg/L and 6.25 mg/L respectively. For each solution a sample was collected in a quartz cuvette and its spectrum was plotted using the ultraviolet-visible spectroscopy with wavelengths between 400 nm and 750 nm. The plot resulting from the spectrum of the different solution is reported in Fig. 2.15. It can be noticed that the trends are similar, but the values of absorbance decrease as the solution is more diluted.
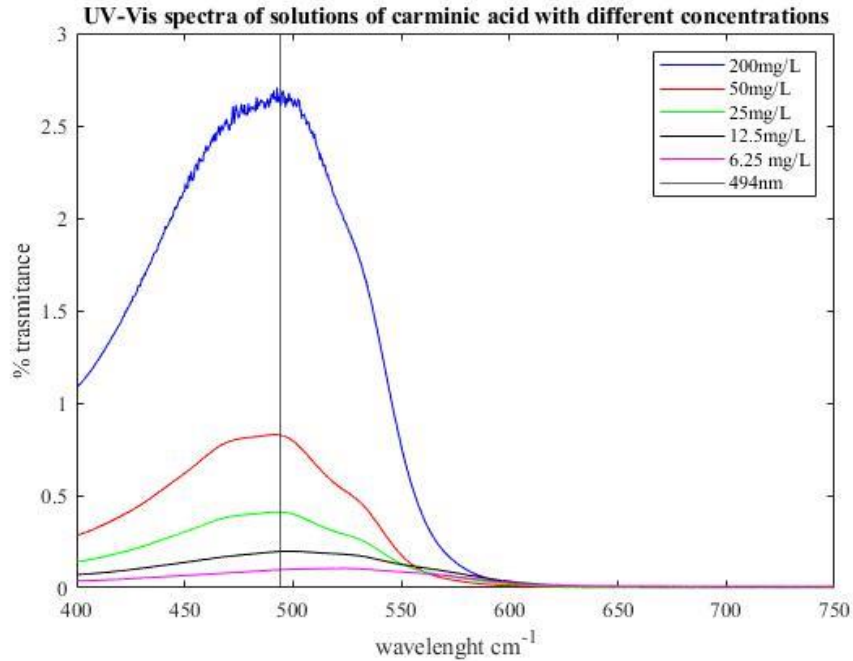
Figure 2.15 Spectra of the carminic acid solutions at different concentrations

A maximum point for each spectrum in the visible region is individuated at the frequency of 495 nm. At this point, concentration and absorbance are known for the different solutions, so the calibration curve can be created in agreement to the Lamber-Beer Law. This choice implies that the curve can be used only for a smaller range of concentrations, but it will be more reliable. The resulting calibration curve plot is reported in Fig. 2.16.
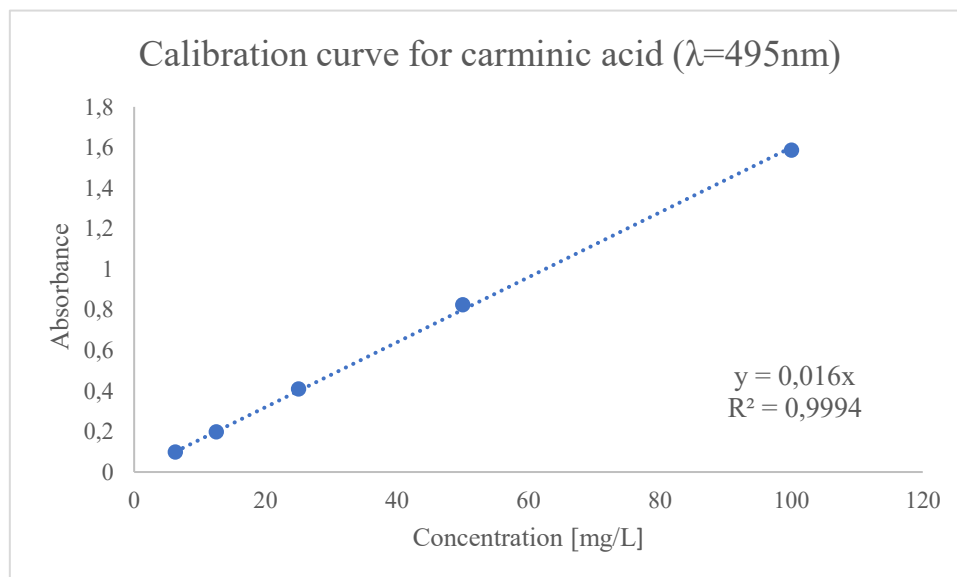
Figure 2.16 Carminic acid calibration curve

The intercept has been set equal to zero. The R^2 is greater than 0.999, so the calibration curve can be trusty used: $y = 0.016x$. The calibration curve has been obtained at a pH of 4.16.

2.6.1 Electrospray ionization

The electrospray ionization is an experimental technique used to study by mass spectrometry the sample composition directly in solution. An electrospray is used to produce ions by applying a high voltage to a liquid to produce an aerosol. In particular, the analyzed solution is introduced into the ionization source, where molecules are first ionized, acquiring positive or negative charges. Depending on their mass/charge ratio, the different ions are then able to travel through the mass analyzer, reaching different points of the detector. Depending on the position on which the ions make contact with the detector, different signals are generated and sent to a computer system. Finally, the computer creates a spectrum showing the relative abundance of the signals according to their mass/charge ratio.

Fig. 2.17 shows the instrument used for the electrospray realization.

Figure 2.17 Instrumentation for the electrospray ionization analysis

2.6.2 Experimental setting for photodegradation experiments

In a glass, a fixed amount of dye solution is disposed, the catalyst and the H_2O_2 are added in the desired quantity. A magnetic anchor is added, and the glass is put on the workstation to start the reaction. It is considered as time 0 the instant on which the glass in disposed on the workstation, from this moment the experiment starts. The experimental setting is composed by a magnetic stirrer on which is disposed the glass containing the reaction environment. Above them a UV lamp, Philips, UVB medical Hg, 9 W, $\lambda=310$ nm, used for the photodegradation experiments, is fixed by means of a clamp anchored to a metal rod with a clip. The clamp assures the stability of the lamp and keep it

in a fixed position, so it is important to verify that sliding is not possible and that the same distance is maintained.

The magnetic stirrer always works with the same frequency, suitable to guarantee the complete suspension of the catalyst particles in the solution and using the same anchor.

The employed glass has always the same dimensions: it is placed always in the centre of the magnetic stirrer and it contains always the same quantity of reactant liquid (200 mL). By this way it is possible to guarantee that in the photodegradation experiments the irradiation conditions are comparable, and the sample is always hit by the same quantity of radiations. The distance between the lamp and the bottom of the glass is of 15,5 cm.

To prevent the dispersion of UV radiations (dangerous) in the laboratory, the experimental setting is insulated, while it is working, by means of a cardboard. By this way it is possible to guarantee that the experiment is run safely.

Fig. 2.18 shows the workstation.

Figure 2.18 Workstation for the adsorption and degradation test

During the experiences, at fixed time intervals, a small quantity of solution is taken using a 5 mL plastic syringe. At this point, a cellulose acetate filter is disposed at the exit of the syringe to trap the powder, allowing to obtain filtered liquid without any suspended solid. The filtered solution is collected on a PMMA cuvette with two knurled surfaces and two smooth surfaces. When the desired samples are collected, the cuvettes are analysed with the UV-visible spectroscopy to obtain the concentration profile during the time.

The remaining solution at the end of the experience is filtered and analysed with the electrospray ionization technique.

2.6.3 Experiments

The set of experiment carried out is collected in Tab 2.10.

Table 2.10 Dyes adsorption and degradation experiments.

Catalyst/Support	Amount [g]	Dye	Solution Volume [mL]	H_2O_2	Amount [mL]	UV light
Photodegradations with titanium oxide						
TiO₂	0.04	Erythrosine B	200mL	No	0	Yes
TiO₂	0.04	Rhodamine	200mL	No	0	Yes
TiO₂	0.04	Carminic Acid	200mL	No	0	Yes
C1:5Ti	1	Erythrosine B	200mL	No	0	Yes
C1:5Ti	1	Rhodamine	200mL	No	0	Yes
C1:5Ti	1	Carminic Acid	200mL	No	0	Yes
Oxidative degradation with Cu-catalysts experiments						
C1:5Cu1:10	0.5	Rhodamine	200mL	No	0	Yes
C1:5Cu1:10	1	Rhodamine	200mL	No	0	Yes
C1:5Cu1:10	2	Rhodamine	200mL	No	0	Yes
C1:5Cu1:10	1	Rhodamine	200mL	Yes	0.5	No
C1:5Cu1:10	1	Rhodamine	200mL	Yes	1	No
C1:5Cu1:10	1	Rhodamine	200mL	Yes	2	No
C1:5Cu1:10	1	Rhodamine	200mL	Yes	1	Yes
C1:5Mn1:10	1	Rhodamine	200mL	Yes	1	No
Oxidative degradation with Fe-catalysts experiments						
SCGs@Fe	0.1	Rhodamine	100mL	Yes	2	No
SCGs@Fe	0.1	Carminic Acid	100mL	Yes	2	No

The experiments can be grouped in three sets.

    a) Experiments with TiO₂

Firstly, experiments have been run using titanium oxide alone, as a reference and titanium oxide-based catalysts C1:5Ti. In the case of the experiments run with titanium oxide, a fixed amount of titanium oxide of 40 mg has been employed for a glass of 200 mL of solution. The experiments have been carried out under the UV light, without H_2O_2.

Considering an average quantity of 5% of titanium oxide (corresponding to 59% of Ti) on the C1:5Ti w/w, it has been decided to use 1 g of catalyst in order to have in the two cases the same total amount of titanium. To distinguish the absorption contribution due to the support porosity from the degradation contribution due to the titanium oxide effect, the experiments with C1:5Ti have been run for the first 8 hours without UV-light and only later switching on the lamp. By this way it is possible

to split the absorption process, that is completed after 8 hours, from the degradation catalytic process that starts only when the lamp is switched on.

Both the pure titanium oxide and the C1:5Ti have been tested with the three dyes.

  b) *Experiments with copper nitrate and manganese nitrate on the spent coffee grounds 1:5 support*

The second set of experiments involved the copper nitrate-based catalyst C1:5Cu1:10 for a modified Fenton reaction based on copper-based catalysts instead of iron-based ones. The rhodamine is the only dye that has been tested.

Initially the adsorption ability of the catalyst has been tested. To do that it has been tried to adsorb the rhodamine with different amounts of catalyst, respectively 0.5 g, 1 g and 2 g. The degradation experiments have been conducted under UV light and in presence of H_2O_2.

The modified-Fenton reaction has been tested using 1g of catalyst and 1mL of hydrogen peroxide for 200 mL of rhodamine solution, without supplying energy by UV radiation. To evaluate the influence of the amount of hydrogen peroxide, other tests have been run using respectively 0.5 mL and 2 mL of hydrogen peroxide.

A Fenton experiment has been run by using the manganese-dispersed catalyst C1:5Mn1:10.

  c) *Experiments with ball milled Fe catalysts*

The third set of experiments aim is to test the catalysts obtained with the ball milling technique in a Fenton reaction. See Section 3.4.

Chapter 3

Results

3.1 General features

In this chapter the results of the analysis carried out to characterize supports and catalysts have been described together with the results achieved concerning the degradation of some dyes promoted by them under different experimental conditions.

As for the characterization of solid supports and catalysts ESEM, XRD and FTIR determinations have been carried out. Only in some cases BET analyses could be carried out for organizational and technical difficulties.

The description of the dye degradation experiments distinguishes three sets: degradations promoted by the titanium dioxide photocatalysis, oxidative degradation with copper catalysts and oxidative degradation promoted by iron catalysts.

As for the dye degradation experiments, three different processes have been carried out:

  a)   Degradation promoted by TiO_2 under UV irradiation.

  b)   Oxidative degradation promoted by copper or manganese salts supported on activated SCGs in the presence of H_2O_2 and UV light.

  c)   Oxidative degradation promoted by SCGs@Fe catalysts.

3.2   Characterization of the solid supports and catalysts

3.2.1 ESEM characterization

By means of an ESEM microscope it has been possible to study the morphology of the samples and a semiquantitative analysis can be achieved by EDX analysis.

3.2.1.1   ESEM Analysis of the raw materials

In Fig. 3.1, Fig. 3.2 and Fig. 3.3 and Fig. 3.4, respectively, the ESEM images of the different raw materials have been reported. Pictures related to spent coffee grounds and wooden ash have been taken with a 700x enlargement, while activated carbon pictures have been taken with a 400x enlargement. The spent coffee grounds (Fig. 3.1) have a leaf-shaped structure. The sample seems to be quite densely packed and impurities are not observable. The wooden ash (Fig. 3.2) is characterized by a completely unregular and not homogeneous morphology. Lot of different corpuscles are present,

each one with its own shape and the matrix appears more fragmentated with respect to the spent coffee grounds. The activated carbon obtained by pyrolysis of spent coffee grounds (Fig. 3.3), shows a smooth surface, full of cavities and characterized by partially flattened cylindrical pores. In the pores, traces of foreign elements (i.e. Mg, Al, Si or S, ≤ 1 %w/w) could be observed. It is to note that the morphology is quite similar to that reported in the literature [73], where the pores observed (μm range) act as channels for the microporous network.

The commercial activated carbon has a structure similar to the structure of the one obtained by pyrolysis of spent coffee grounds, but the matrix is denser, and the pores appear smaller.
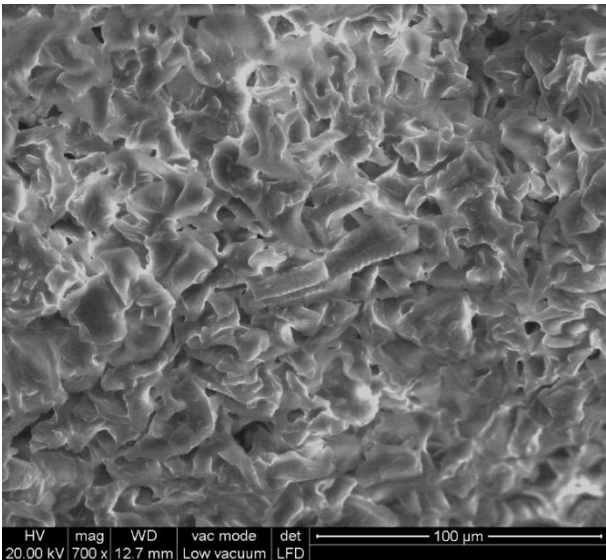
Figure 3.1 Spent coffee grounds morphology
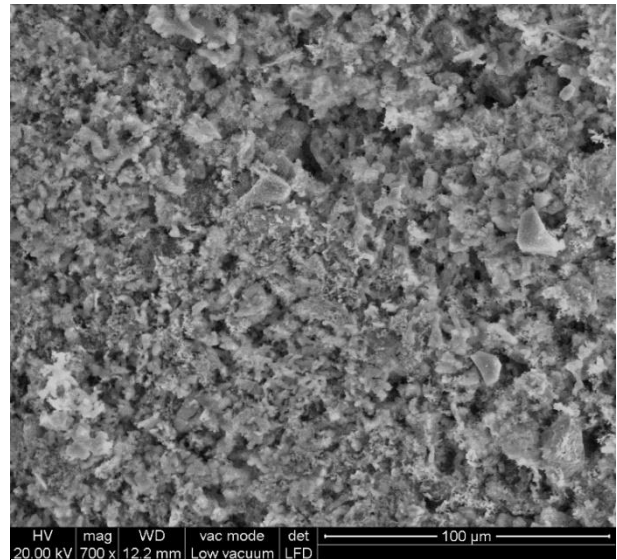
Figure 3.2 Wooden ash morphology
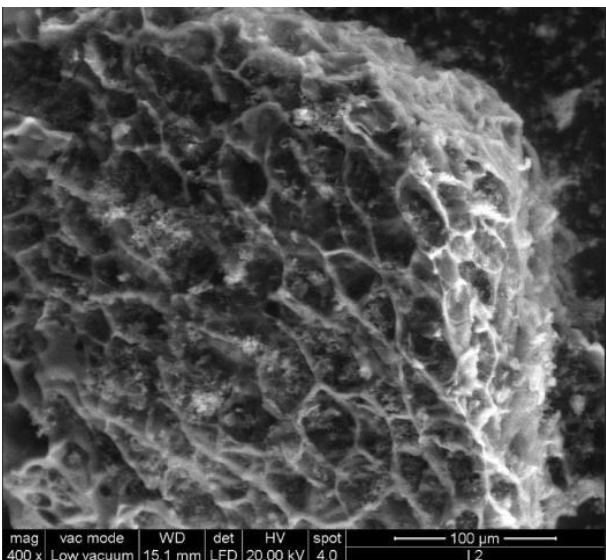
Figure 3.3 Activated carbon from pyrolysis morphology
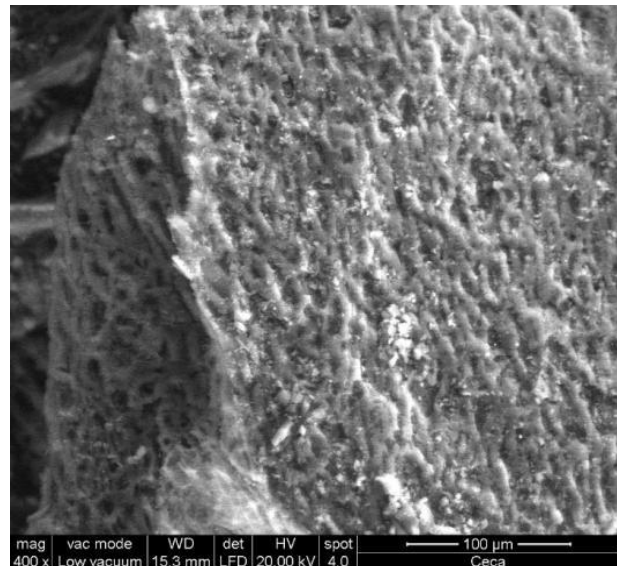
Figure 3.4 Commercial activated carbon morphology

The EDX analyses are collected in Table 3.1 and the plot, as an example for the wooden ash sample, is shown in Fig. 3.5. The information about the composition of the spent coffee grounds, ash and activated carbon from pyrolysis have been collected using a 100x zoom.
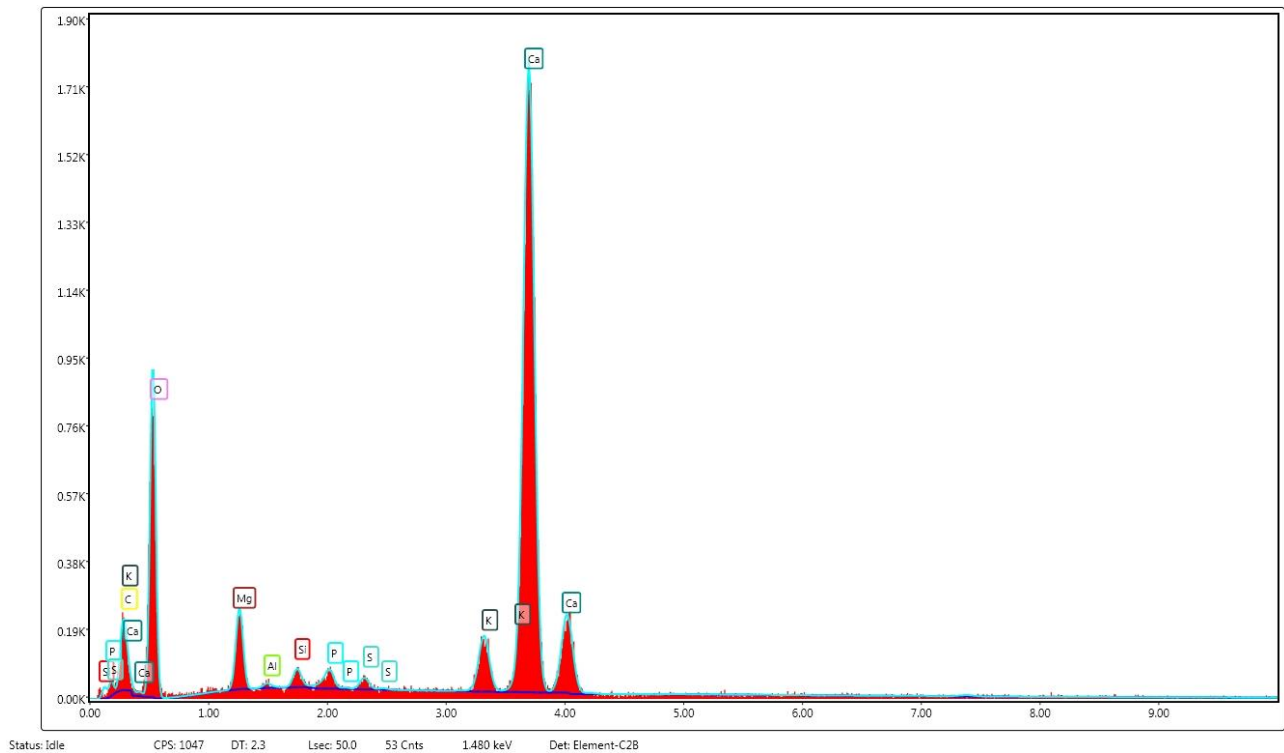
Figure 3.5 Composition of the initial wooden ash

Table 3.1 Element distribution in the four raw materials

Element	SCGs	Ash	AC from SCGs pyrolysis	Commercial AC
C [%]	60.22	3.44	87.35	88.41
O [%]	39.38	64.66	11.65	6.28
Mg [%]	0	3.15	0.74	0
Al [%]	0	0.14	0	0
Si [%]	0	0.47	0	0
P [%]	0	0.53	0	0
S [%]	0	0.32	0	0
Ca [%]	0	25.49	0.26	0
K [%]	0.40	1.80	0	5.31

Spent coffee grounds have a composition typical of organic molecules containing only coffee and oxygen together with potassium traces. In the two activated carbons the carbon percentages are higher than87%, but in the one obtained from spent coffee grounds pyrolysis the oxygen fraction is bigger. In the activated carbon from spent coffee grounds, impurities of magnesium and calcium are present, while in the commercial activated carbon there is a relevant fraction of potassium.

Wooden ash has a carbon weight percentage very low, as a consequence of the combustion process that involved the lignocellulosic biomass, consuming the carbon fraction. The presence of many components in small fractions can be noticed and their presence can be justified considering the origin, represented by a common wood. Most of the components present in the sample are very usually found in lignocellulosic matrices. Calcium, magnesium, phosphor and potassium are nutrient component for the plant, accumulated from the environment with complex mechanisms such as the active adsorption and the ionic exchange during the entire tree life.

Wooden ash morphology and composition has been compared to those of the beech trees by analysing with the ESEM microscope separately the bark and the pulp of the wood before the combustion. Samples have been prepared by grating a log, in the interior side to recover the pulp and externally to recover the bark. Fig. 3.6 and 3.7 show respectively the bark and the pulp.
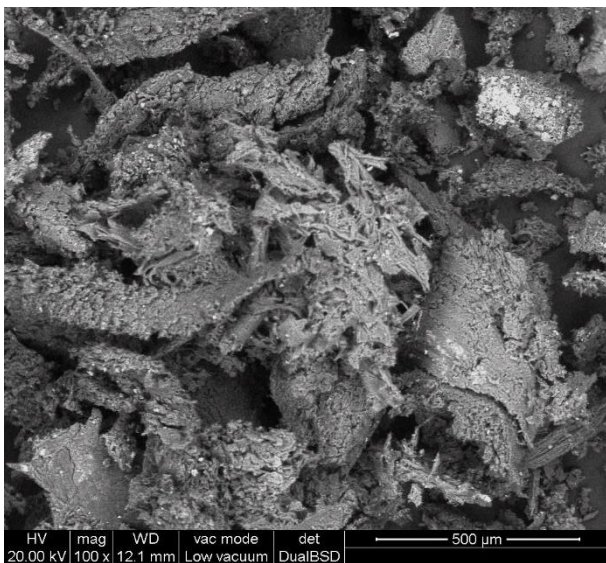
Figure 3.6 Bark morphology
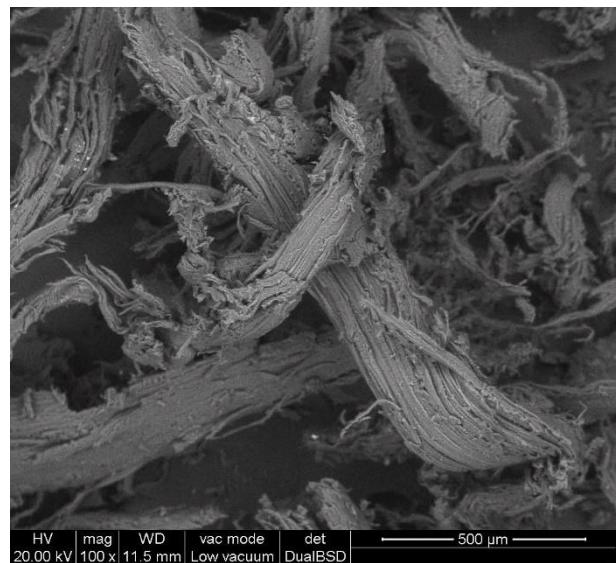
Figure 3.7 Pulp morphology

The bark and the pulp have a completely different morphology from the wooden ash one and each other. Their structure is destroyed by the combustion process leaving ash as residue. Looking at Fig. 3.6 it can be noticed that bark morphology is characterized by the presence of small scrubs, while the pulp, represented in Fig. 3.7, present a fibrous structure. The maintenance of the fibrous structure is a consequence of the fact that it is very difficult to grate the pulp.

Tab. 3.2 reports the composition of the bark and of the pulp as atomic fraction. Results have been obtained by considering an 800x zoom for the bark and a 100x zoom for the pulp. Both the bark and the pulp contain a significant fraction of carbon. The value of the oxygen fraction in the wooden ash is comparable to the beech wood one. Impurities present in the pulp, as the potassium and the calcium, represent an even greater contribution in the wooden ash, because of the disappearance of the carbonic fraction. The silicon represents more than the 12% of the bark concentration because dust is accumulated on the wood bark and it is englobed or trapped during the tree growth process. The decreasing of its fraction in the wooden ash can be explained considering that the bark forms only a thin layer, so it slightly influences the final composition of the sample. Elements as phosphorous and sulphurous are apparently not present in the wood, reasonably masked by the carbon content, but they

appear in the wooden ash composition, even if in a low amount. The heterogeneity of the bark and of the pulp due to the environmental growing conditions and of the wooden ash due to the uncontrolled combustion conditions, must be always kept in consideration.

Table 3.2 Composition of the bark, the pulp and the wooden ash

Element	Bark	Pulp	Ash
C [%]	37.33	53.81	3.44
O [%]	40.89	45.76	64.66
Na [%]	0.64	0	0
Mg [%]	0.35	0	3.15
Al [%]	4.50	0	0.14
Si [%]	12.38	0	0.47
K [%]	0.71	0.21	1.80
P [%]	0	0	0.53
S [%]	0	0	0.32
Ca [%]	1.68	0.22	25.49
Fe [%]	1.53	0	0

It is very difficult to study wooden ash and its derived products because of the significant heterogeneity of the matrix.

3.2.1.2   ESEM Analysis of the spent coffee grounds-based supports

The ESEM analysis has been carried out on the activated spent coffee grounds-based supports: C1:1, C1:2, C1:5. The morphology of the three samples can be considered looking at Fig. 3.8, 3.9 and 3.10. A 100x enlargement has been used for the three figures. C1:1 and C1:2 exhibit very similar morphologies, containing large blocks of spent coffee grounds and some bar shaped corpuscles interposed among them, whose origin is to understand. Blocks have smooth angles and are characterized by a certain degree of porosity. C1:5 instead has a quite different morphology, characterized by smaller blocks, fragmented into small scrubs. Also, in this case some bar shaped corpuscles can be individuated. The different morphology can be explained by the more intense treatment, but also by the fact that in the case of the C1:5 support the bar used to provide mixing is a

cross-shaped one, so it hurts the spent coffee grounds molecules in a different way. Porosity seems to be greater in the case of the C1:5 rather than in the two other supports.
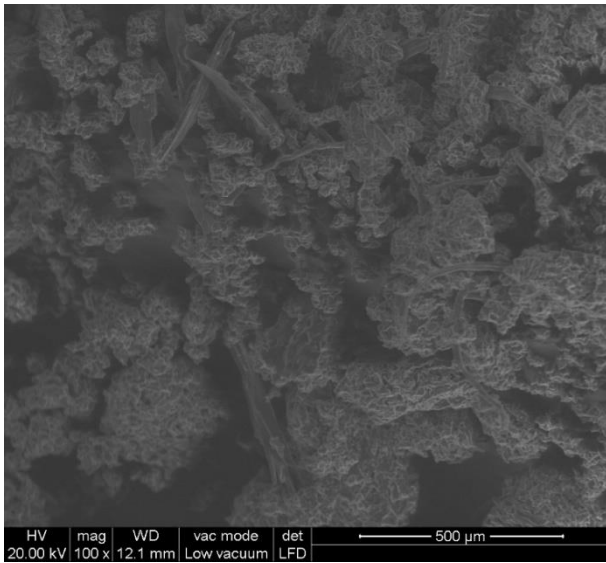

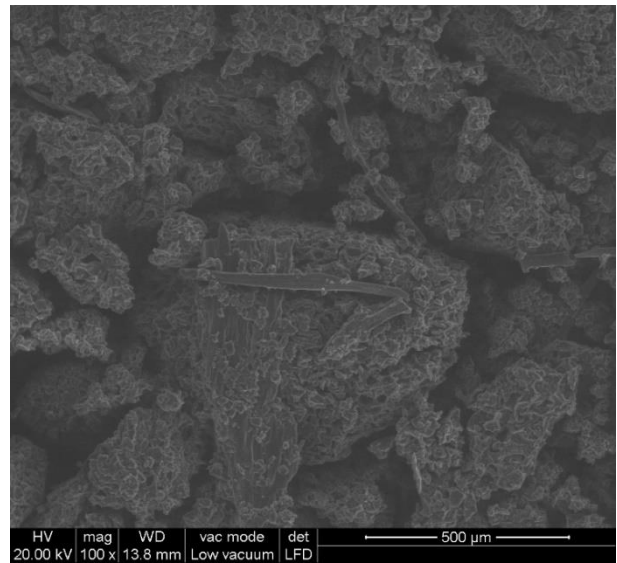*Figure 3.8 C1:1 support morphology*
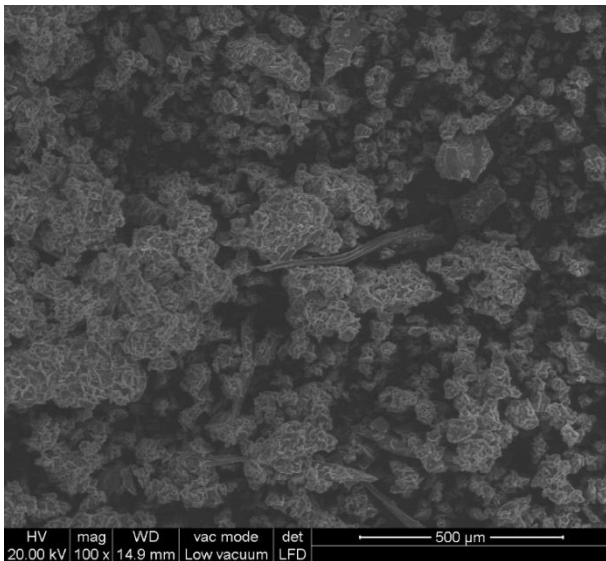

Figure 3.9 C1:2 support morphology

Figure 3.10 C1:5 support morphology

The composition by EDX resulted the same for the three samples and corresponded quite precisely to that of the initial spent coffee grounds. In the three cases it is not possible to find any trace of sodium that can be reconducted to an uncomplete washing after the treatment.

3.2.1.3   ESEM Analysis of the wooden ash-based supports

The morphological result of the ESEM analysis of the wooden ash-based supports, A1:1, A1:2 and A1:5 is reported respectively in Fig. 3.11, 3.12 and 3.13.
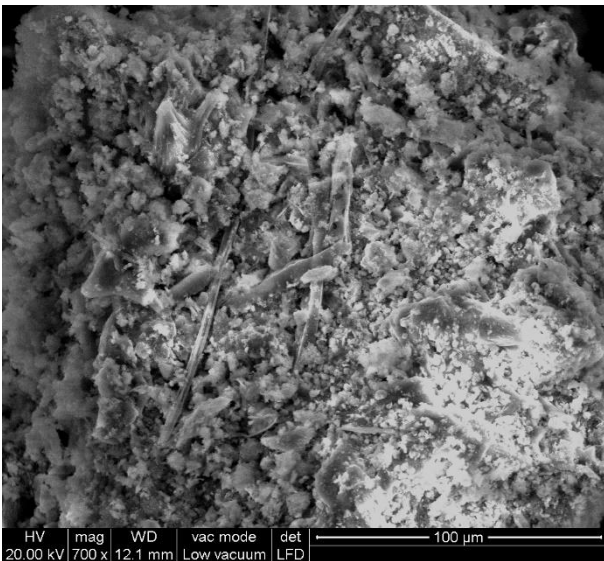
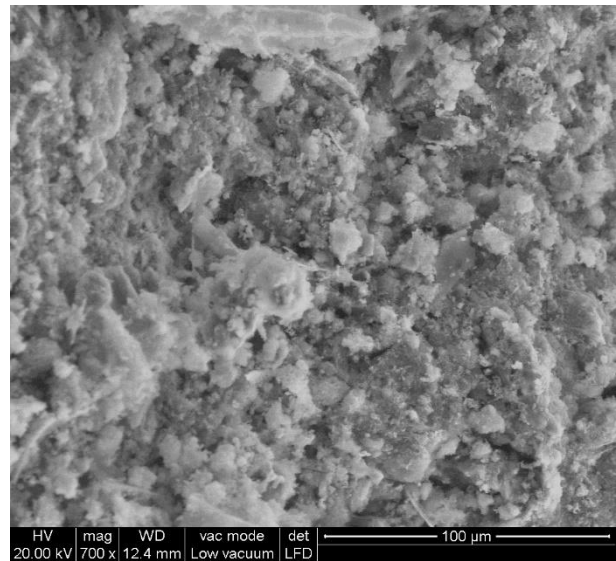Figure 3.11 A1:1 support morphology

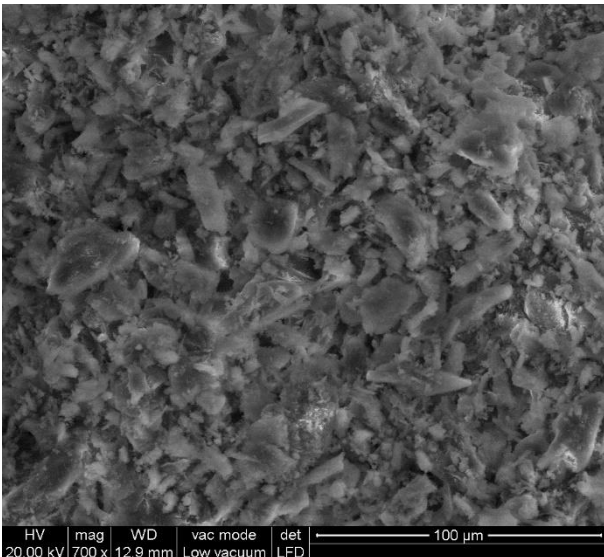

Figure 3.12 A1:2 support morphology

Figure 3.13 A1:5 support morphology

The three figures, that have been collected with the same enlargement, show very different shapes, underlying once again the difficulty of obtaining homogeneous results using wooden ash as raw material. The A1:1 sample is characterized by the presence of many toothpick-shaped corpuscles. The A1:2 sample is much more homogeneous, showing lot of corpuscles with unregular shapes. Finally, the A1:5 present lot of sharp particles. It is difficult to correlate the different shapes and the intensity of the pre-treatment with the sodium bicarbonate and the acetic acid, because of strong differences present in the sample before the pre-treatments and the local heterogeneity.

In Tab 3.3 the EDX data are reported. In the A1:1 and A1:2 some metals are present, as copper and iron, even if in small quantities.

Table 3.3 Composition of the wooden ash-based supports

Element	A1:1	A1:2	A1:5	Ash
C [%]	26.80	12.44	30.05	3.44
O [%]	53.35	61.86	51.43	64.66
Na [%]	2.03	0	5.54	0
Mg [%]	0.58	0.66	0.39	3.15
Al [%]	1.30	3.32	0.63	0.14
Si [%]	4.83	8.01	1.60	0.47
P [%]	1.29	3.25	0.57	0.53
S [%]	0.05	0.08	0.22	0.32
K [%]	0.65	1.53	0.43	1.80
Ca [%]	8.28	7.72	8.94	25.49
Ti [%]	0.20	0.26	0	0
Fe [%]	0.39	0.58	0.20	0
Cu [%]	0.24	0.27	0	0

3.2.1.4   ESEM Analysis of the spent coffee grounds-based catalysts

As for the catalysts prepared using activated spent coffee grounds impregnated with copper nitrate $Cu(NO_3)_2$, in the ratio copper salt:spent coffee ground-based support 2:100 w/w, the EDX analysis data are reported in Table 3.4. The obtained catalysts show a morphology similar to that of the corresponding supports and it is not possible to observe the metal presence from the back-scattering images, suggesting that no salt agglomerates are formed.

The composition of the catalysts obtained by deposition of copper nitrate is reported in Tab. 3.4.

Table 3.4 Composition of the spent coffee grounds-based catalyst obtained with copper nitrate

Element	C1:1Cu	C1:2Cu	C1:5Cu
C [%]	58.58	57.84	61.15
O [%]	41.22	41.94	38.72
Cu [%]	0.19	0.22	0.13

The catalysts are called as the corresponding support, with the adding of the abbreviation Cu that stands for copper nitrate. Traces of potassium have been completely removed, thanks to the washing treatment during the support creation. Only carbon, oxygen and copper are present in the catalysts. The amount of metal on the three sample is quite similar in the three cases, always between 0.10% and 0.20%. The data must be compared with the amount of copper used in the preparation, corresponding to the 0.52%. Thus, less than 50% remains adsorbed on the support.

A catalyst based on the C1:5 support has been prepared using a higher ratio between the metal system and the support of 1:10 w/w. The composition of the catalyst obtained with a greater quantity of copper salt is reported in Tab. 3.5: in terms of atomic copper the amount used was 2.63%, thus indicating that about 50% of copper used remained adsorbed on the support.

Table 3.5 Composition of the C1:5Cu1:10 catalyst

Element	C1:5Cu1:10
C [%]	60.87
O [%]	38.09
Cu [%]	1.04

To evaluate the influence of the counterion, also, copper sulphate ($CuSO_4$) has been employed as metal system instead of copper nitrate with the three different spent coffee grounds-based supports. Copper sulphate is also characterized by a lower solubility in water with respect to copper nitrate. The ratio between the metal salt and the support used is 1:50 w/w, corresponding in terms of atomic copper to 0.64%.

The ESEM analysis has been done for the C1:1solfCu and for the C1:5solfCu, based respectively on the C1:1 and C1:5 supports. Looking at the morphology, as it happened for the catalysts using copper nitrate as metal system, it is not possible to distinguish the metal deposited on the surface, not even using very large enlargements. Considering the composition, results are collected in Tab. 3.6. The analysis has been carried out with a 100x enlargement for the C1:1solfCu and with a 700x enlargement for the C1:5solfCu.

Table 3.6 Composition of the catalysts obtained using copper sulphate

Element	C1:1solfCu	C1:5solfCu
C %	59.54	61.30
O %	40.21	38.34
Cu %	0.25	0.36

The only elements present on the sample surface are carbon, oxygen and copper, as expected after the washing. The final amount of copper present on the surface of the catalysts is greater using copper sulphate, being about 50% in the case of C1:5.

$Mn(NO_3)_2 \cdot 4H_2O$ has been used as metal salt for the deposition of manganese by wet impregnation on the spent coffee grounds-based support surfaces. From the morphological point of view, there are not differences comparing the catalysts to the corresponding supports. The composition on the surface of the three samples is reported in Tab. 3.7.

Table 3.7 Composition of the spent coffee grounds-based catalyst obtained with manganese nitrate 1:50.

Element	C1:1Mn	C1:2Mn	C1:5Mn
C [%]	58.12	58.24	63.86
O [%]	41.61	41.51	35.79
Mn [%]	0.27	0.25	0.35

It can be noticed that catalysts have been completely washed to remove any trace of sodium. The amount of manganese in C1:5, by weight is about 80% of the initial one, greater than the amount of copper in the corresponding catalysts obtained with copper nitrate: the expected amount of atomic Mn is 0.44%. The difference is more pronounced for the C1:5-based catalysts. It can be excluded that the difference is due to physical reasons, considering that copper and manganese have a similar radius.

The manganese nitrate was dispersed on the C1:5 support also with a ratio of 1:10 w/w between metal system and support. The composition of the resulting catalyst is reported in Tab. 3.8.

Table 3.8 Composition of the C1:5Mn1:10 catalyst

Element	C1:5Mn1:10
C [%]	59.54
O [%]	37.92
Mn [%]	0.78
Na [%]	1.76

The amount of manganese is increased respect to the sample with the 1:50 w/w ratio, but less than expected (2.2%). Measurement errors or local heterogeneity can have influenced the result. The result shows a certain amount of sodium in the catalyst, certainly due to an uncomplete washing of the support after the treatment with sodium bicarbonate and acetic acid.

Titanium dioxide (TiO_2) has also been deposited on the C1:5 support surface. The ratio between metal system and support is 1:10 w/w. Fig. 3.14 and Fig. 3.15 show with different enlargements the morphology of the C1:5Ti catalyst.
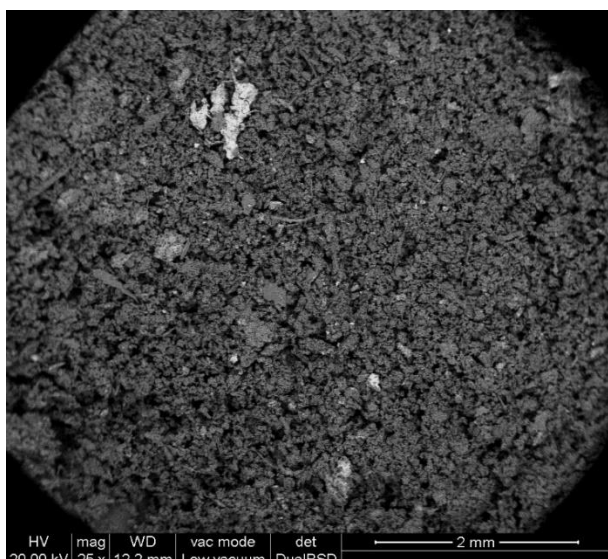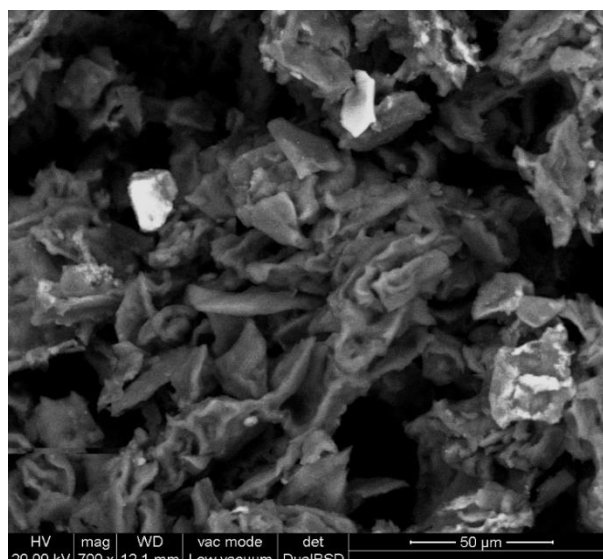
Figure 3.14 C1:5Ti morphology

Figure 3.15 C1:5Ti morphology

Considering the smaller enlargement, in Fig. 3.14, the clearer points represent the titanium dioxide blocks on the spent coffee grounds-based matrix. The sample is characterized by the presence of blocks with very different size. The sample morphology is completely different from the one of the catalysts obtained with copper or manganese salts and evidences the different dispersion mechanism in the case of the titanium dioxide. To overcome the diminution of homogeneity in the result, the sample has to be well grinded to obtain a locally homogeneous catalyst. The bigger enlargement, in Fig. 3.15 underlines the structure of the titanium dioxide crystals, that are characterized by sharp corners.

Information about the composition of the C1:5Ti catalyst are collected in Tab. 3.9.

Table 3.9 Composition of the C1:5Ti

Element	C1:5Ti
C [%]	57.40
O [%]	41.05
Ti [%]	1.55

A region with blocks of medium dimension has been considered for the analysis to obtain representative results. At first it can be noticed that pollutants or traces of sodium bicarbonate due to the pre-treatment are not present on the sample surface. The atomic fraction of titanium, once transformed in mass fraction, tells that the 5.8% in weight of the sample is composed by titanium, so about 30% of the initial titanium oxide is present on the sample.

3.2.1.5   ESEM Analysis of the wooden ash-based catalysts

Copper nitrate, in the ratio 1:50 w/w, is the only metal salt that has been dispersed by wet impregnation on the wooden ash-based supports. The heterogeneity of the raw material makes

difficult the obtainment of results with comparable properties. No aggregates of the copper salt are observed on the A1:1Cu, A1:2Cu and A1:5Cu, in the ESEM images, even using a 100x, a 700x or a 1500x enlargement. The morphology of the different wooden ash-based catalysts appears the same of the corresponding support. The comparison among the different composition is reported in Tab. 3.10.

Table 3.10 Composition of the wooden ash-supported catalysts

Element	A1:1Cu	A1:2Cu	A1:5Cu
C [%]	16.12	22.22	16.37
O [%]	58.48	54.67	58.65
Na [%]	0	0	0.26
Mg [%]	0.42	0,55	0.60
Al [%]	2.75	2.58	2.85
Si [%]	9.77	9.54	7.69
P [%]	2.17	1.60	1.96
K [%]	1.68	1.67	1.52
Ca [%]	7.00	5.55	7.99
Ti [%]	0.27	0.25	0.21
Fe [%]	0.89	0.82	1.14
Cu [%]	0.47	0.53	0.77

Looking at the table it is possible to notice that the copper fraction is relevant in the three catalysts, where about all the atomic Cu expected is present (0.53%). The copper ions might be coordinated by the alkaline groups in the ash, thus being chemically attached to the surface and not physically adsorbed into the matrix. The other components found are the same that have been found on the corresponding supports, even if the fraction changes because of the material heterogeneity and the measurement errors.

3.2.1.6 ESEM Analysis of the spent coffee grounds activated carbon-based (B) catalysts

Copper nitrate and manganese nitrate have been used as metal salts, respectively for the deposition of copper and manganese on the spent-coffee grounds-derived activated carbon in a ratio 1:50 w/w. The ESEM analysis has been carried out on both the catalysts. Activated carbon from spent coffee grounds has also been used for the deposition of TiO_2 in a ratio 1:10 w/w.

Catalysts show a morphology unchanged with respect to the raw material, that is still very porous. The EDX data are reported in Tab. 3.11.

Table 3.11 Composition of the B-Cu and B-Mn

Element	B-Cu	B-Mn	B-Ti
C %	88.74	88.44	96.54
O %	10.51	10.57	0
Mg %	0.30	0.49	0
Ca %	0.25	0.30	0
Cu %	0.20	0	0
Mn %	0	0.19	0
Ti %	0	0	3.46

Considering the common elements, B-Cu e B-Mn show very similar atomic fractions. The presence of magnesium and calcium has been evinced also in the initial activated carbon. Both copper and manganese are found in the corresponding catalyst in percentages which represent the 38% (expected atomic Cu = 0.53%) and 43% (expected atomic Mn = 0.44%), respectively.

As for TiO_2 deposition, it remained on the support in about 63% (expected atomic Ti = 5.86%).
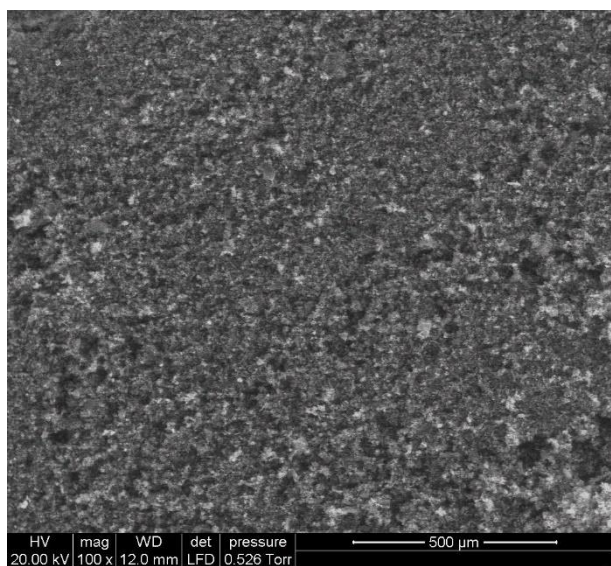
Figure 3.16 B-Ti morphology with a 100x enlargement
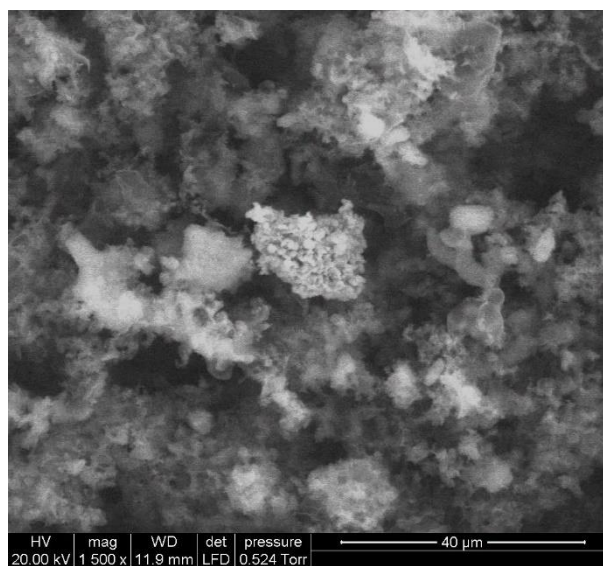
Figure 3.17 B-Ti morphology with a 1500x enlargement

B-Ti morphology is shown in Fig. 3.16 and Fig. 3.17 with two different enlargements.

3.2.1.7 ESEM Analysis of the commercial activated carbon-based (CAC) catalysts

As term of comparison with the spent coffee grounds-derived one, a commercial activated carbon has been employed for the catalyst preparation using copper nitrate and titanium dioxide as metal systems, in 1:10 ratio. Morphologies of the two samples are reported in Fig. 3.18 and Fig. 3.19.

In both cases big blocks and fine powder characterize the morphology. The raw material in fact is composed by pellets, that are partially broken during the preparation of the catalyst. It is easy to individuate the metals in both figures, because they cover wide areas of the carbon blocks. In the case of the copper catalyst the metal salt is adsorbed as agglomerates apparently well dispersed.
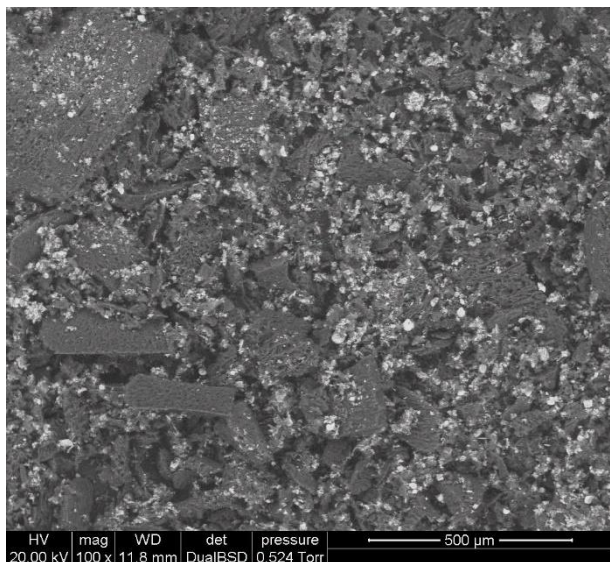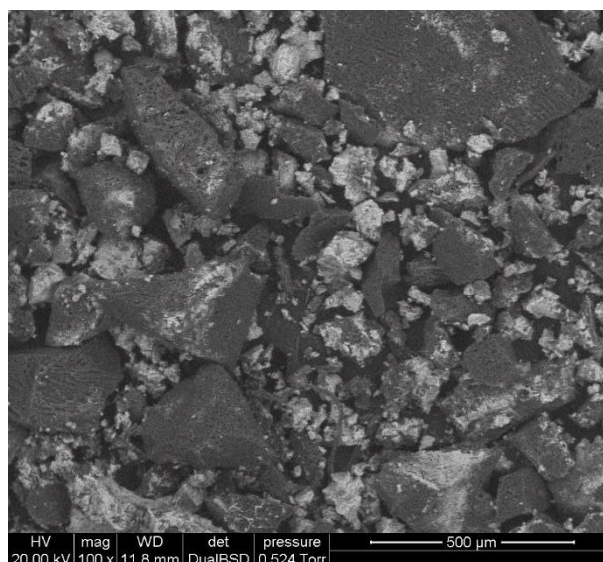

Figure 3.18 CAC-Cu morphology

Figure 3.19 CAC-Ti morphology

To consider the composition of the CAC-Cu and CAC-Ti, Tab. 3.12 can be considered, whose information are collected using a 100x enlargement. Atomic fractions are reported as percentages.

Table 3.12 Composition of the CAC-Cu and CAC-Ti catalysts

Element	CAC-Cu	CAC-Ti
C %	86.98	71.14
O %	10.67	20.08
Cu %	2.35	0
Ti %	0	8.06

Considering the two samples compositions, it can be firstly noticed that there are no impurities. Starting from an initial ratio between precursor and commercial activated carbon of 1:10 w/w, it can be seen that the ratio on the surface of the final catalyst is about 45% in the case of copper and 86% in the case of titanium.

3.2.2 FT-IR spectra

FT-IR results are presented considering separately samples derived from the same raw material. Firstly, the analyses relative to spent coffee grounds and to the supports and catalysts derived from spent coffee grounds are presented. Then, results relative to ash are shown.

All the FT-IR spectra have been collected in the range 4000 cm^{-1} and 250 cm^{-1}. Spectra can give very precise qualitative information about the functional groups present in the sample.

3.2.2.1   FT-IR of the spent coffee grounds-based samples

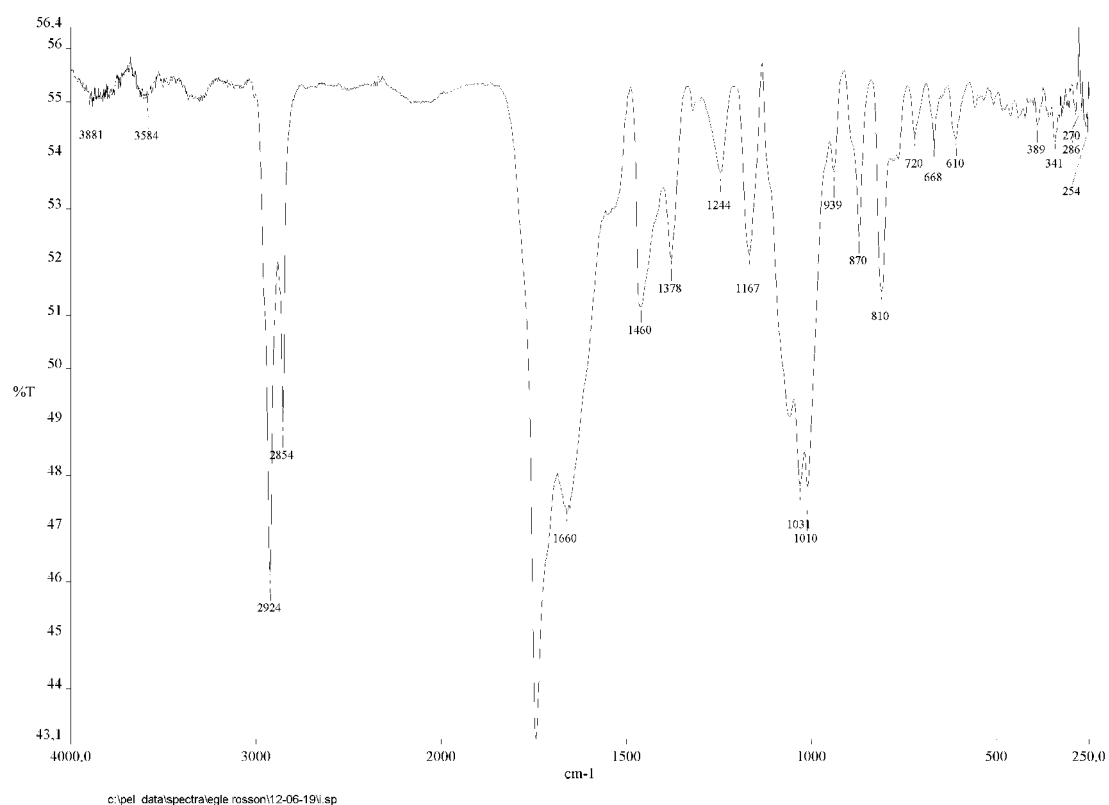In Fig. 3.20 the FTIR spectrum of the starting spent coffee grounds materials is shown.

Figure 3.20 Spent coffee grounds FT-IR spectrum

In the region 3600-500 cm^{-1} broad absorptions of –OH and –NH functional groups of carboxylic acids and amine groups in caffeine and proteins could be observed. The strong absorptions at 2924 and 2854 cm^{-1} were due to asymmetric and symmetric stretching of C-H bond in aliphatic chains of caffeine, lipids and hydrocarbons, and the band at 1440 cm^{-1} was due to the bending of the same moieties. The sharp band at 1743 cm^{-1} was attributed to the C=O absorption in aliphatic esters or triglycerides, while the band at 1660 cm^{-1} could be assigned to C=C vibration of lipids and fatty acids. The bands at 1523 and 1660 cm^{-1} could be ascribed to C=C vibration and carbonyl stretching of lignin, respectively. The bands at 1058, 1113, 1167, 1244 and 1376 cm^{-1} could be attributed to chlorogenic acids which include esters formed by quinic acid and some trans-cinnamic acids. Axial C-O deformation of the chlorogenic, caffeic and coumaric acids occurred in the range 1085-1050 cm^{-1}. The absorptions at 1446, 1378 and 897 cm^{-1} could be attributed to β-linkage in cellulose.

In Fig. 3.21, the spectra of the three activated spent coffee grounds-based supports are reported.
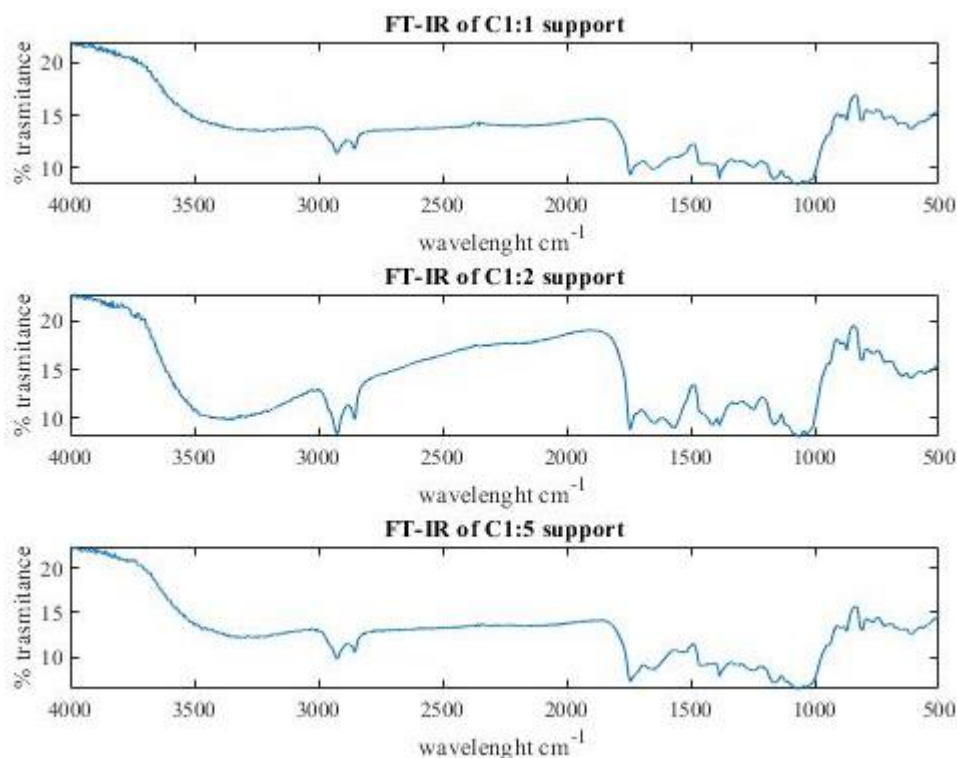

Figure 3.21 FT-IR spectra of the spent coffee ground-based supports

Starting from the top, the three figures represent respectively the spectra of the C1:1, C1:2 and C1:5 supports. They are very similar each other and are characterized by the presence of broad signals at about 3300 cm^{-1} and at 1651 cm^{-1}, indicating the presence of adsorbed water in the samples. The peaks at 2930 cm^{-1} are due to the stretching of the C-H bond. The peak at 1742 cm^{-1}, that is clearly present in the three samples, is due to the carbonyl groups of esters or aldehydes. Finally, the wide band centered at 1060 cm^{-1} indicates the presence of C-O- groups.

To observe the effect of the metal deposition on the spectra, Fig. 3.22 compares the spectrum of the C1:5 support with the one of the C1:5Ti and C1:5Cu1:10 catalysts.
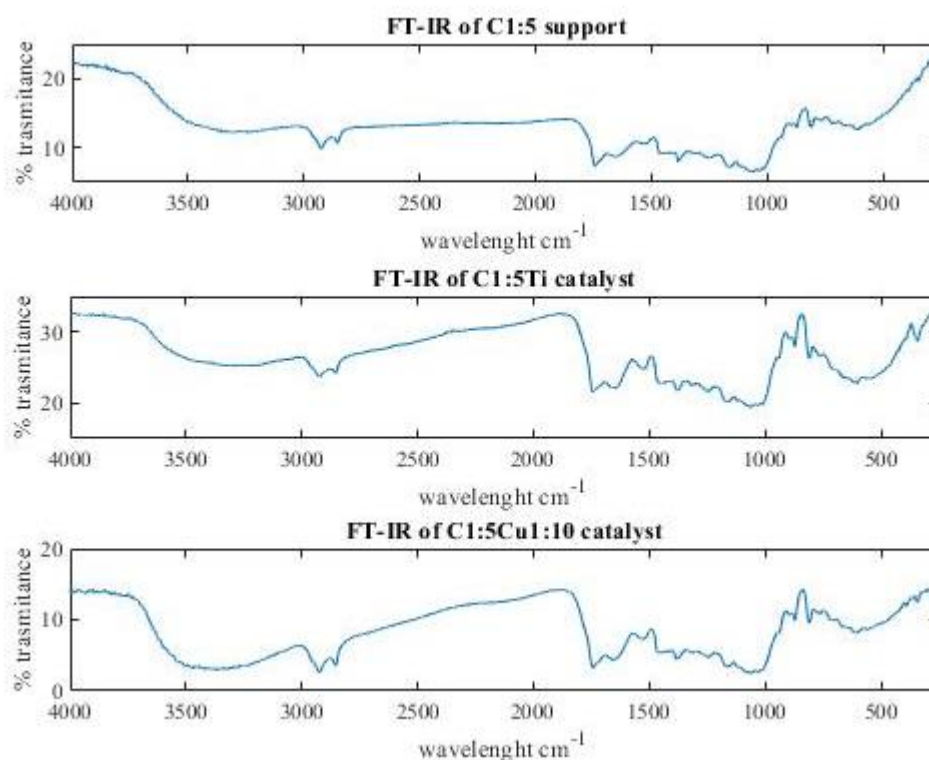

Figure 3.22 Spectra of spent coffee ground-based catalysts

C1:5Ti and C1:5Cu1:10 are obtained with a ratio between metal system and support of 1:10. By looking to Fig. 3.22 it is possible to observe that the major part of the spectra does not change between the support and the two catalysts. In the three cases, the water presence is evidenced by the peak at 1651 cm^{-1} and the band around 3360 cm^{-1}. The stretching of the C-H bond is confirmed by the peaks around 2925 cm^{-1}. The peak at 1742 cm^{-1} wavelength indicates in the support and in the catalysts the presence of carbonyl groups C=O. The C-O- group presence gave the wide band at around 1060 cm^{-1}.

Some difference among the two catalysts and the support regards wavelength between 1460 cm^{-1} and 1160 cm^{-1}, due to OH groups of alcohols. The very sharp peak at 1384 cm^{-1} in the case of the support, moves to 1378 cm^{-1} in the case of the C1:5Ti, to 1382 cm^{-1} in the case of the manganese supporting catalysts and 1377 cm^{-1} in the case of the copper supporting catalysts, reasonably due to OH groups of phenols that interact with the metal systems.

3.2.2.2   FT-IR of the wooden ash-based samples

As for wooden ash, Fourier-Transformed Infrared analysis have been carried on the initial raw material, on the three supports, A1:1, A1:2 and A1:5, and on the catalysts prepared using copper nitrate as metal system, A1:1Cu, A1:2Cu and A1:5Cu.

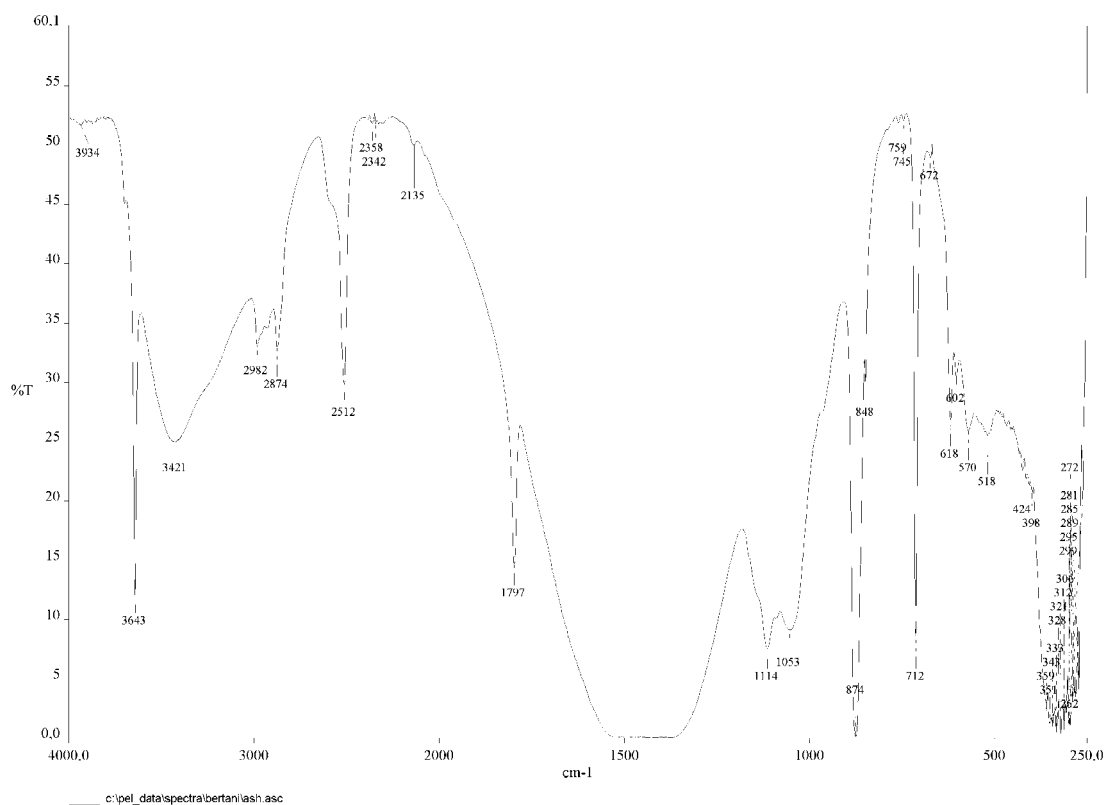In Fig. 3.23 the wooden ash spectrum is reported.

Figure 3.23 Spectrum of the initial wooden ash

Fig. 3.23 shows that the spectrum of the wooden ash is different from the one of the spent coffee grounds. The sharp peak at 3643 cm^{-1} indicates the presence of OH groups regularly distributed on the structure that are due to the presence of calcium hydroxide (Ca(OH)$_2$) present in the wooden ash. A broad adsorption band at around 3421 cm^{-1} is related to random vitrified hydroxyl groups present in the matrix. At about 3300 cm^{-1}, the spectrum presents a broad absorption due to the presence of adsorbed water, whose presence is also confirmed by a peak at around 1600 cm^{-1}, masked by other absorptions.

The peaks at 2982 cm^{-1} and 2874 cm^{-1} are due to the stretching of the C-H bonds. Comparing the peaks amplitude to the one of the corresponding peaks on the spent coffee grounds, in the wooden ash the peaks are smaller for the decreasing of the organic matter, as an effect of the combustion process. At 1797 cm^{-1} a sharp C=O peak of vinyl or aryl esters is observed

The two peaks at 1114 cm^{-1} and 1053 cm^{-1} are respectively related to the asymmetrical stretching of the Si-O bond.

The very deep bond at 874 cm^{-1}, instead, suggests the presence of carbonates. This presence is also proved by the other shard peak centered at 712 cm^{-1}. The peak at 570 cm^{-1}, even if it is small, can be explained by the asymmetrical stretching vibration of the Al-Si-O bond, confirming the presence of alumina-silicates in the initial wooden ash matrix.

Fig. 3.24 compares the spectra of the three ash-based supports.
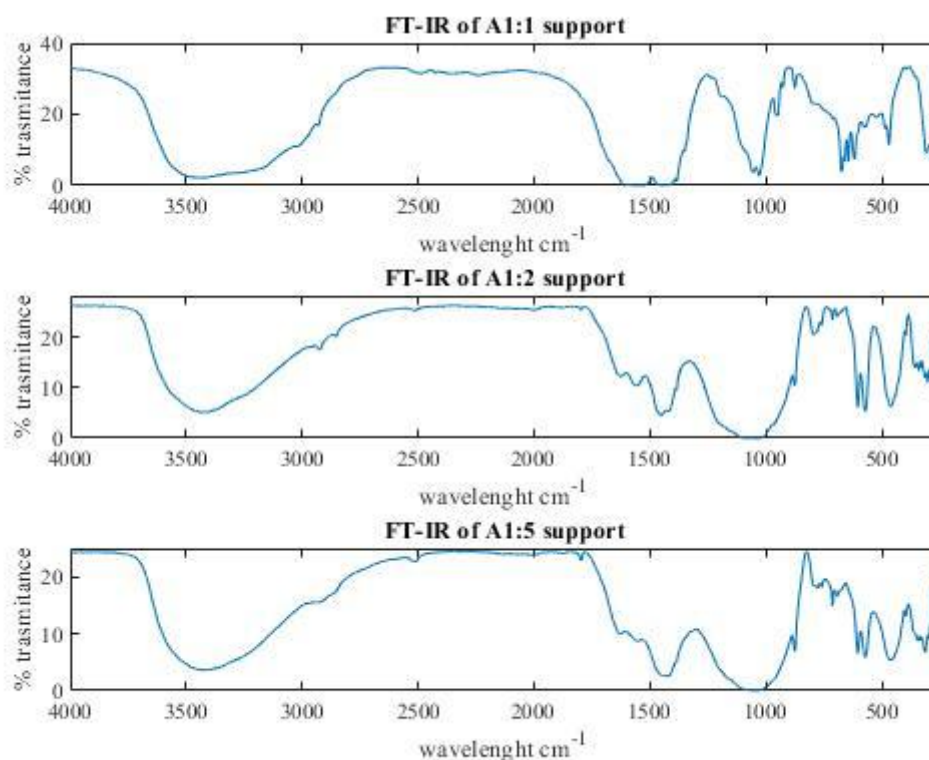

Figure 3.24 FT-IR Spectra of the ash-based supports

Confirming the heterogeneity of the wooden ash, the three spectra reported in Fig. 3.24 are very different, thus indicating that the activation had quite different effects on the ash.

The region with a wavelength between 4000 cm^{-1} and 2000 cm^{-1} is similar in the three cases, but between 2000 cm^{-1} and 250 cm^{-1} qualitative and quantitative differences are underlined in the figures. The C=O peaks disappeared in al the samples. The presence of the carbonates is confirmed in the three case by the other two peaks, respectively at 874 cm^{-1} and 712 cm^{-1}. In the spectra of the three samples peaks between 500 cm^{-1} and 450 cm^{-1} are present. These peaks are broader in the case of the A1:2 and A1:5 supports, while it is sharper in the A1:1. In the starting wooden ash these peaks are not observable so it is reasonable to consider that is presence is strictly related to the pretreatment applied for the support creation.

At this point, referring to Fig. 3.25, it is possible to understand how the deposition of the metal influences the spectrum. As example the support A1:2 and the corresponding A1:2Cu are reported in the figure.
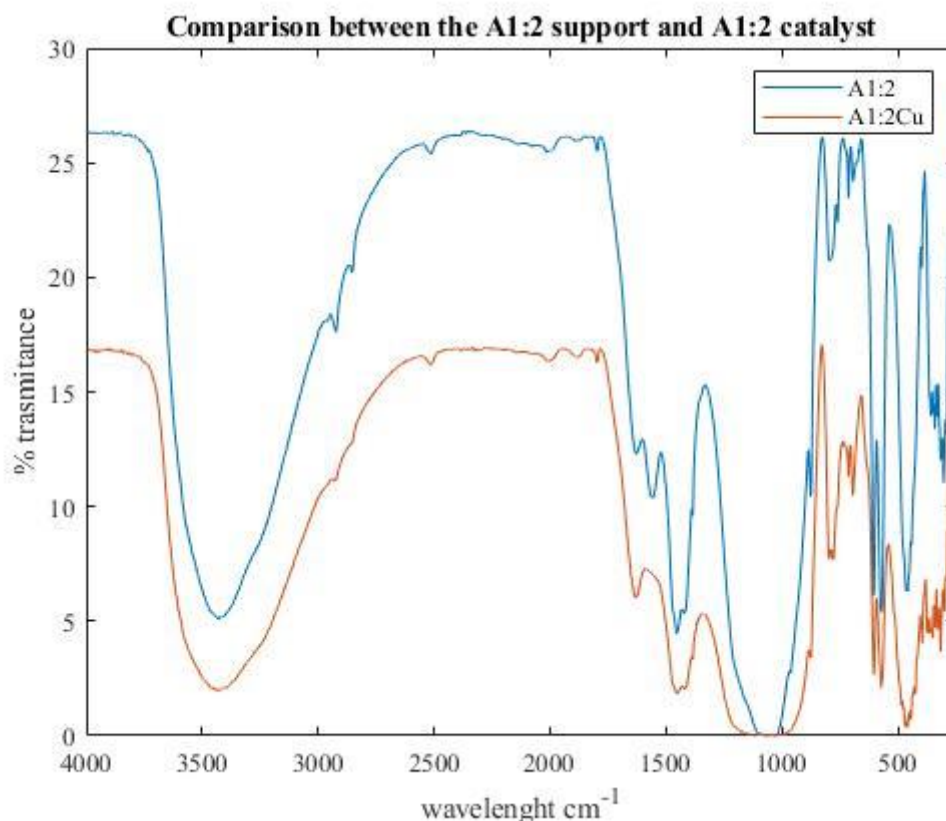
Figure 3.25 Comparison between the A1:2 support and the A1:2Cu catalyst

It is not possible to appreciate in the spectra significant differences in the absorptions attributable to specific functional groups.

3.2.3 XRD spectra

XRD technique has been applied to the three spent coffee grounds-based supports C1:1, C1:2 and C1:5. The only catalyst analyzed with the XRD is the C1:5Ti to see which is the fraction of rutile and anatase deposited on the coffee-based matrix.

The XRD technique has been applied to the ash samples to better understand the structure of the raw material. By comparing its spectrum to the ones of the supports, it would be possible to get an idea about how the pretreatment with the sodium bicarbonate and the acetic acid changed the structure.

3.2.3.1   XRD of the spent coffee grounds-based samples

The XRD spectrum of the C1:1, C1:2 and C:15 samples have been recorded. They show a very similar behavior, determined by their organic matrix. The spectra suggest that the spent coffee ground-based

supports have an amorphous structure. As an example, the spectrum of the C1:1 sample is reported in Fig. 3.26.
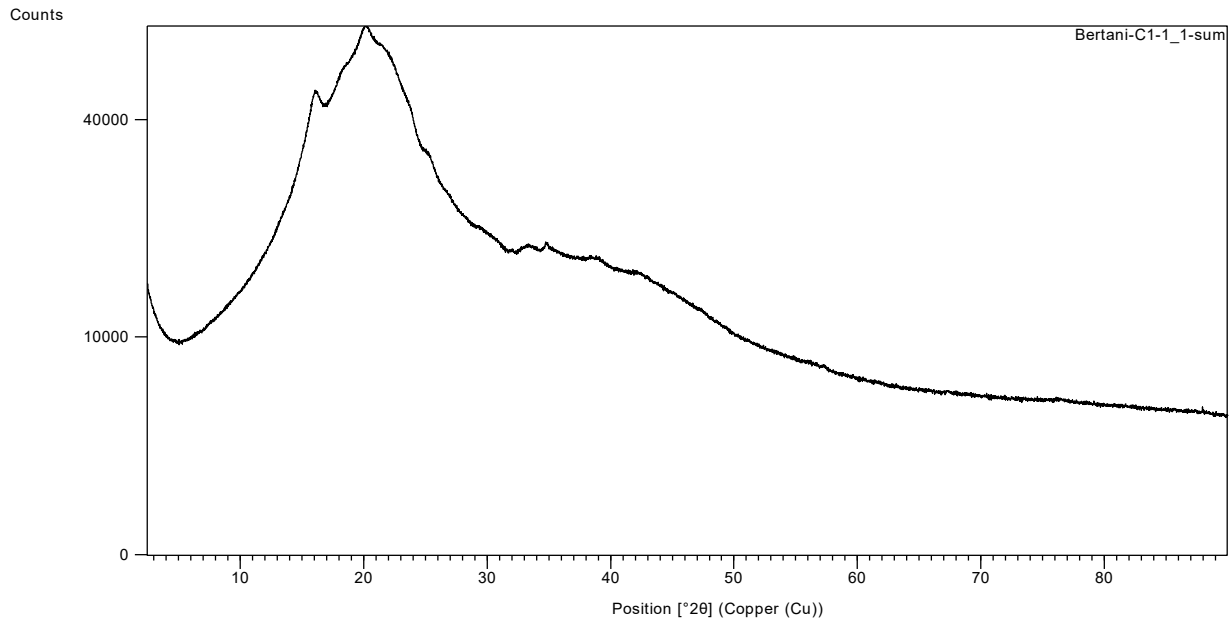

Figure 3.26 XRD of the C1:1 sample

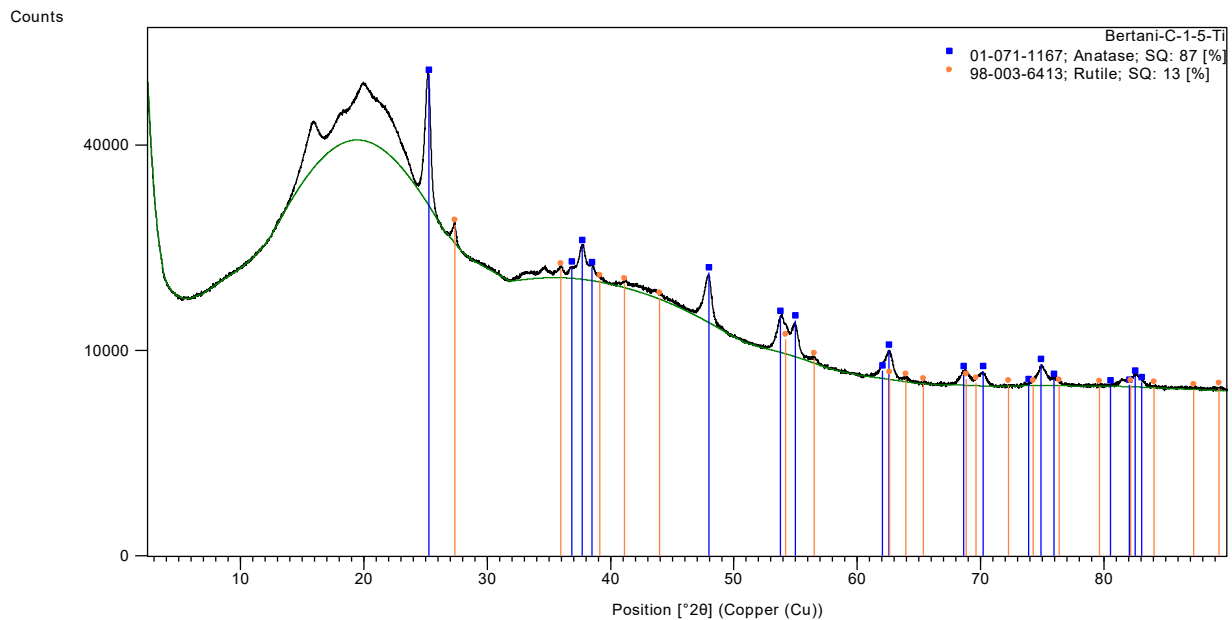Then the spectrum of the C1:5Ti can be considered. It is reported in Fig. 3.27.

Figure 3.27 XRD spectrum of the C1:5Ti sample

Considering the C1:5Ti spectrum it is possible to observe the amorphous structure of the spent coffee grounds supports, but some peaks relative to the TiO_2 presence can be distinguished. Peaks relative

to the anatase are indicated by blue straight lines, while peaks relative to the rutile are indicated by orange straight lines.

A semiquantitative analysis can be reasonably carried out because the peaks related to anatase and rutile have a similar amplitude. The result of the analysis shows that in the sample there is around the 87% of anatase and about the 13% of rutile and corresponds to the composition of the starting titanium dioxide.

3.2.3.2   XRD of the wooden ash-based samples

As for the wooden ash, the initial material has been analyzed to compare the sample with that achieved after the $NaHCO_3/CH_3COOH$ treatment. Fig. 3.28 reports the spectrum of the wooden ash.
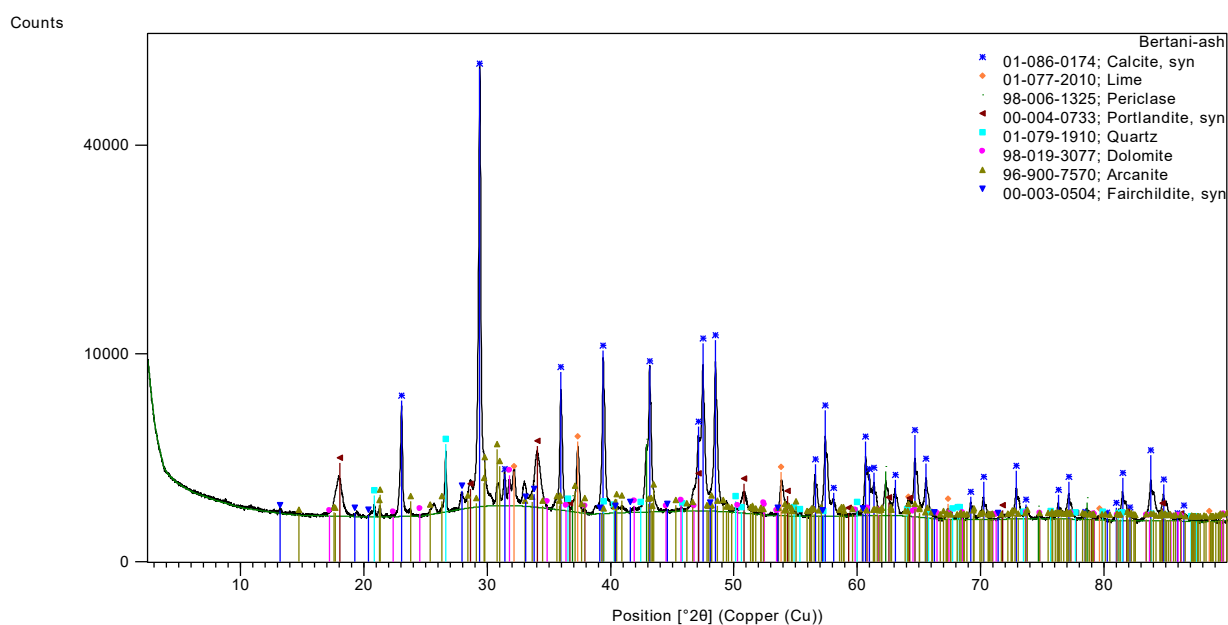

Figure 3.28 XRD of the ash sample

The spectrum underlines the heterogeneity of the wooden ash. The mineral that can be see more clearly is the calcite, that shows very sharp peaks, in agreement with the FT-IR data. Smaller peaks are very difficultly matched with the database information, but some of them can be attributed to lime, portlandite, quartz, dolomite and other minerals. Some of these minerals, as the dolomite, are often found in the lignocellulosic matrices and can be related to the ground where the trees have growth. The presence of quartz, instead, is attributed to an accumulation of dust on the tree bark, that is progressively englobed and fixed by the plant during its growth.

In this case it does not make sense to try to quantify with a semiquantitative analysis the composition, because of the very strong heterogeneity.

The different wooden ash-based supports have been analyzed and the relative spectra are reported in Fig. 3.29.
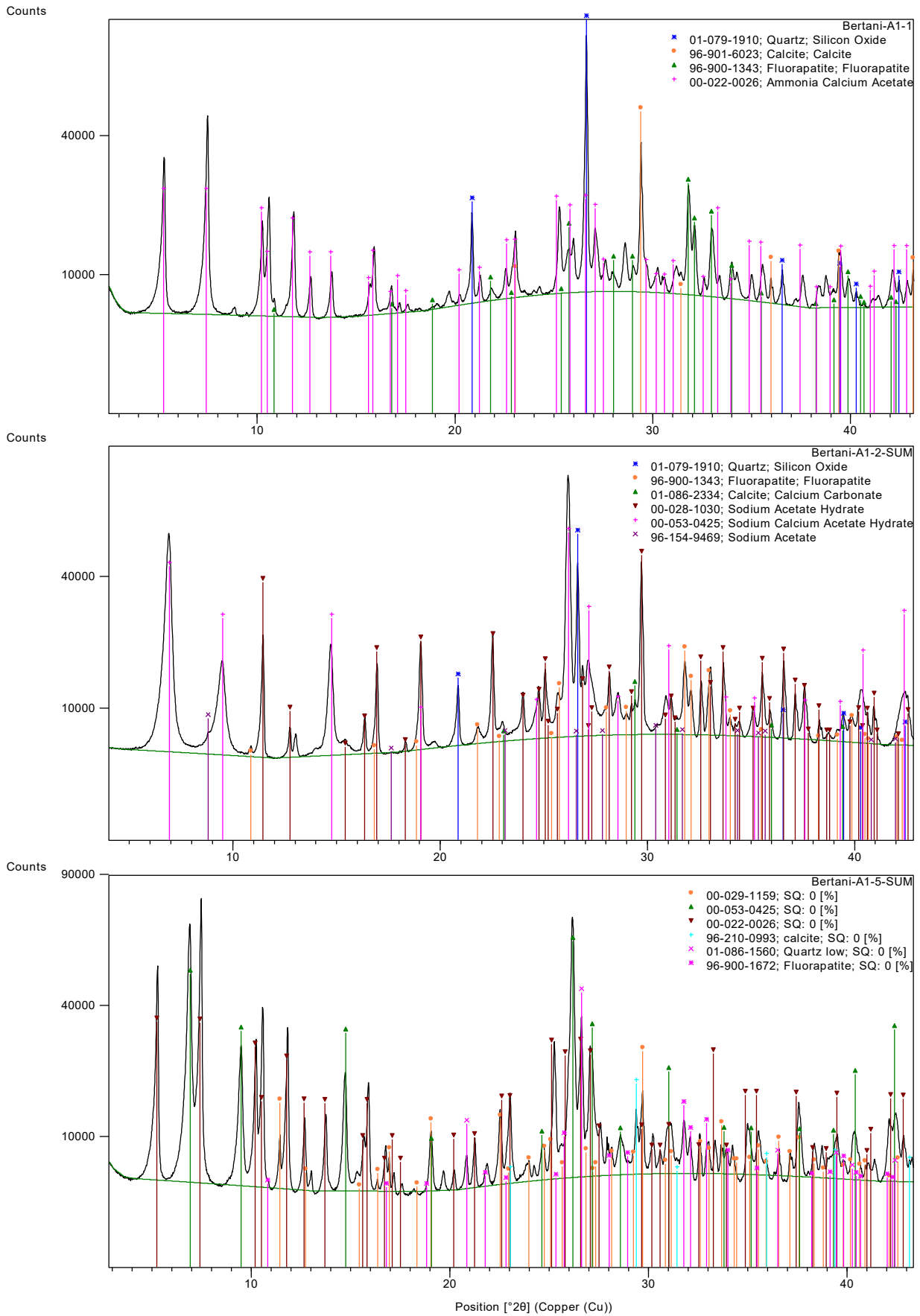
Figure 3.29 XRD spectra of the ash-based supports

The three spectra share many peaks, as for example the one relative to the quartz presence. Apatite are detected in the three samples. Comparing the data with the information available on the database, it seems that the apatite matches very well. It must be considered that the different types of apatite share similar crystallographic parameters, more specifically cells dimensions are almost the same. For this reason, the analysis is likely to confuse the different types of apatite, failing to have characteristics to distinguish them.

The effect of the treatment can be observed in the A1:2 sample, where the presence of sodium acetate, sodium acetate hydrate and sodium calcium acetate hydrate appears as the result of a reaction that has involved the sodium bicarbonate and the acetic acid.

In any case, as indicated also by the FT Spectra, the activation treatments had different effects on the wooden ash. In this thesis, due to the heterogeneity of the material, it was not furtherly used, even if the use of wooden ash as support for catalyst could be of interest, but its application deserve further investigation as for the thermal condition able to achieve reproducible materials in relationship to the starting wood. Other analytical techniques, such as Raman spectroscopy or ICP-MS analyses can help to understand the composition.

3.3 Experiments on dyes adsorption and degradation

In this section of the work some selected catalysts were tested to study their absorption and degradation capacity. For the test, solutions of organic dyes have been employed, respectively with carminic acid, rhodamine and erythrosine B.

It has been decided to exclude from the experience the wooden ash-based catalysts because of their property's heterogeneity. Catalysts prepared with the same procedure show chemical and structural properties drastically different, as underlined respectively by the ESEM analysis and by the XRD analysis. The cause of the heterogeneity is due to the initial matrix. This problem can be probably faced considering controlled combustion conditions and more severe post-combustion treatments to obtain a homogeneous raw material.

The attention has been focused on the spent coffee grounds-supported catalysts. It has been decided to develop experiments using C1:5-derived catalysts.

Experiments done using different catalysts and different organic dyes can be grouped in three sets.

The first ones concern the photodegradations promoted by TiO_2 alone, as a reference, and the TiO_2 based catalyst, C1:5Ti.

The second set of experiments aims to study the oxidative degradation with Cu-catalysts. Experiments have been run in different conditions, considering respectively only the absorption contribution, considering an oxidative Fenton-like system and trying to realize a photo-oxidative photo-Fenton-like reaction. The result of the Fenton-like reaction with Cu-catalyst has been compared with that obtained by using a Mn-supporting catalyst.

The third set of experiments studies the oxidative degradation of rhodamine and carminic acid promoted by a Fe-catalyst.

3.3.1 Photodegradation with TiO₂ alone and TiO₂ supported catalysts

a) Experiments with titanium dioxide alone

The experiments objective was to compare the degradation of organic dyes using pure titanium oxide dispersed in the dye solution with the absorption and degradation of the same dyes using a spent coffee grounds-based catalyst on which titanium oxide has been deposited.

The initial solutions considered are 200 mL of an 80 mg/L solution of rhodamine and 200 mL of a 20 mg/L solution of erythrosine B.

Firstly, experiments using TiO_2 alone have been carried out, suspending 40 mg of TiO_2 in the solution under magnetic stirring.

Experiments have been run under the UV-lamp to provide to the sample the reaction energy needed to activate titanium oxide to transform the organic dyes in degradation byproducts.

The extent of reaction can be intuitively perceived by looking at the solution change of coloration. To have quantitative information, at regular time intervals, a sample is withdrawn and examined with a UV-visible spectroscopy. The results in absorbance terms have been converted in concentration terms according to the calibration curves.

The profiles of absorbance of the rhodamine solution are reported at different times in Fig. 3.30. The absorbance has been measured in the visible range. The absorbance profiles decrease in the time. It can be observed that the form of the bell described by the absorbance profile has constantly the same
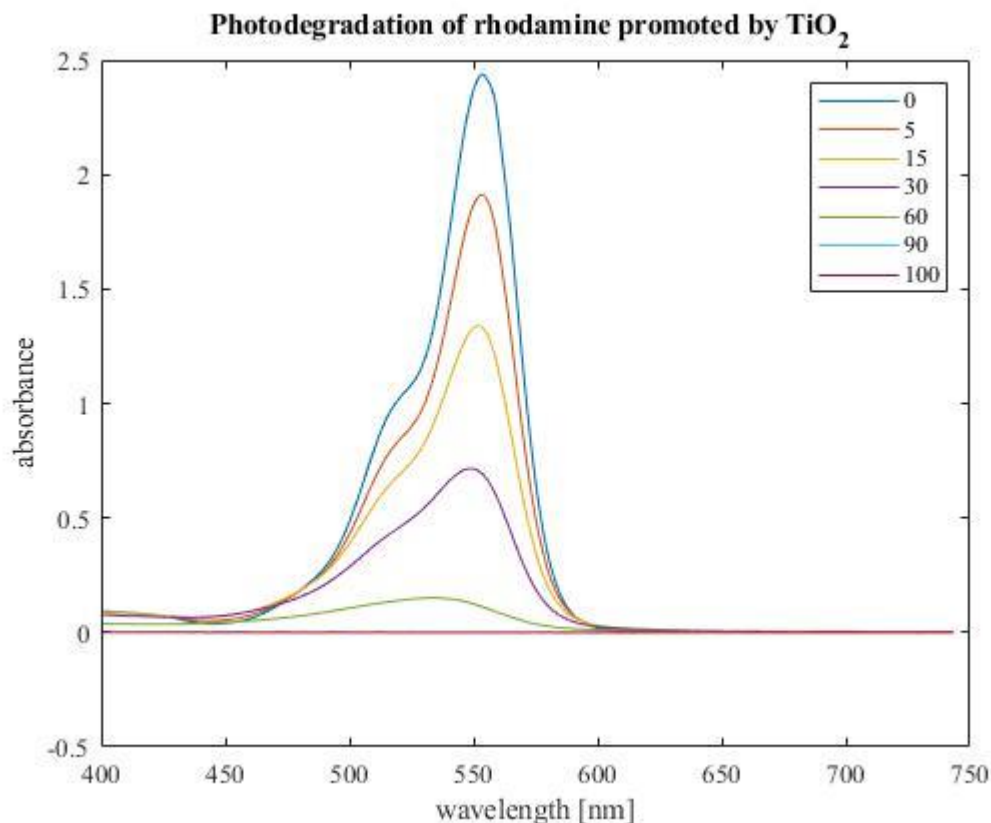

Figure 3.30 Photodegradation of Rhodamine promoted by TiO₂

shape and presents a maximum at the constant wavelength of approximately 553nm, where the Lambert-Beer Law can be applied to determine the concentration profile. in Figure 3.31 the concentration decrease calculated from the absorbance at 553 nm is reported.

The degradation profile of the rhodamine follows a very regular trend. It can be affirmed that after
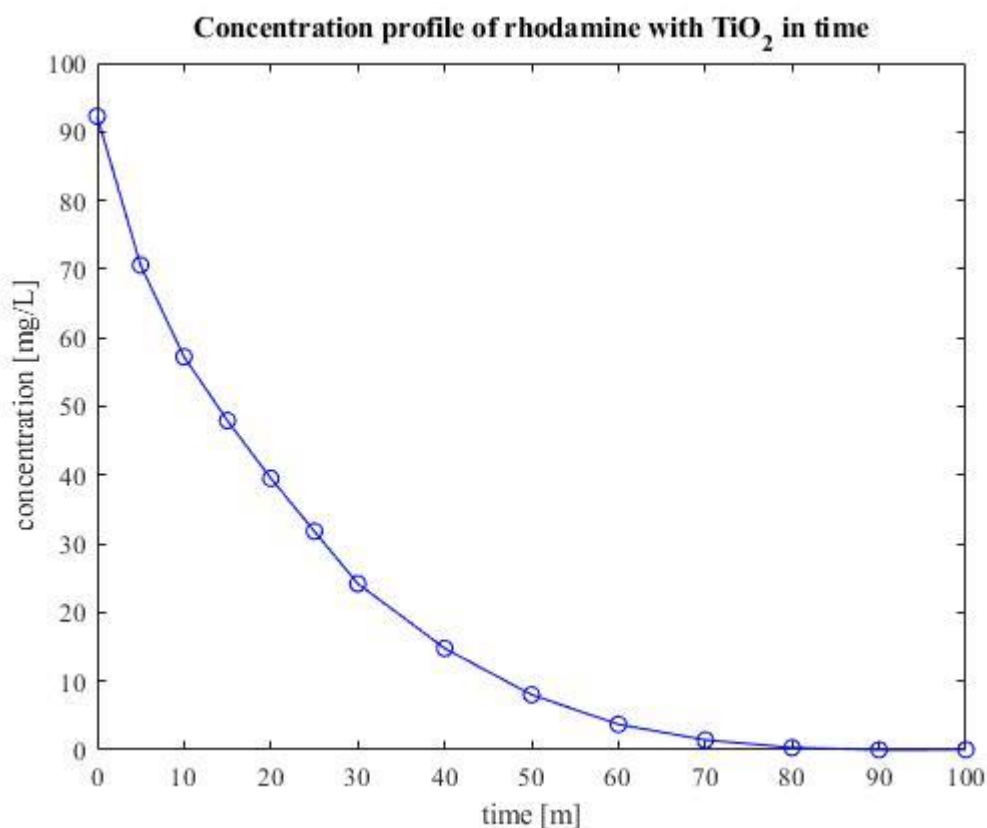

Figure 3.31 Concentration profile of rhodamine acid in time

80 minutes, almost all the rhodamine present in the initial solution is degraded. The degradation velocity progressively decreases in time. Even if we did not perform kinetic studies, the profile has been fit with polynomial function of grade 2 and grade 3 considering values between minute 0 and minute 80, when it can state that the degradation process of the rhodamine is concluded. Resulting equation and the calculated R^2 are collected in Tab. 3.13.

Table 3.13 Polynomial fitting of the experimental degradation curve of rhodamine with TiO_2

Polynomial Degree	Equation	R2
2	$y = 0.0195x^2 - 2.5702x + 84.872$	$R^2 = 0.9877$
3	$y = -0.0002x^3 + 0.0461x^2 - 3.358x + 89.051$	$R^2 = 0.9968$

A fitting with a second order polynomial is quite great, having a very high R^2, but the third order polynomial fitting is again better, having a R^2 close to 100. The kinetics of the reaction has been recently reported in detail: a new model was proposed which resembles a modified Langmuir-Hinshelwood equation: $-dC/dt = [(k_r K_S C)/(1 + K_S C^0)] = k_{app} C^0$

The initial pH of the rhodamine solution was 4.33, which is the optimal for the degradation according to the literature [74]. In our case the degradation is complete after 100 min, as confirmed by the ESI spectrum of the final solution where only noise is detected. It is to note that no organic degradation products are detected, suggesting that the degradation gave essentially CO_2, as indicated by the formation of bubbles in the final solutions.

Then, the degradation of erythrosine B was tested in the same conditions and the resulting concentration profile is reported in Fig. 3.32. Initial pH value is 6.05.
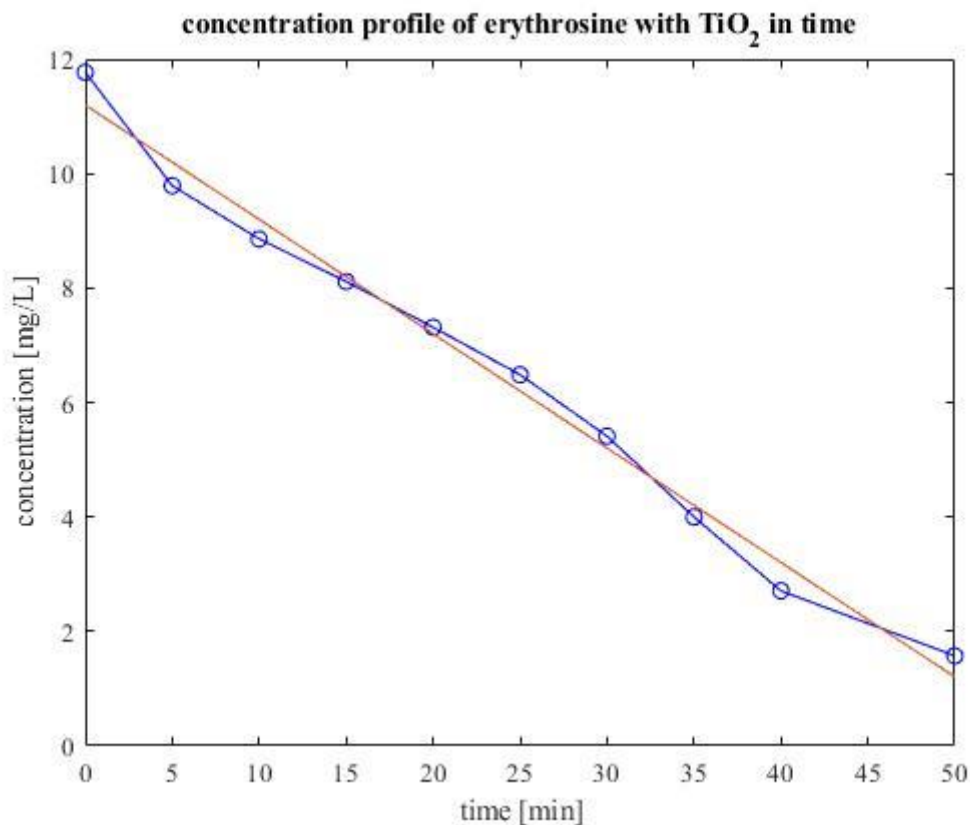

Figure 3.32 Concentration profile of erythrosine B in time

The concentration of erythrosine B decreases in time almost linearly. It is to note that apparently, the effect of the adsorption on titanium dioxide is not observed, reasonably for the its low amount. After 50 minutes the concentration of erythrosine B is not zero.

For the erythrosine B the experimental data have been fit with a first order equation, since it appears the best possible fitting. The equation and the relative R^2 are reported in Tab. 3.14. The straight line individuated by the equation has been reported in Fig. 3.32 in orange.

Table 3.14 Polynomial fitting of the experimental degradation curve of erythrosine B with TiO$_2$

Polynomial Degree	Equation	R2
1	y = -0.1998x + 11.196	R² = 0.9874

The R^2 is not very high but it can be considered acceptable considering that it is a fitting of experimental data, so many errors can affect the measurement, such as an heterogeneity factor of the sample or a different retention of the dye by the syringe filter.

It can be concluded that the rhodamine presents the fastest degradation when TiO_2 is dispersed in it. Erythrosine B degradation promoted by TiO_2 is still very fast and shows a linear profile of concentration differently from the rhodamine, indicating a different degradation mechanism.

b) Experiments with TiO₂ on C1:5

Experiments conducted with the C1:5Ti were then considered. From the ESEM analysis it can be assumed that the TiO_2 has been physically dispersed on the spent coffee ground treated matrix remaining in a quantity equal to the 1.5% as atomic fraction of the total catalyst. For this reason, in order to work with the double quantity of titanium dioxide of the previous experiments, in order to compensate some inhibitory effect due to the adsorption of the dyes on the matrix, it has been decided to employ 1g of catalyst for 20 0mL of solution and using the C1:5Ti, the dye solutions of rhodamine and erythrosine B have been tested with the same concentrations of the previous experiment.

The experiments have been run in two steps. In the first 8 hours they have been run without using the UV lamp and then the lamp has been switched on. By this way it has been possible to distingue the adsorption contribution due to the spent coffee ground matrix from the photodegradation contribution due to the TiO_2-promoted catalysis. It is assumed that the absorption process is exhausted after 8 hours.

Fig 3.33 and Fig. 3.34, respectively, show the adsorption and the photodegradation steps of the rhodamine solution in the presence of C1:5Ti.
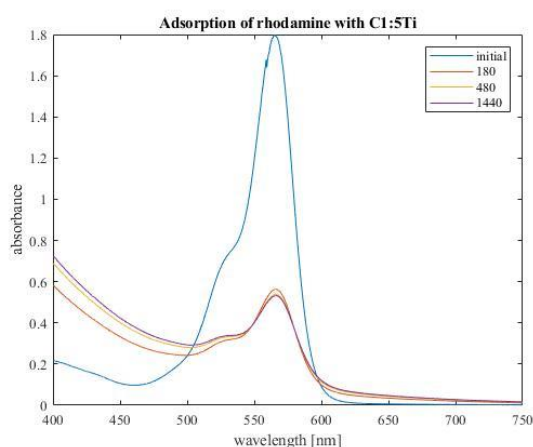

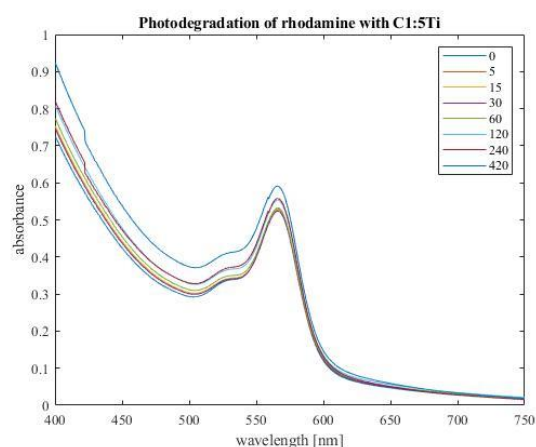Figure 3.33 Adsorption spectra for rhodamine with C1:5Ti

Figure 3.34 Photodegradation spectra for rhodamine with C1:5Ti

The figure in the left shows the absorbance profile during the absorption. It can be noticed that the adsorption effect is very pronounced in the first two hours, resulting in a high decrease in absorbance, which stops when absorbance is reduced of about 50%, thus indicating a saturation of the adsorbent capacity. Even after having switched on the lamp, the absorbance profile remains almost constant. More specifically it is possible to see, during the degradation step, a slight increase of the absorbance

in time. The reason of this behavior can be explained considering that the catalyst molecules are continuously subjected to magnetic stirring that can cause their breakage and the consequent release of some adsorbed dyes. The breakage phenomenon is quite annoying considering the catalyst recovery and reusage for many cycles.

To consider instead erythrosine B, it is possible to observe Fig. 3.35 and 3.36 for the absorption and for the photodegradation steps.
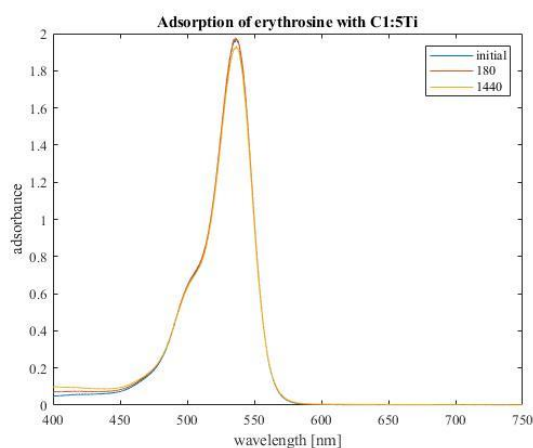

Figure 3.35 Adsorption spectra for erythrosine B with C1:5Ti
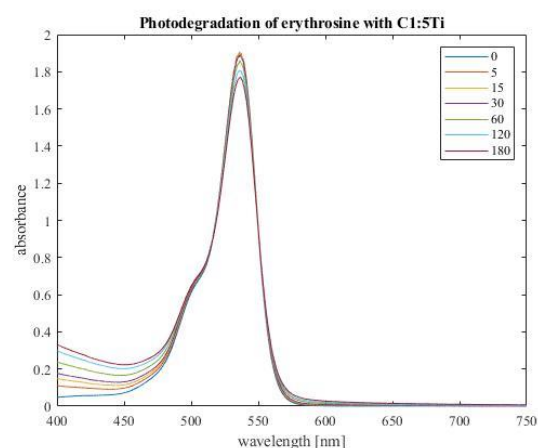

Figure 3.36 Photodegradation spectra for the erythrosine B with C1:5Ti

Fig. 3.35 and Fig. 3.36 show that the adsorption and photodegradation effects of the C1:5Ti catalyst on the erythrosine B are very small. The huge absorption effect see for the rhodamine solution in the first two hours, is not present for the erythrosine B solution and the cause can be due to the bigger size of the erythrosine B molecules. As in the previous case, considering the photodegradation plot, the same effect found for the rhodamine of absorbance increase in time is present. The explanation, as for the rhodamine, can be found considering the spent coffee grounds molecule breakage because of the magnetic stirring. In this case the ESI of the final solution is practically the same of the starting solution, showing a base peak at m/z 836, corresponding to $[M-2Na+H]^+$.

The different effect of the two dyes can be attributed also to their different polarity: rhodamine is a cationic one, while erythrosine B is an anionic one, thus the interaction with an adsorbent material could behave in an opposite way. These results suggest that the C1:5Ti catalyst has a PZC of about 5, so that when the pH of the solution is higher, negative charges arise on the surface, thus inducing a repulsive electrostatic interaction with negative dyes and an attractive one with positive dyes such as rhodamine.

3.3.2 Oxidative degradation with Cu-catalysts

Oxidative degradation experiments have been run using the C1:5Cu1:10 catalyst to degrade an 80mg/L rhodamine solution in three different experiments.

a) The first set aim is to evaluate the absorption capacity of the catalyst.

b) The second set considers an oxidative degradation of the rhodamine solution promoted by the catalyst and hydrogen peroxide, without using the UV light.

c) The third experiment tries to enhance the oxidative degradation with H_2O_2 and UV light. The hydrogen peroxide used for all the experiments has a concentration of 30% approximatively.

For the absorption experiments, a certain quantity of C1:5Cu1:10 was dispersed in the solution by magnetic stirring under UV light and the concentration of the rhodamine in the solution was evaluated at different time steps. Considering a fixed quantity of 200mL of rhodamine solution, three experiments have been run with respectively 0.5 g, 1 g and 2 g of catalyst. Fig. 3.43 shows the concentration profile for the three experiments. As expected, increasing the quantity of catalyst dispersed in the dye solution accelerates the absorption of the dye. The three experiments present after 120 minutes the same dye concentration, corresponding to 5 mg/L. The half time is similar, but the solution with 2 g of catalyst reaches the plateau at constant concentration before than the solution with 1 g and 0.5 g of catalyst.
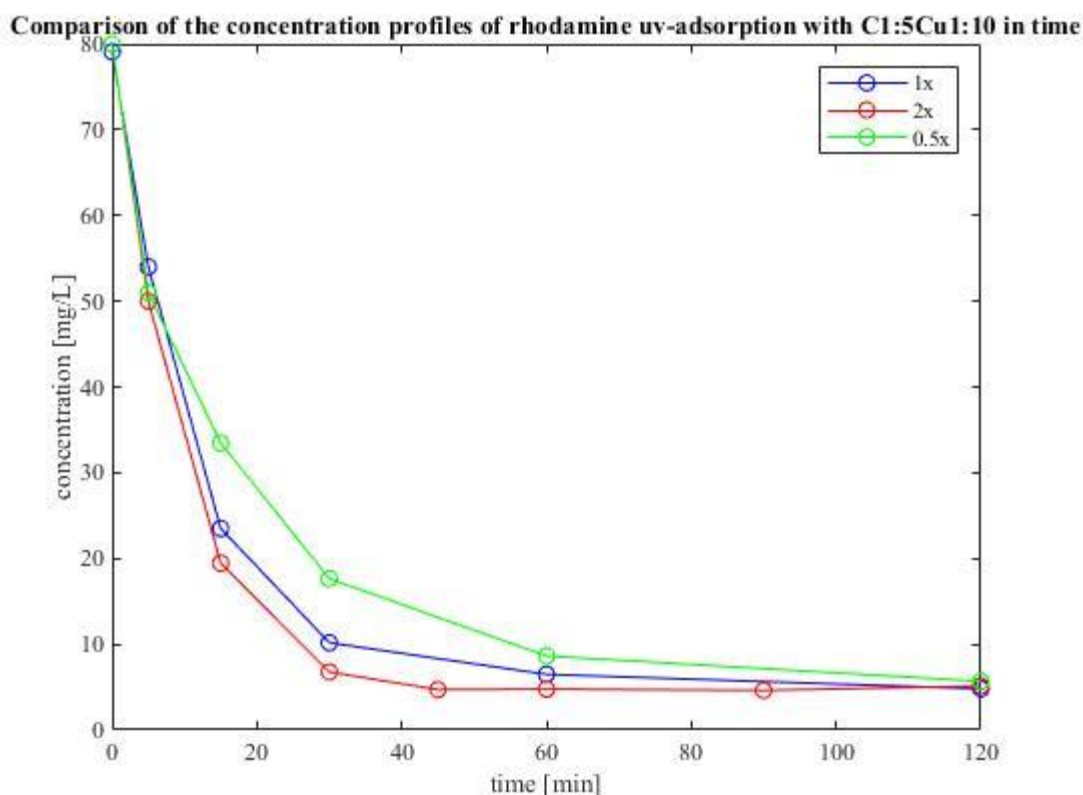

Figure 3.37 Comparison of the different concentration profiles of the absorption experiments with C1:5Cu1:10

The second set of experiments was focused on the oxidative degradation of the dye solution. The same solution with 80 mg/L of rhodamine was used in the presence of the C1:5Cu1:10. In this case a certain amount of hydrogen peroxide H_2O_2 was added and experiments were run without the UV light. Three experiments have been carried out, with 200 mL of rhodamine solution, 1 g of catalyst and respectively 0.5 mL, 1 mL and 2 mL of H_2O_2. The concentration profiles of the three experiments are reported in Fig. 3.38.
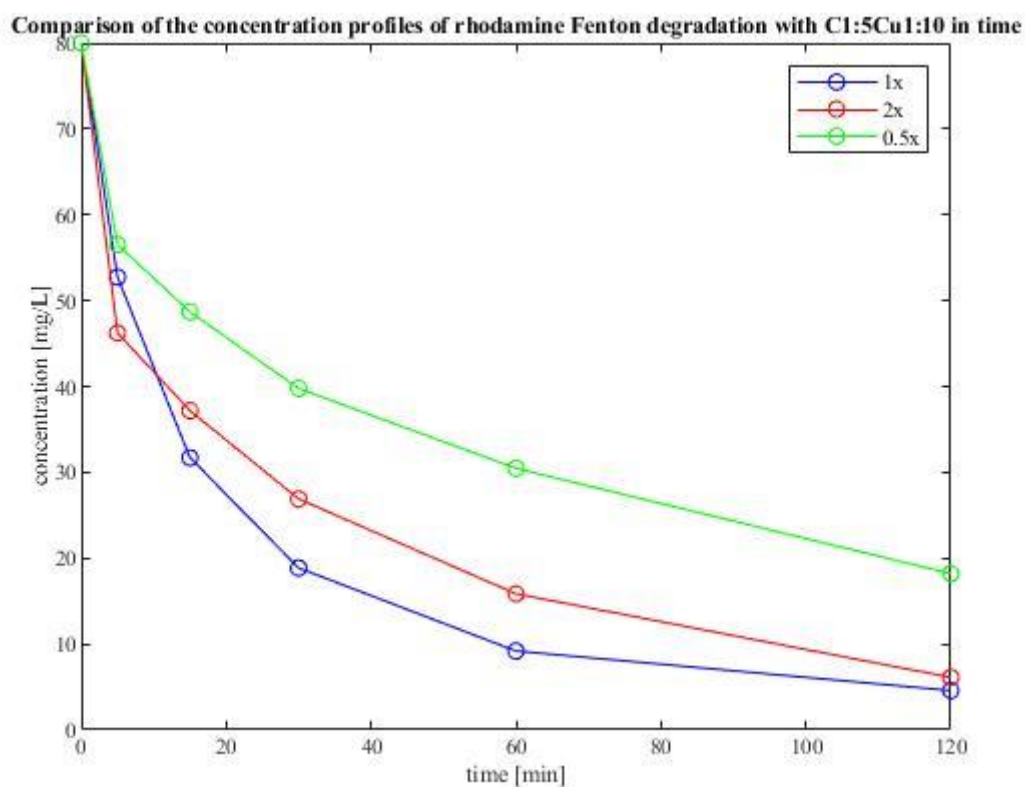

Figure 3.38 Comparison of the different concentration profiles of the oxidative degradation experiments with C1:5Cu1:10

The experiment with the smaller amount of hydrogen peroxide shows the slowest degradation and after 120 minutes has a relevant amount of rhodamine still present. The other two experiments have the same final rhodamine concentration, but they are characterized by different degradation trends. The experiment with 2 mL of hydrogen peroxide, indicated with the red line, initially has the higher degradation rate, but after 5 minutes it slows down, getting a degradation rate smaller compared to the experiment with 1mL of hydrogen peroxide.

The half-life is similar for the experiments with 1 mL and 2 mL of hydrogen peroxide, around 10 minutes, while it is approximately equal to 30 minutes for the experiment with 0.5 mL of hydrogen peroxide.

The experiment has been then repeated switching on the UV lamp. Fig. 3.39 compares experiments run with 200 mL of 80 mg/L solution of rhodamine, 1 g of C1:5Cu1:10 catalyst and with 1mL of H_2O_2. The blue line represents the oxidative degradation experiment, run with and without UV lamp while the red line represents the oxidative photodegradation carried out in the same conditions but

with the UV-light. Even if the sampling points does not exactly correspond, the degradation is clearly enhanced by the UV-light.
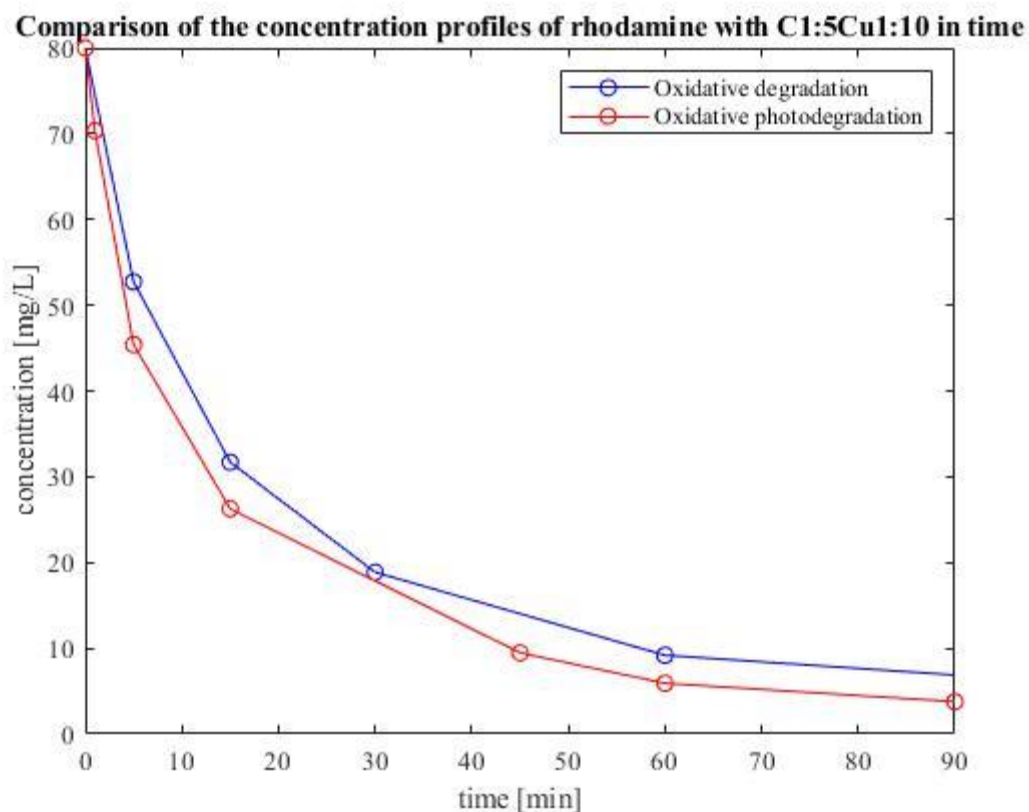

Figure 3.39 Comparison between the oxidative degradation and the oxidative photodegradation of rhodamine with C1:5Cu1:10

Finally, an experience has been carried out by substituting the C1:5Cu1:10 catalyst with the C1:5Mn1:10 one, used in the same amount. The experiment was run with 1mL of H_2O_2 and without UV light. Result is shown in Fig. 3.40, indicating with the blue line the experiment with the C1:5Cu1:10 and with the red line the experiment with the C1:5Mn1:10 catalyst. In the first 30 minutes the two experiments show the same degradation rate, and only at the end the copper-based catalyst is faster, allowing to obtain a smaller concentration of rhodamine in the solution after 120 minutes.
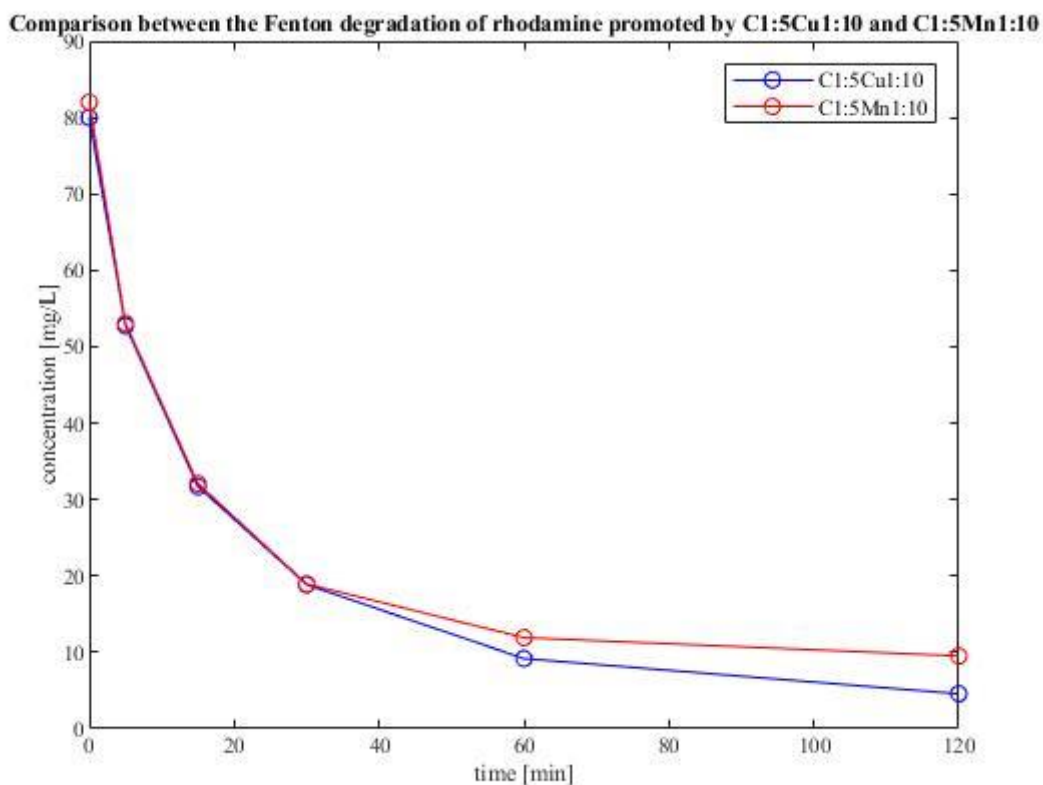
Comparison between the Fenton degradation of rhodamine promoted by C1:5Cu1:10 and C1:5Mn1:10

Figure 3.40 Comparison between the oxidative degradation carried out with C1:5Cu1:10 and with the C1:5Mn1:10

3.4 Preparation and characterization of the SGSs@Fe and CAC@Fe catalysts

a) *Preparation of the catalysts*

Two catalysts, the SCGs@Fe and the CAC@Fe have been prepared using a ball milling technique, followed by a calcination in muffle, in agreement with the experimental conditions of Li et al. [75].

The two raw materials used are respectively spent coffee grounds without any previous treatment and commercial activated carbon. They have been treated with iron sulphate heptahydrate ($FeSO_4 \cdot 7H_2O$) in a 5:2 w/w ratio for both the catalysts.

The support and the iron salt have been weighted and homogenized by mean of a pestle and a mortar. Then the powder has been separated in two parts having approximatively the same weight. Each one has been inserted in a steel cylinder. The two cylinders, containing a steel ball, have been closed and fixed in the device. At this point the device has been switched on. After 10 minutes, once the device has been switched off, the cylinders have been removed and the powder has been collected. In the case of the coffee-based catalyst, the material was quite packed, probably because of the humidity of the initial raw material and the higher susceptibility to the heating during the milling in the case of the organic SCGs matrix. For this reason, it has been quite difficult to recover the material from inside the cylinder. After the se of the cylinders for the preparation of one catalyst, before switching to a

different raw material it is important to well clean the cylinders and the ball by milling an inert sand for some minutes to prevent sample contamination.

Once the materials have been collected, they have been dried in an oven for 96 hours at 120°C. At this point both the samples still have the initial colour of the coffee and of the commercial activated carbon.

The final operation is the calcination. This treatment allows to change the oxidation state of the iron by means of heating supply: the two powders have been disposed on ceramic crucibles, previously cleaned with paper. The crucibles have been inserted in a muffle, initially at room temperature. The muffle temperature has been set equal to 300°C and it has switched off after two hours from the moment at which the required temperature has been achieved.

Once the muffle has cooled down, the two samples have been collected in glass jars. The final samples have turned they colour into red, indicating the change of the oxidation state of iron, as shown in Fig. 3.41 : in the left the catalyst from SCGs before the treatment in the muffle is represented, in the right how it appears after the treatment.
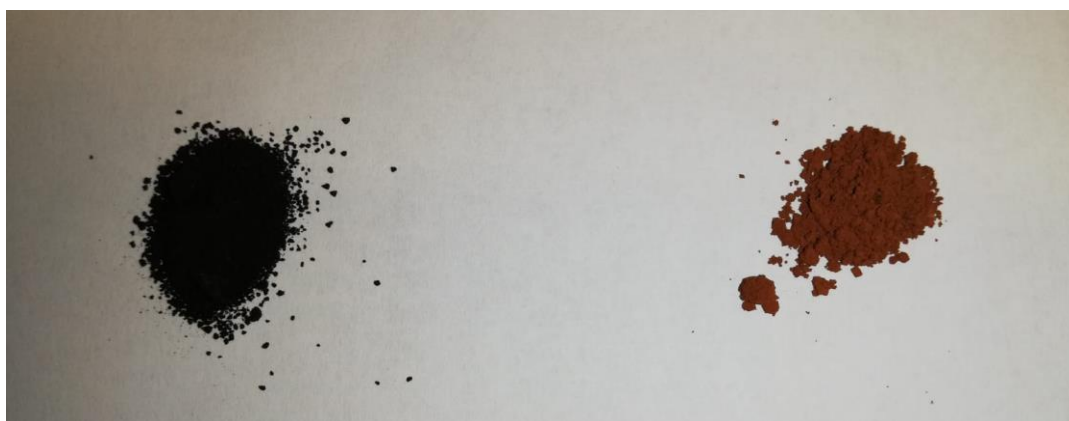

Figure 3.41 Catalyst obtained by ball milling before and after the treatment with the muffle.

Looking at Fig. 3.42 it can be seen the instrumentation for the ball milling. Inside the chamber two supports are placed on which cylinders containing the material to be treated and the ball can be disposed. The chamber is isolated by a resistant plastic box, that prevents damages in the case of accidental detachment of the cylinders from their supports. On the top a panel is disposed and allows to set the desired frequency of agitation of the cylinders and the time of the process. Usually the time chosen does not exceed some minutes to prevent an overheating of the cylinders with a possible degradation of the material processed.

The final yields of the catalysts where 15 % and 19% for SCGs@Fe and for CAC@Fe, respectively. In Tab. 3.15 the catalysts prepared by ball milling and the amount of support and iron precursor employed are summarized.
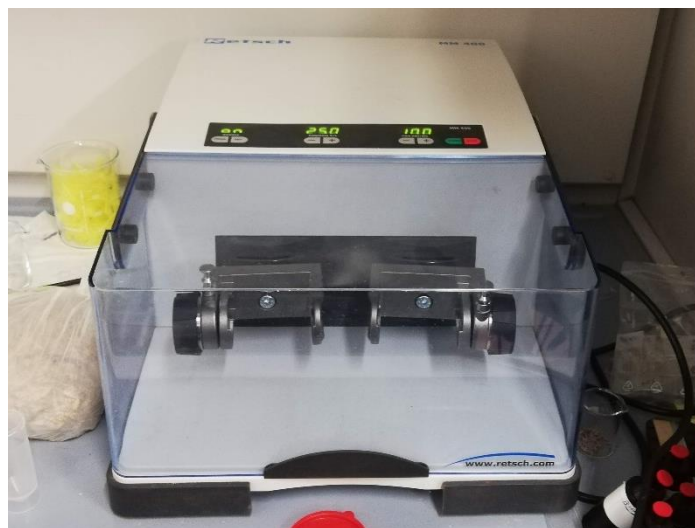
Figure 3.42 Instrument for ball milling

Table 3.15 Recapitulative table of the catalysts obtained by ball milling

	Support	**Precursor**	**Amount of Support [g]**	**Amount of Precursor [g]**
SCGs@Fe	Spent coffee grounds	$FeSO_4$	5	2
CAC@Fe	CAC	$FeSO_4$	5	2

The main purpose of this part of work is to verify the feasibility of synthesizing tar-based monometallic catalyst (but the method in principle could be applied to different metals thus achieving multi-metallic catalysts) by mechanochemical synthesis under green solvent-free conditions. Further studies will be developed in this frame, such as the investigation of the effect of different calcination temperatures, different iron salts and amounts, the presence of other metals (such as Ni, Cu, Mn or Zn) on the catalytic activity in oxidation processes.

b) *Characterization of the catalysts*

The ESEM images for both catalysts are reported in Fig.3.43 and 3.44 with a 100x enlargement.

In the case of the SCG@Fe catalyst, the morphology appears very homogeneous and the matrix seems to be porous. The commercial activated carbon catalyst seems less homogeneous, and some

carbonaceous blocks can be individuated. The matrix of the CAC@Fe appears porous. Bigger enlargements, reported in Fig. 3.45 and 3.46, show the porosity of the two catalysts.
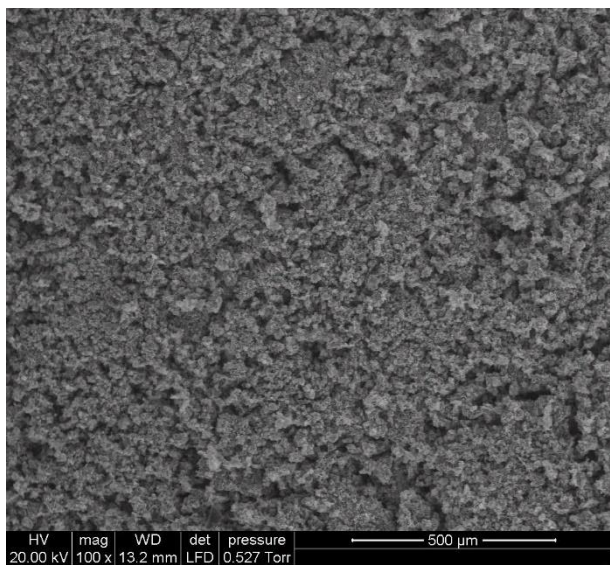

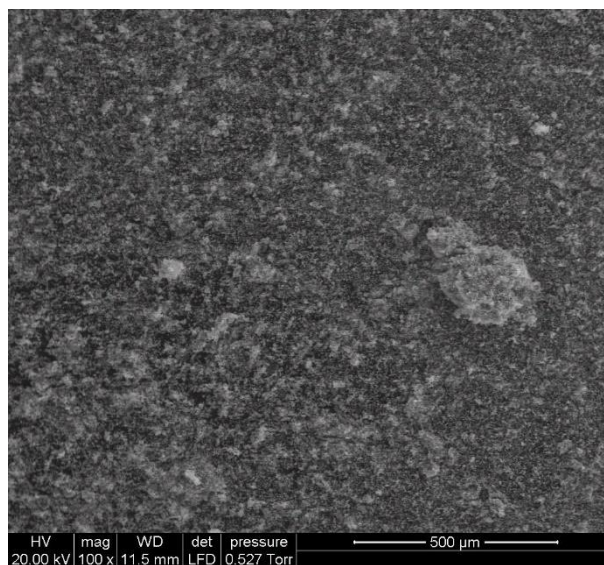*Figure 3.43 SCGs@Fe morphology with a 100x enlargement*

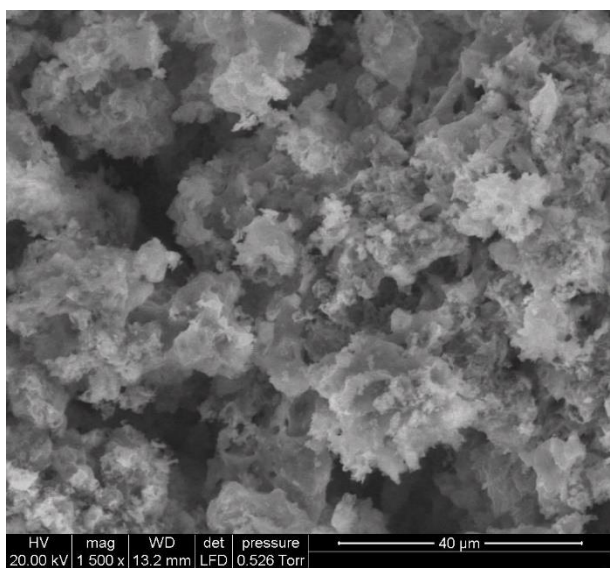*Figure 3.44 CAC@Fe morphology with a 100x enlargement*

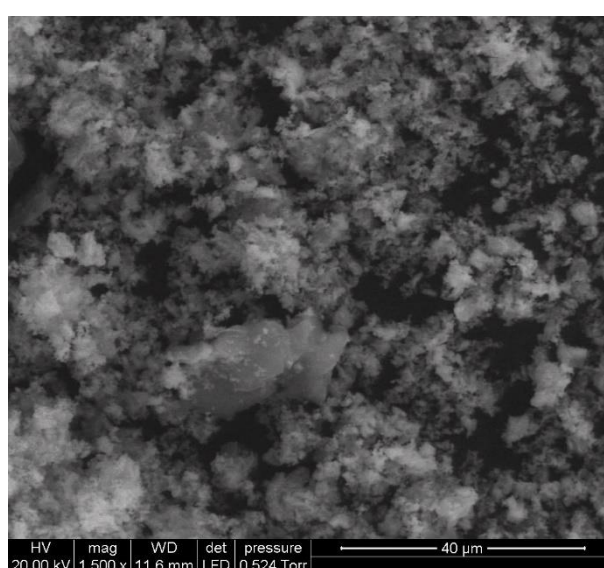*Figure 3.45 SCGs@Fe morphology with a 1500x enlargement*

Figure 3.46 CAC@Fe morphology with a 1500x enlargement

Unfortunately, we were not able to achieve a BET analysis for the two catalyst, until now. Composition of both samples, calculated considering a 100x enlargement, is reported in Tab. 3.16. In the SCGs@Fe catalyst, the carbon fraction is almost disappeared due to calcination. The iron is present in large amount, but there are other elements whose presence is hardly justifiable. Among them the most abundant one is sodium whose presence is due reasonably, to a release from the crucible. The ceramic material was impregnated with these pollutants and the cleaning operation with paper was not effective for the problem resolution. The CAC@Fe carbon fraction is larger than the

one of the coffee-based catalyst, being the commercial carbon, reasonably, previously thermally treated, thus being more resistant to calcination. Iron is represented by a large fraction and also in this case small amounts of pollutants is detected, such as sodium, aluminum and silicon.

Table 3.16 Composition of the SCGs@Fe and CAC@Fe catalysts.

Element	SCGs@Fe	CAC@Fe
C %	2.61	32.69
O %	43.25	48.91
Na %	36.79	1.99
S %	0.45	0
K %	1.30	3.01
Fe %	15.60	12.04
Al %	0	0.68
Si %	0	0.67

Figure 3.47 XPS of SCGs@Fe catalyst in the region of iron
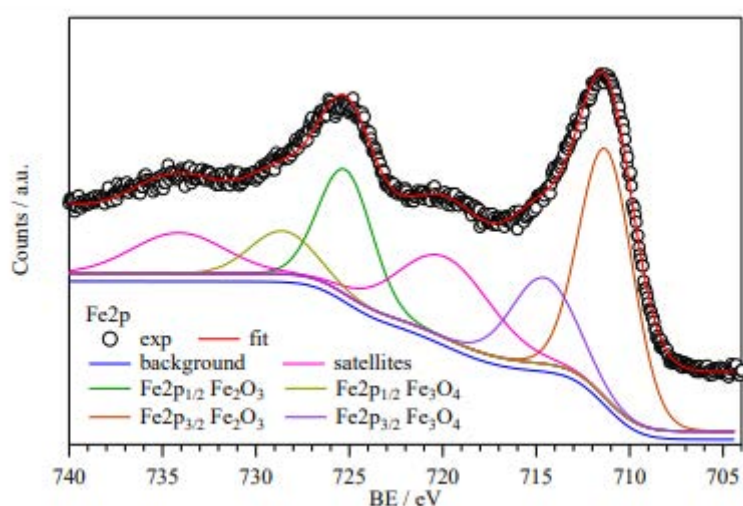
To start the characterization of the catalysts, an XPS analysis on SCGs@Fe was carried out. Fig. 3.47 shows XPS in the region of iron where the presence of different iron species can be observed.

c) *Oxidative degradations with the SCGs@Fe catalyst*

Both the degradation of the rhodamine and the degradation of the carminic acid (see Section 3.5) have been tested.

The first test was the degradation of 200 mL of an 80 mg/L solution of rhodamine. 100 mg of SCGs@Fe were employed. The catalyst has been dispersed in the solution by magnetic stirring. The solution pH was adjusted to 3.5 with the addition of a 0.1 M HCl solution. Then 2 mL of hydrogen peroxide were added and from this moment the reaction starts. After 30 minutes, 30 mg of Fe(III) were added. Fig. 3.48 shows the concentration profile for the experiment.
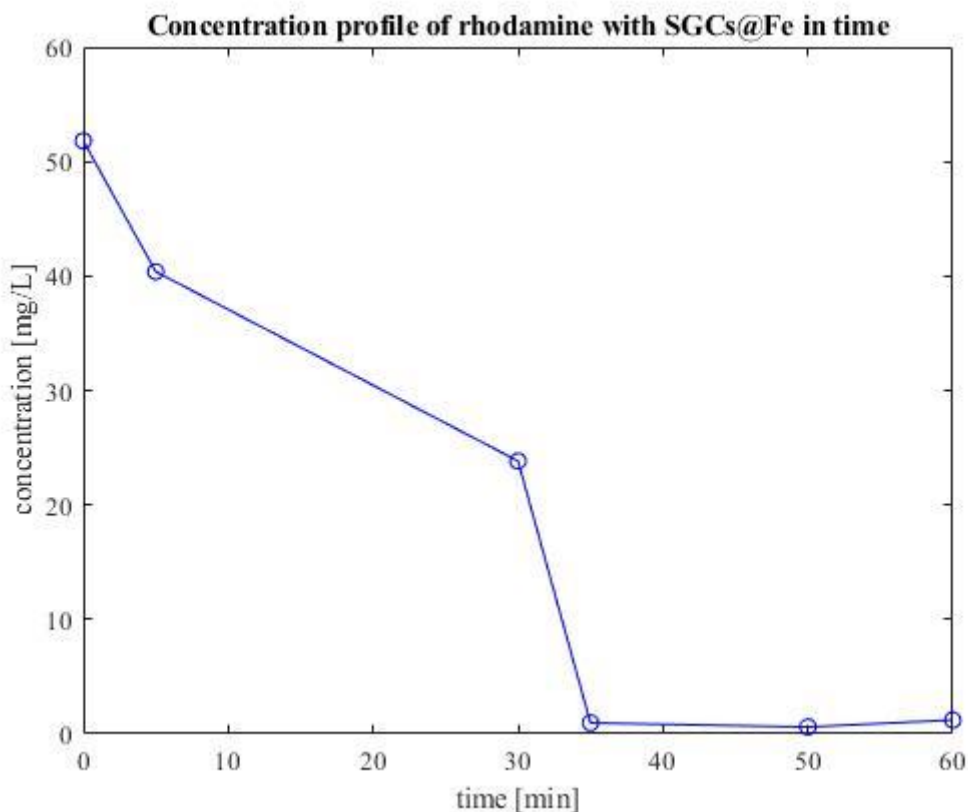

Figure 3.48 Concentration profile of rhodamine degraded with SCGs@Fe

The initial concentration does not correspond to that of the initial dye solutions because of the dilution with hydrochloric acid. The pH 3.5 is considered, on the basis of the literature [75] the optimized value to observe the catalytic activity.

Within the first 30 minutes the rhodamine concentration is reduced about of 50%. After 30 min 30 mg of $FeCl_3$ are added: immediately the rhodamine disappears.

This result suggests that a very active heterogeneous Fenton catalyst was prepared, thus confirming that it is possible to prepare catalyst with this procedure.

In traditional Fenton reaction H_2O_2 is activated by iron ions and then decomposed to generate OH· radicals. The rate determining step is considered the Fe^{3+} → Fe^{2+} reduction for OH· generation. The presence of a carbonaceous material could provide delocalized π-electrons exchange. The dispersion of catalysts particles on the surface of carbonaceous materials can also improve the hydrogen peroxide decomposition.

3.5   The case of carminic acid

Carminic acid is naturally produced by scale insects of the type cochineal (Doctylopius coccus), primarily sessile parasite native to the tropical and subtropical parts of South America, Mexico and Arizona living on cacti of the genus Opuntia. Carminic acid (CA) can be extracted from the insect's dried body and eggs and is used to produce carmine dye through the addition of aluminum or calcium. It was also synthesized with a long stepwise process [76]. The interest for carminic acid derived from the fact that carmine is widely used as a natural coloring food additive (approved by FAO and WHO expert's committee), in drugs and cosmetics and in lake pigments.

E120 is the red dye extensively used in food. It comprises the whole family of cochineal red, such as carminic acid, carmine and amino-carmine [77].

A serious issue in food and beverage products is represented by degradation of the food additive promoted by sunlight irradiation which depends also from the other ingredients present, from which many compounds can be formed, some of which potentially dangerous.

The molecule contains an anthraquinone ring linking with a glycosyl group by C-C bond as shown in Fig. 3.49.
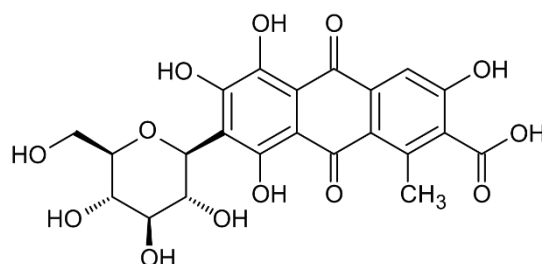
Figure 3.49 Structure of the carminic acid molecule

Despite its relatively high chemical and biological stability, the use of it as colorant or additive is controlled by laws and regulations because of its potential risk to human health.

Carminic acid possesses a variety of biological activities:

- Carminic acid interaction with DNA was reported forming intercalation complexes and was studied under different experimental condition and through different biological tests. Carminic acid has been reported to possess antitumor activity, but the presence of a sugar unit seemed to reduce the cardiotoxicity associated to anthracyclines [78].
- Carminic acid was demonstrated to have an antioxidant effect to protect DNA and

erythrocytes against radical induced oxidation [79].
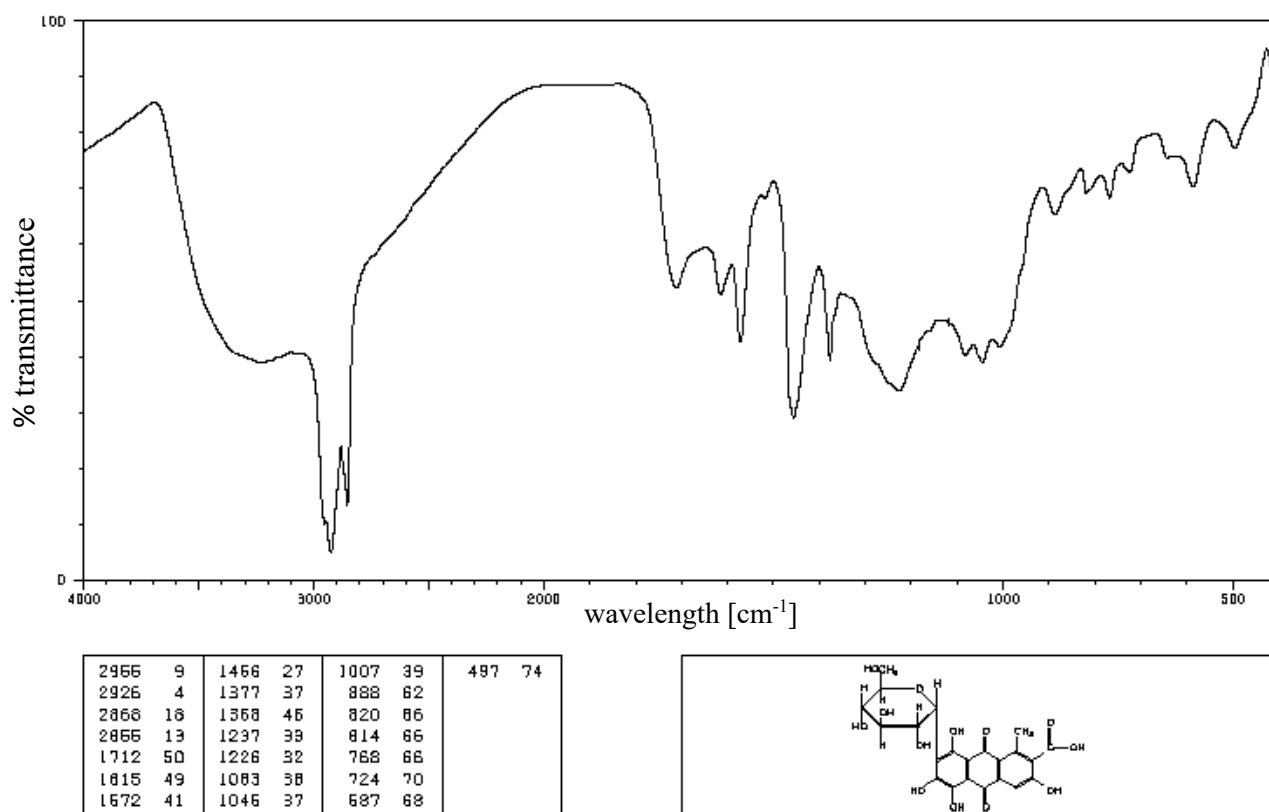

2966	9	1466	27	1007	39	497	74		
2926	4	1377	37	888	62				
2866	18	1368	46	820	66				
2866	13	1237	39	814	66				
1712	50	1226	32	768	66				
1615	49	1063	38	724	70				
1672	41	1046	37	687	68				

Figure 3.50 FT-IR spectrum of the carminic acid

In the FT-IR spectrum is reported in Fig. 3.50, a broad absorption at about 3300 cm^{-1} due to the n(OH) can be observed, together with signals at 2966 and 2866 cm^{-1} of the n(CH); at 1712 cm^{-1} of the n(C=O); at 1460 cm^{-1} of the d(OH); in the region 1450-1400 cm^{-1} of the d(CH)+d(OH); at 1300 cm^{-1} of the d(OH).

Carminic acid is a molecule with several acidic centers: in water it is considered tetraprotic or pentaprotic. The formation of deprotonated forms of carminic acid at a given pH is coupled with an intense color change from yellow – orange (pH=2) to violet to pH =12.

Figure 3.51 Carminic acid solution coloration at different pH values

Considering a carminic acid solution with an initial pH of 3.5, the pH has been changed adding the SCGs@Fe catalyst to 9, then it has been reported to 6 and finally to 3.5 with a hydrochloric acid

solution. The different coloration of the carminic acid varying the pH are represented in Fig. 3.51. The fourth cuvette appears clearer respect to the first one, but it is mainly due to the dilution effect caused by the hydrochloric acid addition. The absorbance profile is reported for the four samples in Fig. 3.52.
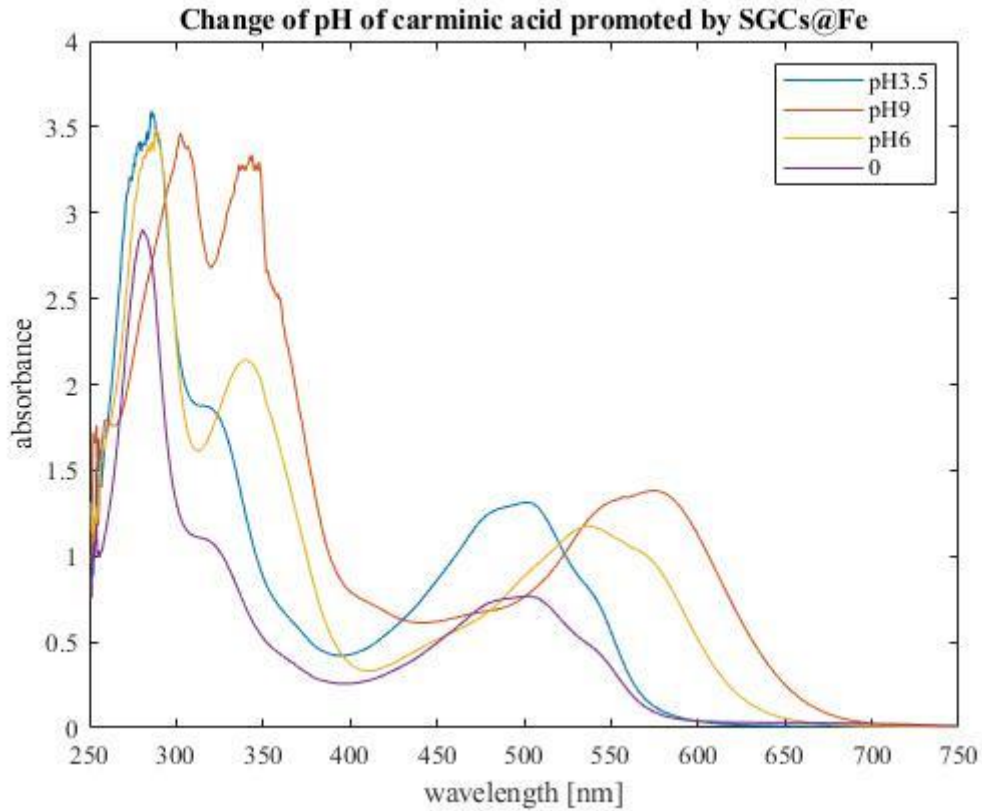

Figure 3.52 Absorption profile of carminic acid solution at different pH

Comparing the final profile, indicated as "0" with the initial curve, having a pH of 3.5 it can be seen that the curve profile is the same, even if the dilution effect causes an attenuation of the absorbance value.
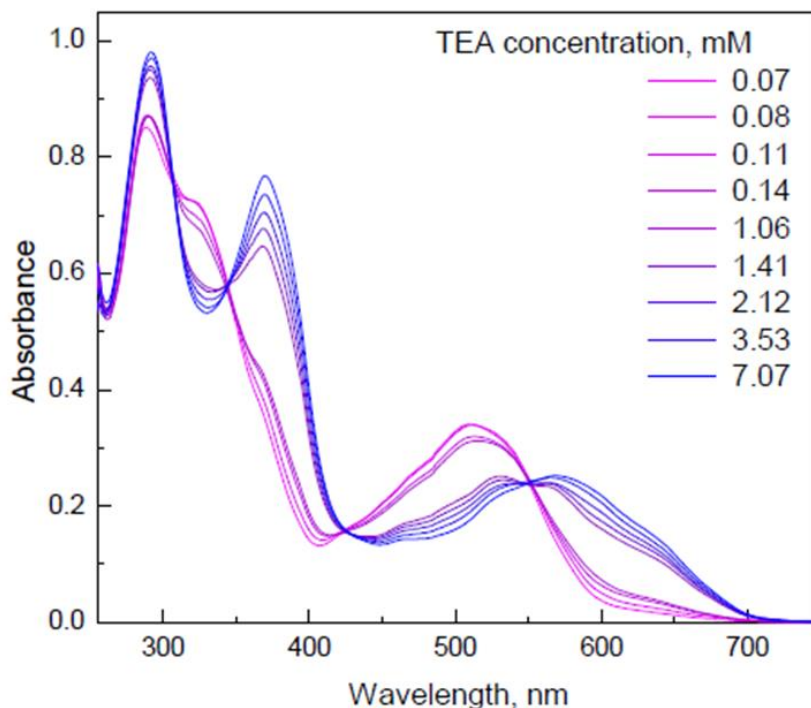
Figure 3.53 Carminic acid titration with triethylamine

Fig. 3.53 shows the carminic acid titration with triethylamine. The first deprotonation involves the carboxylic group (λ_{max} 504 nm), then the gradual deprotonation of the OH group in position 6 (λ_{max} 535 nm); then the OH in position 3 (λ_{max} 567 nm), then the OH group in position 8 [80].

*Figure 3.54 Tautomers of carminic acid: : 9,19- **I**; 1,4- **IV**; 1,10- **II** and **III**; 2,9- **V** and **VI**; 1,7-**VII**; 1,2- **VIII**.*

CA exists as an equilibrium mixture of 9,10-, 1,4-, 1,10-, 2,9- and 1,7-anthraquinoid tautomers to which λ_{max} have been assigned, according to quantum-chemical studies and to the corresponding anions [81].

Table 3.17 λ_{max} of the carminic acid tautomers in different media
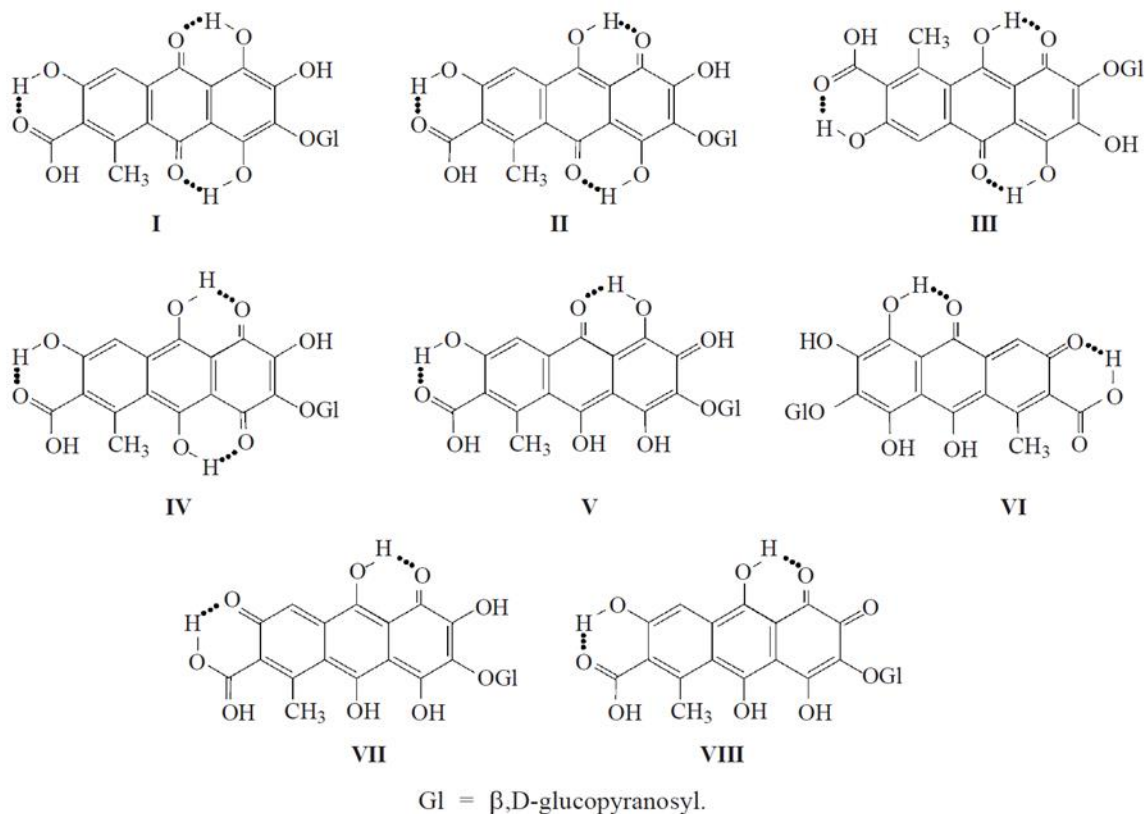
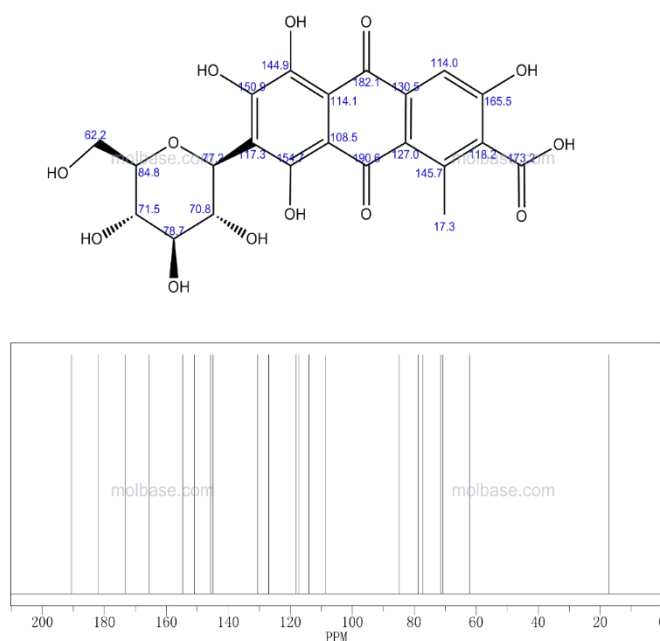| Medium	λ_{max} [nm]					
	I	IV	VI	II	VII	V
Water, pH 2		490				
Water, pH 2.4			500			
Water, pH 4		490				
Water, pH4+ Be(II)				530		580
Water, PH 5			500			
Water, pH 5.5				530		
Water	469		497	533		
Water			500	540		
Water					560	
Ethanol	470.7		499.2	535.7		
Methanol		491		540 sh		
λ_{calc}, [nm]	477	498	504	539	562	579

Figure 3.55 ^{1}H NMR of carminic acid in CDCl$_3$.

^{1}H NMR of carminic acid in CDCl$_3$ is reported in Fig. 3.55. In Fig 3.56, the ^{13}C NMR spectrum of carminic acid is reported
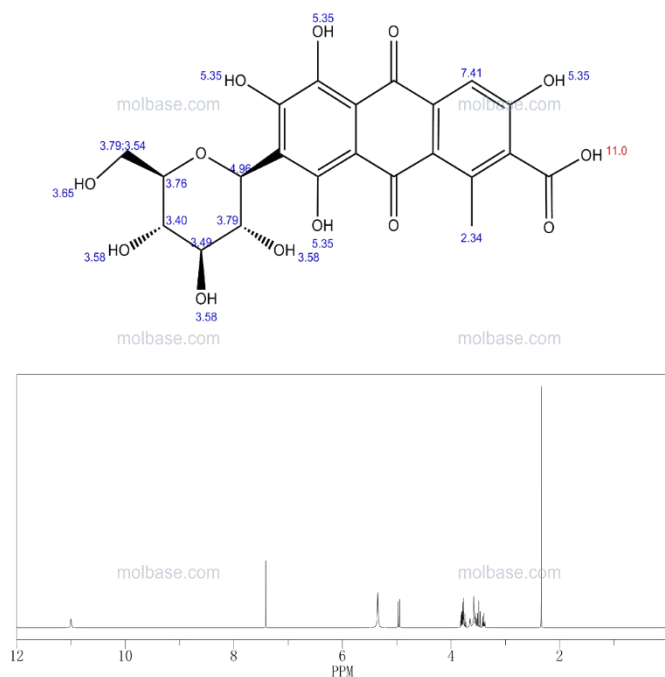
Figure 3.56 ^{13}C NMR spectrum of carminic acid.

We studied the degradation of carminic acid in solution under different experimental conditions.

a) *With TiO₂ (80 mg/L solution with a pH=4.01); irradiation with UV lamp λ310nm.*
Considering the degradation of the carminic acid, the absorbance profiles at different time steps has been represented in the wave range 400-750 nm in Fig. 3.57. Fig. 3.57 reports the time in minutes. It can be intuited from the plot that the degreasing of the absorbance velocity changes in time. Fig. 3.58 shows more precisely the decrease in concentration, accordingly with the calibration curve.

By looking at Fig. 3.58 three different steps can be observed. In the first 5 minutes, the decreasing of the absorbance is very fast, going from the initial 80mg/L to approximatively 60mg/L in less than 5 min. Around the 25% of the catalyst is degraded in the first 5 minutes. After the first 5 minutes the degradation process slows down and assumes approximatively a linear trend until 120 min. In the final part of the plot, after 120 minutes, the degradation seems to further slowdown. It was observed that the degradation resulted to be complete after about 165 min.

It is to note that TiO_2 has been reported to react with carminic acid to which TiO_2 can be anchored via the carboxylate and phenolate groups in a very strong way, with no changes into the spectrum of the chromophore. The formed material is stable in water, with slow hydrolysis and carminic acid desorption observed only in alkaline solution [82].
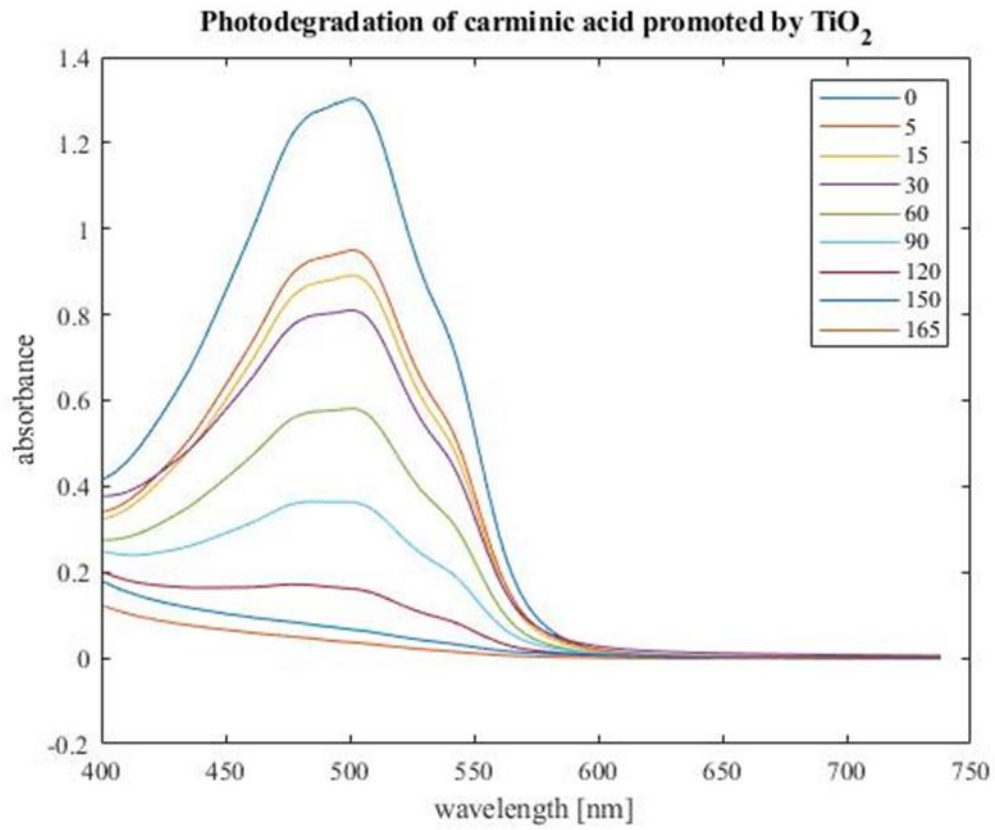
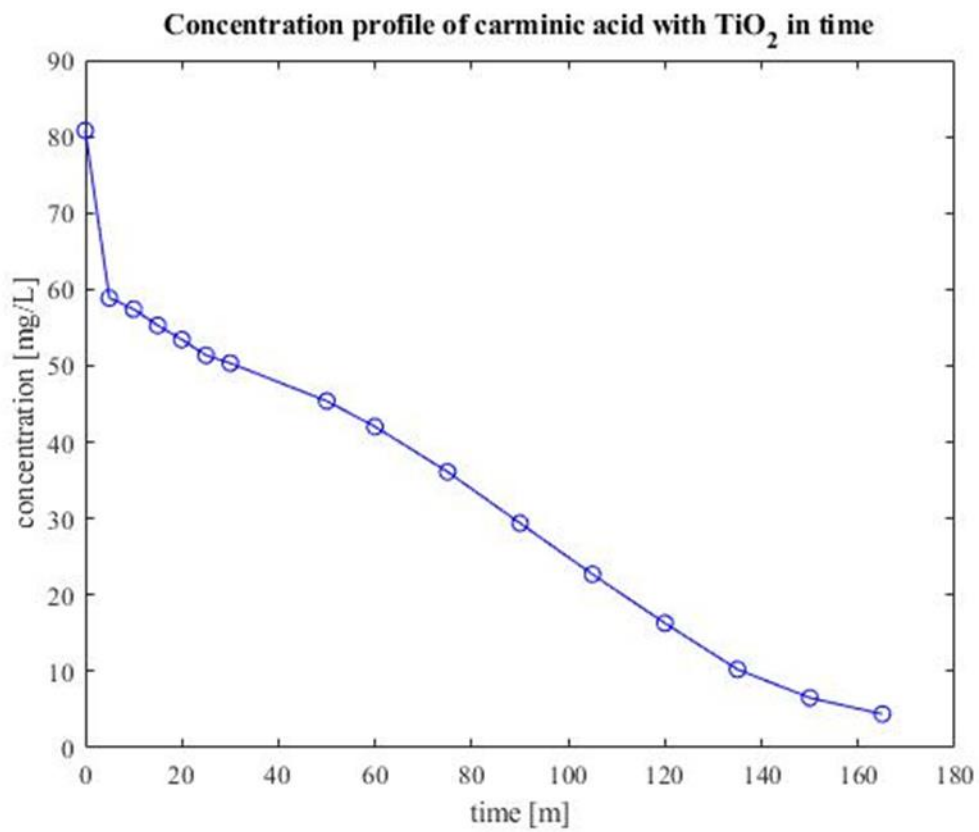*Figure 3.57 Absorbance profile of the carminic acid solution in the time*

Figure 3.58 Concentration profile of the carminic acid solution in the time

Thus, the complex degradation pathway, which deserves deeper investigation, results from the combination of different processes:

1. Formation of the carminic acid-TiO$_2$ complex
2. Desorption of carminic acid
3. Photodegradation induced by TiO$_2$ and by carminic acid-TiO$_2$ complex, which was reported to exhibit pronounced photosensitization toward visible and UV light [82].
4. Finally, the carminic acid has the slowest degradation being not completely degraded after 2 hours.

   b) *Degradation of carminic acid in the presence of C1:5Ti.*

The experiments have been run in two steps. In the first 8 hours they have been run without using the UV lamp and then the lamp has been switched on. By this way it has been possible to distingue the adsorption contribution due to the spent coffee ground matrix from the photodegradation contribution due to the TiO$_2$-promoted catalysis. It is assumed that the absorption process is exhausted after 8 hours.
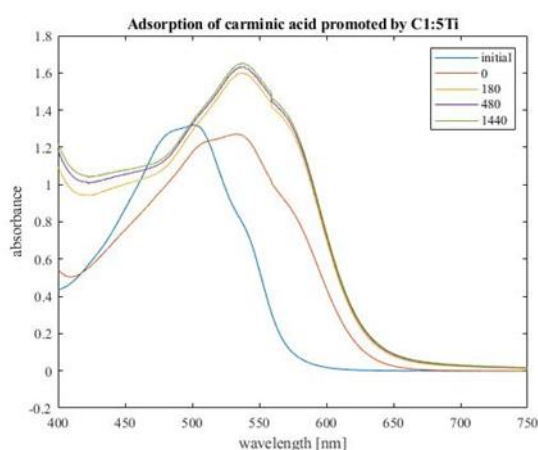
Figure 3.59 Absorption spectra for carminic acid with C1:5Ti
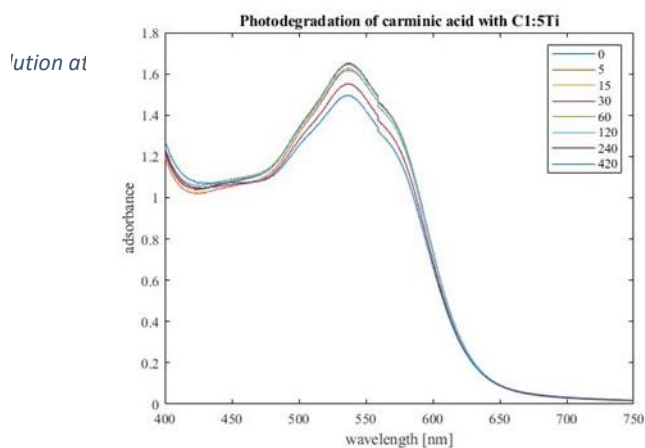
Figure 3.60 Photodegradation spectra for carminic acid with C1:5Ti

Fig. 3.59 and Fig. 3.60 respectively represent the absorption step and the photodegradation step for the carminic acid solution with the C1:5Ti catalyst.

Considering the absorption step, the line indicated as "initial" corresponds to the carminic acid absorption profile before the adding of the C1:5Ti. The line indicated as "0" corresponds to the effective first instant of the reaction, considered as the moment at which the catalyst is completely dispersed in the liquid solution. It can be observed that the bell before the adding of the catalyst and the bell at time "0" have different shapes and are centered at different wavelengths. The reason of the shift is the change of pH of the solution due to the catalyst presence from 4.01 to 6.96.

After the shift of the spectrum, it can be observed that the absorbance values increase, reasonably due to the formation of the carminic acid-TiO$_2$ complex adsorbed on the carbonaceous material.

Considering instead the photodegradation step, it is possible to notice that the absorbance profiles slightly decrease in time, even if apparently the TiO$_2$ seems to be masked by the carbonaceous support, thus decreasing significantly its catalytic capacity.

c) *Photodegradation of 50mL of an 80 mg/L carminic acid solution in the presence of 100 mg of SCGs@Fe catalyst and 2 mL H$_2$O$_2$.*

In Fig 3.61 the concentration profile of carminic acid degradation in the presence of SCGs@Fe catalyst is reported.
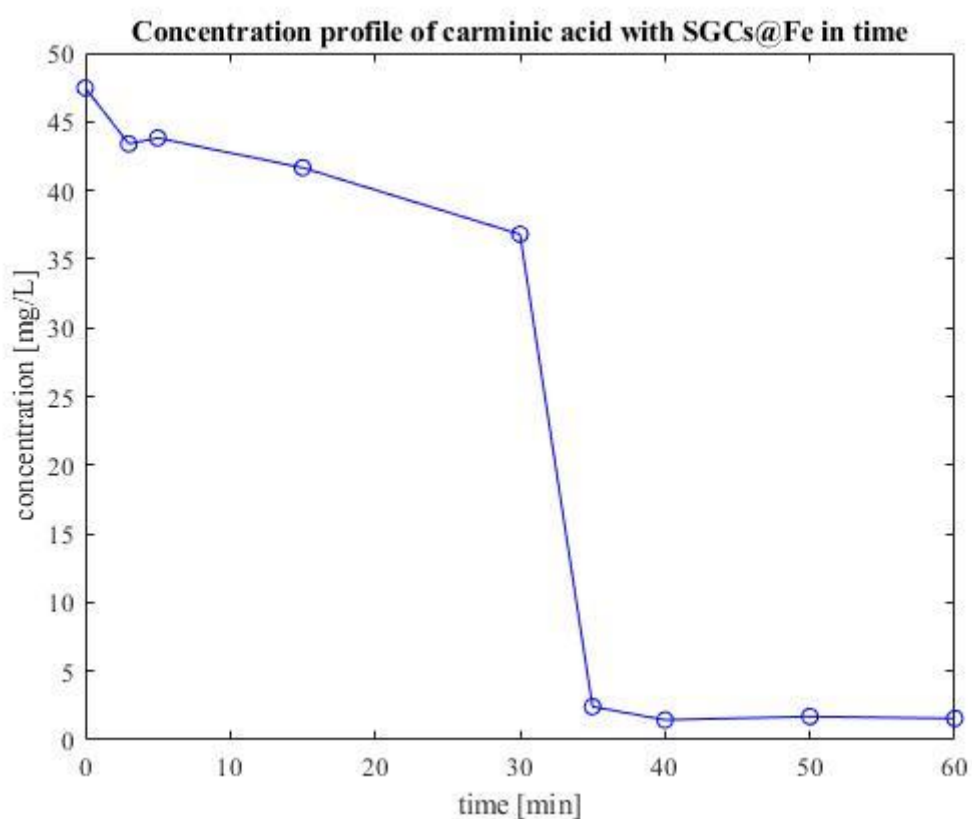
Figure 3.61 Concentration profile of carminic acid solution with SCGs@Fe.

The initial alkaline pH, that was equal to 9, was reduced to 3.5 by addition of HCl solution (0.1 M). The concentration profile has been reported in Figure 3.63. The initial absorbance decreasing was due to the dilution by HCl addition, then the degradation started with a degradation of about 10% along 30 min. The slow process can be explained with the ability of carminic acid to scavenge radicals (in this case ·OH) as demonstrated by the antioxidant activity in biological systems [79].

After 30 min 30 mg of FeCl$_3$ have been added: the total degradation was immediately observed.

Even if this process will deserve further studies, nevertheless our hypothesis is that the presence of

iron species in different oxidation states in the SCGs@Fe together with a soluble Fe(III) species can promote the Fe^{3+}/Fe^{2+} cycle and then enhance the performance for the degradation of carminic acid. In figure 3.62 the ESI mass spectrum in positive ions and in Figure 3.63 in negative ions of carminic acid are shown.

From Fig. 3.62, the following peaks can be assigned:

- at m/z 515 (relative abundance 4%) ions $[M+Na]^+$
- at m/z 413 (relative abundance 100 %, base peak) ions $[M-CO_2-2H_2O +H]^+$
- at m/z 537 (relative abundance 14%) ions $[M+2Na-H]^+$

From Fig. 3.63 the following peaks can be assigned:

- at m/z 491 (relative abundance 100%, base peak and molecular ion) ions $[M-H]^-$
- at m/z 447 (relative abundance 13 %) ions $[M-CO_2-H]^-$

The very poor fragmentation, either in the positive or in negative modes, confirms the chemical stability of the molecule.

The ESI mass spectra of the final solution confirms the complete oxidative degradation to CO_2. No new organic compounds are formed and in the ESI spectra only noise can be detected.
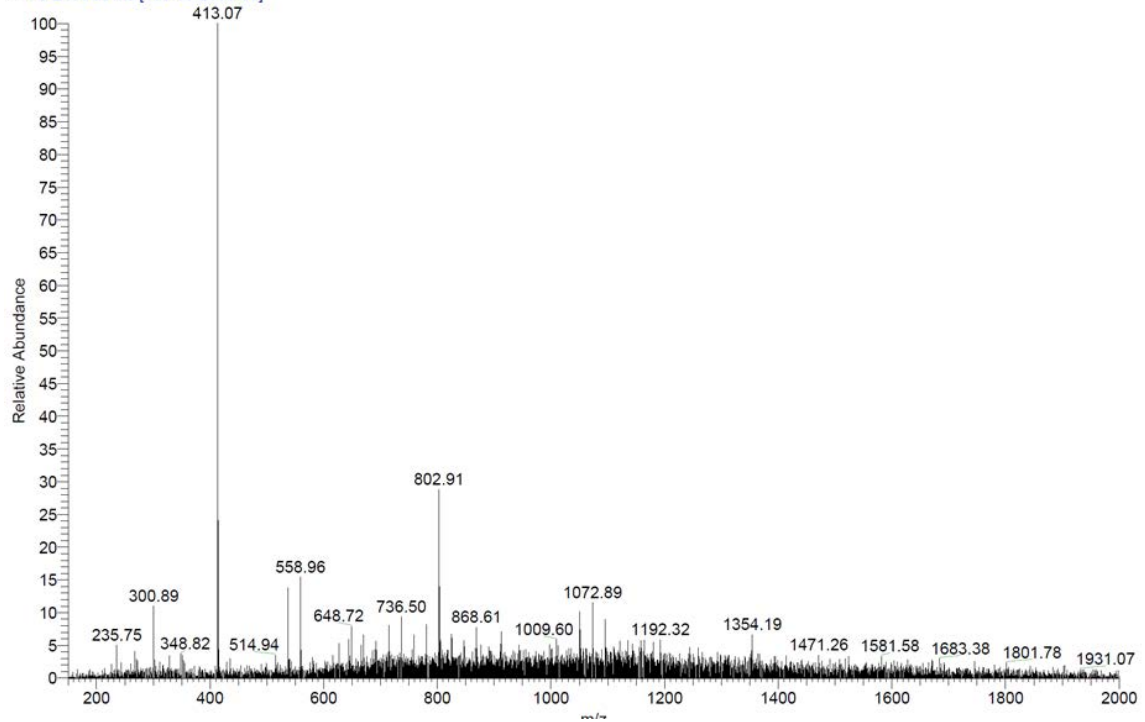
Figure 3.62 ESI mass spectrum in positive ions
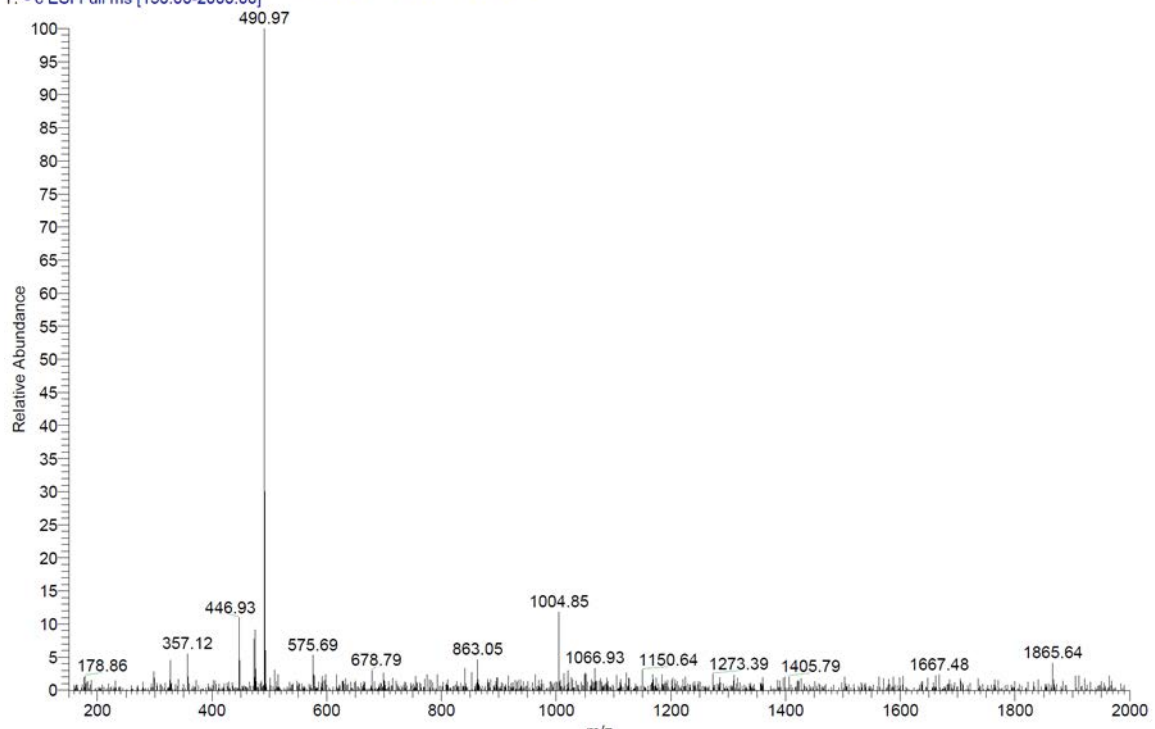
Figure 3.63 ESI mass spectrum in negative ions

Chapter 4

Conclusions and Perspectives

The thesis work is articulated in two parts. In the first part waste materials such as spent coffee grounds and wooden ash have were investigated for their application as raw material for the preparation of supports suitable to deposit metal systems, with the aim to achieve "green" catalysts. In the second part some catalysts were tested in dyes degradations.

Considering the catalysts preparation, it can be concluded that:

- Spent coffee grounds and wooden ash are interesting wastes because they are renewable and are constantly produced in huge amounts worldwide. Spent coffee grounds are a food industry waste that does not contain dangerous components and their application has been considered in many studies. Wooden ashes in the past were disposed in landfills, but, being a source of pollution because of the fine particulate matter easily transported by the wind, their management has become a relevant issue.

- Previous studies showed that spent coffee grounds can be pyrolyzed to obtain activate carbon that can be used as catalyst support. Activated carbon from spent coffee grounds is characterized by very high porosity, even greater than the commercial activated carbon one.

- The activating pretreatment of spent coffee grounds has shown some effect only using big amounts of sodium bicarbonate (1:5 w/w), even if some relevant data are not available up to now for the characterization of this material.

- As for wooden ash, the heterogeneity of the matrix and the loss of material during the processing make the wooden ash not suitable for the application. The heterogeneity is due to the biomass and to the combustion process. Setting precise combustion conditions would help to obtain a more homogeneous raw material. The loss in weight is relevant during the treatment to develop porosity and during the metal system deposition. Further investigations are required to minimize the loss in weight to justify the usage of wooden ash as raw material.

- The deposition of metal salts in a ratio 1:10 w/w with respect to the support is suitable for the preparation of catalysts to characterize in a deeper way.

- Titanium dioxide has been dispersed on the C1:5 support in a ratio of 1:10 w/w. The dispersion will be improved in order to achieve more homogeneous materials.

- The ball milling technique has been applied successfully to the spent coffee grounds and to the commercial activated carbon in the preparation of iron catalysts active in oxidative degradation of dyes.

Degradation of organic dyes has been studied by means of different experiments. Firstly, rhodamine and erythrosine B. It is to note that rhodamine is considered a model for oxidative degradation

processes, to apply not only to dyes but also to emerging pollutants. Some considerations can be formulated, even if we did not perform kinetic studies.

a) *Photodegradation of rhodamine and erythrosine B with TiO$_2$*

It can be concluded that the rhodamine presents the fastest degradation when TiO$_2$ is dispersed in it. Erythrosine B degradation promoted by TiO$_2$ is still very fast and shows a linear profile of concentration differently from that of rhodamine, indicating a different degradation mechanism. Kinetic studies will be carried out as for the reactions under our experimental conditions.

b) *Photodegradation of rhodamine and erythrosine B promoted by C1:5Ti*

The experiments were conducted in such a way that it was possible to separate the absorption contribution from the photodegradation. Rhodamine shows a very strong absorption contribution, while erythrosine B is almost not absorbed. Two factors can influence the different behavior:

1. The different molecule dimension: erythrosine B molecules are bigger than the rhodamine ones.
2. The different polarity: rhodamine is a cationic dye, while erythrosine B is an anionic dye, thus the interaction with an adsorbent material could behave in an opposite way. These results suggest that the C1:5Ti catalyst has a PZC of about 5, so that when the pH of the solution is higher, negative charges arise on the surface, thus inducing a repulsive electrostatic interaction with negative dyes and an attractive one with positive dyes such as rhodamine.

The photodegradation does not proceed: the spent coffee grounds support probably inhibit the TiO$_2$ activity.

c) *Oxidative degradations of rhodamine promoted by C1:5Cu1:10*

The absorption contribution of the activated spent coffee ground matrix has been tested using different amounts of catalysts. It has been underlined how the higher quantity of catalyst accelerate the decreasing of dye concentration in the solution.

Tests have also been run with different amounts of H$_2$O$_2$: a larger amount of hydrogen peroxide allows to degrade faster the dye.

The process carried out with C1:5Mn1:10, gives quite similar results.

d) *Oxidative degradation of rhodamine promoted by SCGs@Fe*

The reaction has been run in the first 30 minutes, observing about 50% degradation. Then upon addition of FeCl$_3$, rhodamine immediately disappears.

Particular attention is paid to carminic acid, being extensively used as food additive and representing an environmental problem due to its biological activity and chemical stability.

a) *Photodegradation of carminic acid promoted by TiO$_2$*

It has been individuated a complex degradation pathway, which deserves deeper investigation, resulting from the combination of different processes:

5. Formation of the carminic acid-TiO$_2$ complex
6. Desorption of carminic acid
7. Photodegradation induced by TiO$_2$ and by carminic acid-TiO$_2$ complex, which was reported to exhibit pronounced photosensitization toward visible and UV light.
8. Carminic acid is not completely degraded after 2 hours.

b) *Photodegradation of carminic acid promoted by C1:5Ti*

Absorption and degradation steps have been studied separately. In the absorption step it is possible to see immediately a shift in the UV-Visible spectrum, corresponding to a change of pH due to the catalyst presence. As for the photodegradation step, the absorbance profiles slightly decrease in the time, even if apparently the TiO$_2$ seems to be masked by the carbonaceous support, thus decreasing significantly its catalytic capacity.

c) *Oxidative degradation of carminic acid promoted by SCGs@Fe*

In the first 30 minutes the degradation corresponded to about 10%. Once a small amount of FeCl$_3$ is added, carminic acid immediately disappears. Even if this process will deserve further studies, nevertheless our hypothesis is that the presence of iron species in different oxidation states in the SCGs@Fe together with a soluble Fe(III) species can promote the Fe^{3+}/Fe^{2+} cycle and then enhance the performance for the degradation of carminic acid.

The ESI mass spectra of the final solution confirms the complete oxidative degradation to CO$_2$. No new organic compounds are formed and in the ESI spectra only noise can be detected.

This result is particular intriguing: the new "green" catalyst will be characterized completely in order to optimize composition, preparation and conditions of applications in specific chemical processes of industrial interest such as cyclohexane oxidation to cyclohexanone/cyclohexanol, to study in terms of yield and selectivity.

Bibliography

1. Porter, Michael E. and Claas van der Linde. "Toward a new conception of the environment-competitiveness Relationship." *Journal of Economic Perspectives*, 9, 4, 97-118. 1995.

2. https://www.resourcepanel.org/

3. Ellen McArthur Foundation. "Circular economy report - towards the circular economy" Vol. 1. 2013.

4. https://www.footprintnetwork.org/

5. https://www.europarl.europa.eu/portal

6. Anastas, P. and J.C. Warner. "Green chemistry: theory and practice." *Oxford University Press*, Oxford. 1998.

7. Sheldon, R. A., I. Arends and U. Hanefeld. "Green chemistry and catalysis". *Wiley-VCH*, Weinheim. 2007.

8. Abraham, M. *Envron. Prog.* 23, 4, p. 266. 2004.

9. Galanakis, C. "Handbook of coffee processing by-product: sustainable applications." *Academic Press*. London. 2017

10. Mussato, S.I, E.M.S. Machado, S. Martins, J.A. Teixeira. "Production, composition and application of coffee and its industrial residues." *Food Bioprocess Technol.* 2011. 4. 661-672.

11. Girotto, F., A. Pivato, R. Cossu, G.E. Nkeng, M. C. Lavagnolo. "The broad spectrum of possibilities for spent coffee grounds valorization." *J.Mater. Cycles Waste Manag.* 2018. 20. 695-701.

12. Ballesteros, L.F., J.A. Texeira, S.I. Mussato. "Chemical, functional and structural properties of spent coffee grounds and coffee silverskin". *Food Bioprocess Technol*. 2014. 7. 3493-3503.

13. Campos-Vega, R., G. Loarca-Pina, H.A. Vergara-Castaneda, B.D. Oomah. "Spent coffee grounds: a review on current research and future prospects." *Trends in Food Science & Technol.* 2015. 45. 24-36.

14. Peshev. D., D. Mitev, L. Peeva. G. Peev. "Valorization of spent coffee grounds – A new approach." *Separation and Purification Technology.* 2018. 192. 271-277.

15. Nguyen Q.A., E.J. Cho, D.S. Lee, H.J. Bae. "Development of an advanced integrative process to create valuable biosugars including manno-oligosaccharides and mannose from spent coffee grounds." *Bioresource Technology*. 2019. 272. 209-216.

16. Ramon-Goncalves M., L. Alcarez, S. Perez-Ferreras, M.E. Leon-Gonzalez, N. Rosales-Conrado, F.A. Lopez. "Extraction of polyphenols and synthesis of new activated carbon from spent coffee grounds." *Scientific Reports*. 2019. 9. 17706.

17. Karmee SK. "A spent coffee grounds based biorefinery for the production of biofuels, biopolymers, antioxidants and biocomposites." *Waste Management*. 2018. 72. 240-254.

18. Tongcumpou C., P. Usapein, and N.Tuntiwiwattanapun. "Complete utilization of wet spent coffee grounds waste as a novel feedstock for antioxidant, biodiesel, and bio-char production." *Industrial Crops & Products*. 2019. 138. 111484.

19. Moustafa H., C. Guizani, and A. Dufresne. «Sustainable biodegradable coffee grounds filler and its effect on the hydrophobicity, mechanical and thermal properties of biodegradable PBAT composites." *J. Applied Polymer Science.* 2017. 44498-44509.

20. Mendoza Martinez C.L. E.P. Alves Rocha, A.C. Oliveira Carneiro, F.J. Borges Gomes, L.A. Ribas Batalha, E. Vakkilainen, M. Cardoso. "Characterization of residual biomasses from the coffee production chain and assessment the potential for energy purposes." *Biomass and Bioenergy.* 2019. 120. 68-76.

21. Kookos I.K. "Technoeconomic and environmental assessment of a process for biodiesel production from spent coffee grounds (SCGs)." *Resources, Conservation & Recycling.* 2018. 134. 156-164.

22. Silva M.A., S.A. Nebra, M.J. Machado Silva, C.G. Sanchez. "The use of biomass residues in the Brazilian soluble coffee industry." *Biomass Bioenerg*. 1998. 14 (5-6), 457-467.

23. Machado E.M.S., R.M. Rodriguez-Jasso, J.A. Teixeira, S.I. Mussato. "Growth of fungal strains on coffee industry residues with removal of polyphenolic compounds." *Biochem. Eng. J.* 2012. 60. 87-90.

24. Rocha M.V.P., L.J.B.L de Matos, L.P.D. Lima, P.M.D.S. Figueiredo, I.L. Lucena, F.A.N. Fernandes, L.R.B. Gonçalves. "Ultrasound-assisted production of biodiesel and ethanol from spent coffee grounds." *Biores. Technol.* 2014. 167. 343-348.

25. Cruz R., E. Mendes, A. Torrinha, S. Morais, J.A. Pereira, P. Baptista, S. Casal. "Revalorization of spent coffee residues by a direct agronomic approach." *Food Research International*. 2015. 71. 190-196.

26. Elbl J., L. Plošek, A. Kintl, J. Přichystalová, J. Záhora, J. K. Friedel. "The effect of increased doses of compost on leaching of mineral nitrogen from arable land." *Pol. J. Environ. Stud.* 2014. 23(3). 697–703

27. Jutakrisada P., C. Prajaksud, L. Kuboonya-Aruk, S. Theerakulpisut, K. Kamwilaisak. "Adsorption characteristics of activated carbon prepared from spent ground coffee." *Clean Technol. Environ. Policy.* 2016. 18. 639-645.

28. Alcaraz. L., M.E. Escudero, F.J. Alguacil, I. Llorente, A. Urbieta, P. Fernandez, F.A. Lopez. "Dysprosium removal from water using active carbons obtained from spent coffee ground." *Nanomaterials.* 2019. 9. 1372-1387.

29. Paredes-Laverde M., J. Silva-Agredo, R.A. Torres-Palma. "Removal of norfloxacin in deionized, municipal water and urine using rice (Oryza sativa) and coffee (Coffea arabica) husk waters as natural adsorbents." *J. Environmental Management.* 2018. 213. 98-108.

30. Babu, N.A., D.S. Reddy, G.S. Kumar, K. Ravindhranath, G.V.K. Mohan. "Removal of lead and fluorine from contaminated water using exhausted coffee grounds based bio-sorbent." *J. Environmental Management.* 2018. 218. 602-612.

31. Wen. X., H. Liu, L. Zhang, J. Zhang, C. Fu, X. Shi, X. Chen, E. Mijowska, M.J. Chen, D.Y. Wang. "Large-scale converting waste coffee grounds into functional carbon materials as high-efficient adsorbent for organic dyes". *Bioresource Technology.* 2019. 272. 92-98.

32. Fonseca Alves, A.C., R.V.P. Antero, S.B. de Oliveira, S. A. Ojala, P.S. Scalize. "Activated carbon produced from waste coffee grounds for an effective removal of bisphenol-A in aqueous medium." *Environmental Science and Pollution Research.* 2019. 26. 24850-24862.

33. Dos Santos D.C., M.A. Adebayo, E.C. Lima, S.F.P. Pereira, R. Cataluna, C. Saucier, P.S. Thue, F.M. Machado. "Application of carbon composite adsorbents prepared from coffee waste and clay for the removal of reactive dyes from aqueous solutions." *J. Braz. Chem. Soc.* 2015. 26. 924-938.

34. Boudrahem F., A. Soualah, F. Aissani-Benissad. "Pb(II) and Cd(II) removal from aqueous solutions using activated carbon developed from coffee residue activated with phosphoric acid and zinc chloride." *J. Chemical and Engineering Data.* 2011. 56. 1946-1955.

35. Suganya S., P.S. Kumar. "Influence of ultrasonic waves on preparation of active carbon from coffee waste for the reclamation of effluents containing Cr(VI) ions." *J. Industrial Engineering Chemistry.* 2018. 60. 418-430.

36. Yeung P.T., P.Y Chung, H.C. Tsang, J.C.O Tang, G.Y.M. Cheng, R. Gambari, C.H. Chui, K.M. Lam. "Preparation and characterization of bio-safe activated charcoal derived from coffee waste residue and its application for removal of lead and copper ions." *RSC Adv.* 4. 38839-38847.

37. Ching S.L., M.S. Yusoff, H.A. Aziz, M. Umar. "Influence of impregnation ratio on coffee ground activated carbon as landfill leachate adsorbent for removal of total iron and orthophosphate." *Desalination.* 2011. 279. 225-234.

38. Kim H.B., S.H. Kim, E.K. Jeon. D.H. Kim, D.C.W. Tsang, D.S. Alessi, E.E. Kwon, K. Baek. "Effect of dissolved organic carbon from sludge, rice straw and spent coffee ground biochar on the mobility of arsenic in soil." *Science of the Total Environment.* 2018. 636. 1241-1248.

39. Kim Y., H.G. Min, N. Koo, J. Park, S.H. Lee, G.I. Bak, J.G. Kim. "The effectiveness of spent coffee grounds and its biochar on the amelioration of heavy metals-contaminated water and soil using chemical and biological assessments." *J. Environmental Management.* 2014. 146. 124-130.

40. Rovani. S., M.T. Censi, Jr. S.L. Pedrotti, E.C. Lima, R. Cataluna, A.N. Fernandes. "Development of a new adsorbent from agro-industrial waste and its potential use in endocrine disruptor compound removal." *J. Hazardous Materials.* 2014. 271. 311-320.

41. Querejeta N., M.V. Gil, C. Pevida, T.A. Centeno. "Standing out the key role of ultramicroporosity to tailor biomass-derived carbons for CO_2 capture." *J. CO_2 Utilization.* 2018. 26. 1-7.

42. Travis W., S. Gadipelli, Z. Guo. "Superior CO_2 adsorption from waste coffee ground derived carbons." *RCS Advances. 2015.* 5. 29558-29562.

43. Nowicki P., P. Skibiszewska, R. Pietrzak. "Hydrogen sulphide removal on carbonaceous adsorbents prepared from coffee industry waste materials." *Chemical Engineering Journal.* 2014. 248. 208-215.

44. Kante K., C. Nieto-Delgado, J.R. Rangel-Mendez, T.J. Bandosz. "Spent coffee-based activated carbon: specific surface features and their importance for H_2S separation process." *J. Hazardous Materials.* 2012. 201-202. 141-147.

45. Kemp K.C., S.B. Baek, W.G. Lee, M. Meyyappan, K.S. Kim. "Activated carbon derived from waste coffee grounds for stable methane storage." *Nanotechnology.* 2015. 26. 385602-385609.

46. Akasaka H., T. Takahata, I. Toda, H. Ono, S. Ohshio, S. Himeno, T. Kokubu, H. Saitoh. "Hydrogen storage ability of porous carbon material fabricated from coffee bean wastes." *International J. Hydrogen Energy.* 2011. 36. 580-585.

47. Um J.H., Y. Kim, C.Y. Ahn, J. Kim, Y.E. Sung, Y.H. Cho, S.S: Kim, W.S. Yoon. Biomass waste, coffee grounds-derived carbon for lithium storage." *J. Electrochim. Sci. Technol.* 2018. 9. 163-168.

48. Oh W.D., G. Lisak, R.D. Webster, Y.N. Liang, A. Veksha, A. Giannis, J.G.S. Moo, J.W. Lim, T.T. Lim. "Insight into the thermolytic transformation of lignocellulosic biomass waste to redox-active carbocatalyst: durability of surface active sites." *Applied Catalysis B: Environment.* 2018. 233. 120-129.

49. Goncalves M., M.C. Guerreiro, L.C. Alves de Oliveira, C. Soares de Castro. "A friendly environmental material: iron dioxide dispersed over activated carbon from coffee husk for organic pollutants removal." *J. Environmental Management.* 2013. 127. 206-211.

50. Lee H.K., Y.G. Park, T. Jeong, Y.S. Song. "Green nanocomposites filled with spent coffee grounds." *J. Applied Polymer Science.* 2015. 42043-42049.

51. Zhao P., M.H. Aboonasr, H. Zhu, Y. Liu, L. Tao, J. Liu. "Hierarchically porous carbon from waste coffee grounds for high-performance Li-Se batteries." *Electrochimica Acta.* 2019. 325. 134931-134938.

52. Givens D.I., W.P. Barber. "In vivo evaluation of spent coffee grounds as a ruminant feed." *Agr. Wastes.* 1986. 18 (1). 69-72.

53. Sampaio A., G. Dragone, M. Vilanova, J.M. Oliveira, J.A. Teixeira, S.I. Mussato. "Production, chemical characterization, and sensory profile of a novel spirit elaborated from spent coffee ground." *LWT. Food Sci. Technol.* 2013. 54 (2). 557-563.

54. Demeyer A., J.CVoundi Nkana, M.GVerloo. "Characteristics of wood ash and influence on soil properties and nutrient uptake: an overview." *Bioresource Technology.* 2001. 77 (3). 287-295.

55. Etiégni L., A.G. Campbell. "Physical and chemical characteristics of wood ash." *Bioresource Technology.* 1991. 37 (2). 173-178.

56. Cheah C.B., M. Ramli. "The implementation of wood waste ash as a partial cement replacement material in the production of structural grade concrete and mortar: An overview." *Resources, Conservation and Recycling*. 2011. 55 (7). 669-685.

57. Vassilev S.V., C.G. Vassileva. "A new approach for the classification of coal fly ashes based on their origin, composition, properties, and behaviour." *Fuel.* 2007. 86 (10-11). 1490-1512.

58. Vassilev S.V., D. Baxter, L.K. Andersen, C.G. Vassileva. "An overview of the composition and application of biomass ash.: Part 2. Potential utilisation, technological and ecological advantages and challenges." *Fuel.* 2013. 105. 19-39.

59. Kalembkiewicz J., D. Galas, E. Sitarz-Palczak. "The physicochemical properties and composition of biomass ash and evaluating directions of its applications." *Pol. J. Environ. Stud.* 2018. 27 (6). 1-11.

60. Schwarzenbach R.P., P.M. Gschwend, D.M. Imboden. "Environmental organic chemistry." 3rd edition, 2016, Whiley.

61. Pera-Titus M., V. García-Molina, M. A Baños, J. Giménez, S. Esplugasa. "Degradation of chlorophenols by means of advanced oxidation processes: a general review." *Applied Catalysis B: Environmental.* 2004. 47 (4), 219-256.

62. Al-Hamdi A.M., M. Sillanpää, J. Dutta. "Photocatalytic degradation of phenol by iodine doped tin oxide nanoparticles under UV and sunlight irradiation." *Journal of Alloys and Compounds.* 2015. 618. 366-371.

63. Strong P.J., J.E. Burgess. "Treatment methods for wine-related and distillery wastewaters: a review." *Bioremediation Journal*. 2008. 12 (2). 70-87.

64. Bellona C., J.E. Drewes, P. Xu, G: Amy. "Factors affecting the rejection of organic solutes during NF/RO treatment—a literature review." *Water Research.* 2004. 38 (12). 2795-2809.

65. Fujishima A., X. Zhang, and D.A. Tryk. "Heterogeneous photocatalysis: From water photolysis to applications in environmental cleanup." *International Journal of Hydrogen Energy.* 2007. 32 (14). 2664-2672.

66. Ikehata K., M.G. El-Din. "Degradation of recalcitrant surfactants in wastewater by ozonation and advanced oxidation processes: a review." *Ozone: Science & Engineering.* 2010. 26 (4). 327-343.

67. Rossetto E., D.I. Petkowicz, J.H.Z. dos Santos, S.B.C. Perghera F.G. Penhaa. "Bentonites impregnated with TiO_2 for photodegradation of methylene blue." *Applied Clay Science.* 2010. 48 (4). 602-606.

68. Yurdakal S., G. Palmisano, V. Loddo, V. Augugliaro, L. Palmisano. "Nanostructured Rutile TiO_2 for Selective Photocatalytic Oxidation of Aromatic Alcohols to Aldehydes in Water." *J. Am. Chem. Soc.* 2008. 130 (5). 1568-1569.

69. Li J., A.N. Pham, R. Dai, Z. Wang, D. Waite. "Recent advances in Cu-Fenton systems for the treatment of industrial wastewaters: Role of Cu complexes and Cu composites." *Journal of Hazardous Materials.* 2020. 392. 122261.

70. Crini G. "Non-conventional low-cost adsorbents for dye removal: A review." *Bioresource Technology.* 2006. 97 (9). 1061-1085.

71. Wang C.H., W.C. Wen, H.C. Hsu, B.Y. Yao. "High-capacitance KOH-activated nitrogen-containing porous carbon material from waste coffee grounds in supercapacitor." *Advanced Powder Technology.* 2016. 27 (4). 1387-1395.

72. Satterfield C N. "Heterogeneous catalysis in industrial practice." 2nd edition. 1991. United States.

73. Laksaci, H., A. Khelifi, M. Trari, A. Addou. "Synthesis and characterization of microporous activated carbon from coffee grounds using potassium hydroxide". *J. Cleaner production.* 2017. 147. 254-262.

74. Kiwaan K.A., T.M. Atwee, E.A. Azab, A.A. El-Bindary. "Photocatalytic degradation of organic dyes in the presence of nanostructured titanium dioxide." *Journal of Molecular Structure.* 2020. 1200. 127115.

75. Li D., T. Yang, Y. Li, Z. Liu, W. Jiao. "Facile and green synthesis of highly dispersed tar-based heterogeneous Fenton catalytic nanoparticles for the degradation of methylene blue." *Journal of Cleaner Production.* 2020. 246. 119033.

76. Allevi P., M. Anastasia, S. Bingham, P. Ciuffreda, A. Fiecchi, G. Cighetti, M. Muir, A. Scala, J. Tyman. "Synthesis of carminic acid, the colourant principle of cochineal." *J. Chem. Soc.,* Perkin Trans. 1998. 1. 575.

77. Gosetti F., U. Chiuminatto, E. Mazzucco, R. Mastroianni, E. Marengo. "Ultra-high-performance liquid chromatography/tandem high-resolution mass spectrometry analysis of sixteen red beverages containing carminic acid: Identification of degradation products by using principal component analysis/discriminant analysis." *Food Chemistry.* 2015. 167. 454-462.

78. Das P., C.K. Jain, S. Roychoudhury, H. K. Majumder, S. Das. "Design, synthesis and in vitro anticancer activity of a Cu(II) complex of carminic acid: a novel small molecule inhibitor of human DNA topoisomerase I and topoisomerase II." *Chemistry Select.* 2016. 1. 6623-6631.

79. Li G. X., Z.Q. Liu, D. Wu. "Carminic acid: an antioxidant to protect erythrocytes and DNA against radical-induced oxidation." *J. Phys. Org. Chem.* 2009. 22. 883–887.

80. Machatová Z., Z. Barbieriková, P. Poliak, V. Jančovičova, V. Lukeš, V. Brezová. "Study of natural anthraquinone colorants by EPR and UV/vis spectroscopy." *Dyes and pigments.* 2016. 132. 79-93.

81. Fain V. Ya., B.E. Zaitsev, M.A. Rayabov. "Tautomerism and ionization of carminic acid." *Russian Journal of General Chemistry.* 2007. 77 (10). 1769-1774.

82. Gawęda S., S. Grażyna, K. Szaciłowski. "Photosensitization and photocurrent switching in carminic acid/titanium dioxide hybrid material." *J. Phys. Chem. C.* 2008. 112 (48). 19131-19141.

Ringraziamenti

Desidero ricordare tutti coloro che mi hanno aiutato nel lavoro di tesi, con suggerimenti, critiche ed osservazioni: a loro va la mia gratitudine.

In primo luogo, ringrazio la Professoressa Roberta Bertani per la disponibilità e lo spirito di collaborazione con cui mi ha accompagnato nel lavoro degli ultimi mesi.

Ringrazio inoltre il Dottor Paolo Sgarbossa e il Dottor Federico Zorzi per il tempo dedicatomi e per i preziosi consigli e confronti.

Ringrazio la Dottoressa Ana da Costa Ribeiro per aver contribuito a guidare, anche se a distanza, il progetto.

Ringrazio i miei colleghi Dottor Giovanni Nardin e Dottor Luca Troncon per l'intesa costruttiva.

Infine, ringrazio tutti coloro che, non solo negli ultimi mesi, ma durante l'intero percorso di studi, mi hanno supportato e accompagnato.